



**Michigan
Technological
University**

Michigan Technological University
Digital Commons @ Michigan Tech

Dissertations, Master's Theses and Master's Reports

2017

An Optimal Energy Management Strategy for Hybrid Electric Vehicles

Amir Rezaei

Michigan Technological University, arezaei@mtu.edu

Copyright 2017 Amir Rezaei

Recommended Citation

Rezaei, Amir, "An Optimal Energy Management Strategy for Hybrid Electric Vehicles", Open Access Dissertation, Michigan Technological University, 2017.
<https://digitalcommons.mtu.edu/etdr/378>

Follow this and additional works at: <https://digitalcommons.mtu.edu/etdr>



Part of the [Automotive Engineering Commons](#), and the [Controls and Control Theory Commons](#)

AN OPTIMAL ENERGY MANAGEMENT STRATEGY FOR HYBRID
ELECTRIC VEHICLES

By

Amir Rezaei

A DISSERTATION

Submitted in partial fulfillment of the requirements for the degree of

DOCTOR OF PHILOSOPHY

In Electrical Engineering

MICHIGAN TECHNOLOGICAL UNIVERSITY

2017

Copyright 2017 Amir Rezaei

This dissertation has been approved in partial fulfillment of the requirements for the Degree of DOCTOR OF PHILOSOPHY in Electrical Engineering.

Department of Electrical and Computer Engineering

Dissertation Advisor: *Dr. Jeffrey B. Burl*

Committee Member: *Dr. Bo Chen*

Committee Member: *Dr. Mahdi Shahbakhti*

Committee Member: *Dr. Wayne W. Weaver*

Committee Member: *Dr. Darrell L. Robinette*

Department Chair: *Dr. Daniel R. Fuhrmann*

Dedication

To my parents, advisor and friends

who supported me during the years I spent to complete my degree. Surely, I would not be here today if it was not for their patience, help, and support.

Contents

List of Figures	xi
List of Tables	xv
Preface	xvii
List of Abbreviations	xix
Abstract	xxi
1 Introduction	1
2 Effects of Time Horizon on Model Predictive Control for Hybrid Electric Vehicles	7
2.1 Introduction	7
2.2 A review on control strategies	9
2.2.1 Rule-based control	9
2.2.2 Instantaneous optimal control (IOC)	10
2.2.3 Model Predictive Control (MPC)	11
2.3 Applied approach for analyzing MPC	12

2.3.1	Simulation approaches	12
2.3.2	HEV configuration and equations	13
2.3.3	Cost function and optimization method	16
2.3.4	Vehicle model	18
2.4	Simulation results	20
2.4.1	MPC performance versus time horizon	20
2.5	Conclusion	21

3 Estimation of the ECMS Equivalent Factor Bounds for Hybrid

Electric Vehicles	23	
3.1	Introduction	23
3.2	Pontryagin’s Minimum Principle (PMP) AND ECMS	27
3.2.1	Vehicle Model	27
3.2.2	Control Problem	30
3.3	Bounds of the Optimal ECMS Equivalent Factor	33
3.3.1	Lower Bound for Optimal ECMS Equivalent Factor	34
3.3.2	Upper Bound for Optimal ECMS Equivalent Factor	36
3.3.3	summary	43
3.4	A Real-Time Adaptive ECMS	45
3.5	Simulation Results	48
3.6	Conclusion	53

4	A Real-Time Optimal Energy Management Strategy for Parallel Hybrid Electric Vehicles	55
4.1	Introduction	55
4.2	Problem Statement	59
4.3	Catch Energy Saving Opportunities (CESO), The Proposed Optimal EM Strategy	65
4.3.1	Deriving the ECMS-CESO Equations	67
4.3.2	Achieving Hard SOC Constraints With ECMS-CESO	75
4.3.3	Achieving Driver Requested Power With ECMS-CESO	79
4.4	Simulation Results	80
4.5	Conclusion	85
5	A Real-Time Optimal Energy Management Strategy for Series Hybrid Electric Vehicles	87
5.1	Introduction	87
5.2	Problem Statement	88
5.3	Optimal Equivalent Factor Bounds For Series HEVs	93
5.4	The Proposed Energy Management Strategy, ECMS-CESO, For Series HEVs	96
5.5	Achieving The Hard SOC Constraints	103
5.6	Experimental Setup	106
5.7	Simulation Results	108

5.8 Conclusion	113
References	115
A Vehicle Modeling And Simulation	129
B Letters of Permission	135

List of Figures

2.1	A representation of different control strategies	9
2.2	Units of a model predictive controller	12
2.3	Effect of predicted horizon on fuel economy in the city (UDDS) and Highway (HWFET) driving (The high values for mpg comes from using the plant model as the actual plant in simulations)	20
3.1	Typical configuration of a parallel HEV.	27
3.2	A new ECMS with an adaptive equivalent factor $\lambda(t)$ as a linear function of SOC bounds and calculated λ^* bounds.	47
3.3	The SOC trajectory of the Full HEV for 3 different controllers on the NEDC drive-cycle (The speed profile is plotted with free offset/scale).	52
4.1	The configuration of the power-train in a parallel HEV.	59
4.2	(a) Replacing the SOC hard bounds in (4.5) with soft constraints SOC_L^{soft} and SOC_H^{soft} . x_1 is allowed to exceed the soft bounds by at most θ_{max} . (b) ECMS-CESO maintains $\lambda(t)$ inside the range (4.30).	66
4.3	ECMS-CESO sets $\lambda(t)$ based on the current value of SOC.	72

4.4	The SOC and fuel consumption trajectories for 4 different EM strategies: (a) mild parallel HEV on UDDS (b) full parallel HEV on US06.	83
4.5	Normalized FEs for two HEVs with different initial SOC.	85
5.1	The configuration of the powertrain in a series HEV in this study. .	91
5.2	ECMS-CESO defines new soft bounds for the SOC inside the actual hard limits SOC_L and SOC_H . ECMS-CESO is allowed to exceed the soft bounds by $\theta(t)$ when there is an energy saving opportunity. When the soft bounds are exceeded, the equivalent factor is modified. If $\theta(t) = \theta_{max}$, the equivalent factor becomes modified enough that it prevents the ECMS-CESO from violating (5.5).	97
5.3	Developed hybrid electric powertrain experimental setup connected to a double-ended 465 hp AC dynamometer at Michigan TEchnological University.	106
5.4	Trajectories of SOC and fuel consumption rate for the UDDS drivecycle	111
A.1	High fidelity parallel HEV model in AMESim (19 state variables). .	130
A.2	High fidelity series HEV model in AMESim (22 state variables). . .	131
A.3	Co-simulation between Simulink and AMESim: The energy management strategies are developed in Simulink.	132

A.4 Simulation requires two model of the HEV: the model inside the EM strategy for the optimization algorithm, and the actual HEV model which simulates the real plant. 133

A.5 The quasi static model (the right top block) created in Simulink and was validated with AMESim model. 133

A.6 AMESim model vs. quasi-static model on HWFET drivecycle for the parallel HEV. Both models are triggered with identical control actions. The dark blue lines are AMESim, and the red lines are created by the quasi-static model. The light blue line in the top window is the reference velocity. 134

List of Tables

2.1	Validation of model performance with manufacturer data	19
2.2	Improvement of fuel economy (MPG) by different control strategies.	21
3.1	Vehicle parameters used in the simulations. The initial SOC is 68.5% and the allowed SOC range is 50% to 70%.	49
3.2	λ^* values for 2 different HEVs on different drive-cycles with the boundary condition: $x(0) = x(t_f)$. The results are provided to validate (3.28), which gives $1 \leq Q_{thv}\lambda^* \leq 3.38$ for the mild HEV, and $1 \leq Q_{thv}\lambda^* \leq 3.74$ for the full HEV.	50
3.3	Simulation results for a mild and a full parallel HEV for several drive-cycles, comparing the achieved MPG by 3 different EM strategies. .	53
4.1	Vehicle Parameters Used in the Simulations.	81
4.2	Results for a mild parallel HEV.	84
4.3	Results for a full parallel HEV.	84
5.1	Parameters of the SI engine in this study	107
5.2	Battery specifications.	108

5.3	Vehicle specifications.	109
5.4	Fuel economy (MPG) and final SOC $x_1(t_f)$ results for different control strategies. All simulations start at $x_1(0) = 60\%$. The SOC range in (5.5) is from 40% to 70%. For ECMS-CESO: $\theta_{max} = 6\%$, and $1 \leq Q_{lhv}\lambda^* \leq 4.78$. For all of simulations, the average and variance of speed tracking error are in orders of 0.005 (m/s) and 0.001, respectively .	111

Preface

This dissertation is organized based on the previously published papers or the papers that are still under review. The letters of permission for using these papers are provided in Appendix B. The order of authors for each paper reflects their contribution.

The material contained in Chapter 2 is previously published: *A. Rezaei and J. B. Burl, "Effects of Time Horizon on Model Predictive Control for Hybrid Electric Vehicles," IFAC PapersOnLine, vol. 48, no. 15, pp. 252–256, Aug. 2015.* This paper is an original work developed and written by the dissertation author. Coauthor, professor J. B. Burl contributed as the research advisor. He helped in developing the idea of the work and reviewing and revising the manuscript. © 2015, IFAC. Published in IFAC PapersOnLine, vol. 48, no. 15, pp. 252–256.

The material contained in Chapter 3 is under review by the IEEE Transactions on Control Systems Technology: *A. Rezaei, Jeffrey B. Burl, and Bin Zhou, "Estimation of the ECMS Penalty Factor Bounds for Hybrid Electric Vehicles," IEEE Transactions on Control Systems Technology, Under Review, 2017.* This paper is an original work developed and written by the dissertation author. Coauthor, professor J. B. Burl provided research direction and helped with developing the idea of the work. He also helped in reviewing and revising the manuscript. Coauthor, B. Zhou contributed

by running and debugging the simulation models.

The material contained in Chapter 4 is under review by the IEEE Transactions on Control Systems Technology: *Amir Rezaei, Jeffrey Burl, Bin Zhou, and Mohammad Rezaei, "A new real-time optimal energy management strategy for hybrid electric vehicles," IEEE Transactions on Control Systems Technology, Under Review, 2016.* This paper is an original work developed and written by the dissertation author. Coauthor, professor J. B. Burl provided research direction and helped with developing the idea of the work. He also helped in reviewing and revising the manuscript. Coauthors, B. Zhou and M. Rezaei contributed by running and debugging the simulation models.

The material contained in Chapter 5 is in preparation for submission to the Journal of Energy Conversion and Management soon: *Amir Rezaei, Jeffrey B. Burl, Ali Solouk, Bin Zhou, Mohammad Rezaei, and Mahdi Shahbakhti, "ECMS-CESO for series hybrid electric vehicles," Applied Energy, To be submitted, 2017.* This paper is an original work developed and written by the dissertation author. Coauthor, professor J. B. Burl provided research direction and helped with developing the idea of the work. He also helped in reviewing and revising the manuscript. Coauthor, A. Solouk provided data for the simulation model. He also wrote the experimental setup section. Coauthors, B. Zhou and M. Rezaei contributed by running and debugging the simulation models. Coauthor, M. Shahbakhti contributed by providing data for simulations and helped in reviewing and revising the paper.

List of Abbreviations

A-ECMS	Adaptive Equivalence Consumption Minimization Strategy
ACF	Auto-Correlation Function
ANN	Artificial Neural Network
AR	Auto-Regressive
ARMA	Auto-Regressive Moving Average
bom	battery only mode
CESO	Catch Energy Saving Opportunity
CD	Charge Depletion
cm	charge mode
CS	Charge Sustaining
CV	Conventional Vehicle
DDV	Driver Desired Velocity
DP	Dynamic Programming
E-machine	Electric Machine
ECMS	Equivalence Consumption Minimization Strategy
EM	Energy Management
eom	engine only mode
EV	Electric Vehicle

FE	Fuel Economy
GIS	Geographical Information System
GOC	Global Optimal Controller
GPS	Global Positioning System
HEV	Hybrid Electric Vehicle
hm	Hybrid mode
IOC	Instantaneous Optimal Controller
MA	Moving Average
MPC	Model Predictive Control
MPG	Miles Per Gallon
MPGe	Miles Per Gallon Equivalence
PACF	Partial Auto-Correlation Function
P_D	Driver's Requested power on the wheels
PMP	Pontryagin's Minimum Principle
RBC	Rule-Based Control
SOC	State Of Charge

Abstract

Hybrid Electric Vehicles (HEVs) are used to overcome the short-range and long charging time problems of purely electric vehicles. HEVs have at least two power sources. Therefore, the Energy Management (EM) strategy for dividing the driver requested power between the available power sources plays an important role in achieving good HEV performance.

This work, proposes a novel real-time EM strategy for HEVs which is named ECMS-CESO. ECMS-CESO is based on the Equivalent Consumption Minimization Strategy (ECMS) and is designed to Catch Energy Saving Opportunities (CESO) while operating the vehicle. ECMS-CESO is an instantaneous optimal controller, i. e., it does not require prediction of the future demanded power by the driver. Therefore, ECMS-CESO is tractable for real-time operation.

Under certain conditions ECMS achieves the maximum fuel economy. The main challenge in employing ECMS is the estimation of the optimal equivalence factor λ^* . Unfortunately, λ^* is drive-cycle dependent, i. e., it changes from driver to driver and/or route to route. The lack of knowledge about λ^* has been a motivation for studying a new class of EM strategies known as Adaptive ECMS (A-ECMS). A-ECMS yields a causal controller that calculates $\lambda(t)$ at each moment t as an estimate of λ^* .

Existing A-ECMS algorithms estimate λ^* , by heuristic approaches. Here, instead of direct estimation of λ^* , analytic bounds on λ^* are determined which are independent of the drive-cycle. Knowledge about the range of λ^* , can be used to adaptively set $\lambda(t)$ as performed by the ECMS-CESO algorithm.

ECMS-CESO also defines soft constraints on the battery state of charge (SOC) and a penalty for exceeding the soft constraints. ECMS-CESO is allowed to exceed a SOC soft constraint when an energy saving opportunity is available. ECMS-CESO is efficient since there is no need for prediction and the intensive calculations for finding the optimal control over the predicted horizon are not required. Simulation results for 3 different HEVs are used to confirm the expected performance of ECMS-CESO.

This work also investigates the performance of the model predictive control with respect to the predicated horizon length.

Chapter 1

Introduction

Unlike conventional vehicles, hybrid electric vehicles (HEVs) have more than one energy source. The strategy for dividing the driver requested energy among the available energy sources significantly impacts the fuel economy of the HEV, [1] [2]. Many energy management (EM) strategies have been suggested to improve the HEV fuel economy. For instance, model predictive control (MPC) [2] [3][4][5] [6][7], equivalent consumption minimization strategy (ECMS) [8] [9][10] [11] [12][13] [14] [15][16], dynamic programming (DP) [2][16][17], and rule-based control (RBC) [18][19][20] are some of well studied EM strategies for HEVs.

Rule-based control strategies are more common for commercial vehicles than the other EM strategies [19][21]. RBCs are easy to implement, fast for real-time applications,

and reliable for safety concerns. However, finding efficient rules requires extensive simulations and tests on the vehicle, which generally takes more development time than optimal controllers [19] [22]. In addition, theoretically optimal controllers can achieve better fuel economy in comparison with RBCs [2] [7] [12] [23].

Globally optimized control (GOC) yields the maximum fuel economy, or miles per gallon (MPGmax). The GOC can be obtained using DP. The main challenge for implementing GOC is acquiring advanced knowledge of the whole drive-cycle or Driver's Demanded Power $P_D(t)$ [24]. In addition, given P_D , finding the optimal solution requires intensive calculation, which is time-consuming. However, assuming the problem of computational time can be resolved by a powerful on-board computational processor, the uncertainty on the predicted P_D still affects the expected optimal fuel economy [24].

MPC can yield a suboptimal solution close to MPGmax [7]. In addition, unlike GOC, model predictive control is based on short term $P_D(t)$ prediction. Therefore, the effect of prediction uncertainty on MPC is less severe in comparison with GOC [24]. However, like GOC, MPC suffers from model uncertainty.

ECMS is based on the calculus of variations or Pontryagins Minimum Principle (PMP) [9]. The main challenge for employing ECMS is estimating the optimal trajectory of the battery equivalent factor λ^* [10][12][23][25]. In fact, since PMP generally yields a two point boundary value problem, the numerical solution requires an iterative

approach with full knowledge of $P_D(t)$ over the whole drive-cycle. For real-time applications, such advance knowledge of $P_D(t)$ either is not available, or is subject to uncertainty [24] [26]. Therefore, many approaches have been proposed to estimate the optimal trajectory of the ECMS equivalent factor, λ^* , for causal systems [10][11][12][13] [23] .

This work, determines the upper and lower bounds for λ^* , which can be employed to estimate λ^* in other applications such as adaptive ECMS (A-ECMS) [10][25]. Whereas, λ^* depends on the drive-cycle, the proposed bounds for λ^* are independent of the drive-cycle, which is useful in estimating λ^* . For instance, this work develops two types of A-ECMS algorithms based on λ^* bounds: 1) a simple A-ECMS presented in chapter 3, and 2) an advanced A-ECMS, i. e. EMCS-CESO, presented in chapters 4 and 5. The term CESO stands for Catch Energy Saving Opportunity, which is the fundamental idea in developing ECMS-CESO. The performance of both introduced A-ECMS algorithms are compared with another A-EMCS algorithm which has been previously introduced in [12]. Simulation results show the introduced A-ECMS results have comparable performance to global optimal, thanks to employing the bounds on λ^* . ECMS-CESO has one main advantage over the simple A-ECMS developed in chapter 3. In order to catch energy saving opportunities, soft constraints are defined for the SOC and ECMS-CESO is allowed to exceed these soft constraints. However, ECMS-CESO is penalized for exceeding the soft constraints. This technique improves the performance of ECMS-CESO in terms of being robust for delivering driver's

desired power. In addition, thanks to the soft constraints, ECMS-CESO is less likely to be restricted by a depleted or full battery, which allows more flexibility in applying optimal control actions. Furthermore, unlike the A-ECMS in [12], no speed prediction is required for the ECMS-CESO, which makes it easier to implement and faster for real-time applications.

This work, is organized as follows:

Chapter 2 presents a review of different control strategies for HEVs, including rule-based control, ECMS, MPC, and DP. In addition, chapter 2 investigates the performance of MPC with regard to the predicted time horizon of future driver's desired power. Simulation results are presented in section 2.4.

Chapter 3 introduces the lower and upper bounds on the ECMS optimal equivalence factor λ^* for parallel HEVs. It is shown that the bounds are independent of the drive-cycle. The detailed derivation procedure for λ^* bounds is presented in section 3.3. To demonstrate an application of the λ^* bounds, a simple and efficient real-time EM strategy is introduced and simulated in section 3.5. The analytically determined bounds are employed for developing ECMS-CESO in following chapters.

Chapter 4 introduces ECMS-CESO, the novel real-time EM strategy that is the main contribution of this work. Section 4.2 presents the optimal control problem for parallel HEVs. Section 4.3, introduces ECMS-CESO and the equations for applying

ECMS-CESO to a parallel HEV are derived. In this section, it is also proved that ECMS-CESO maintains the SOC limits in charge-sustaining mode. In addition, the robustness of ECMS-CESO in terms of providing P_D is discussed. Finally, in Section 4.4, the simulation results are presented, comparing ECMS-CESO with RBC and PMP, and an instantaneous A-ECMS.

The λ^* bounds in chapter 3 and the ECMS-CESO algorithm in chapter 4 are for parallel HEVs. Therefore, chapter 5 is dedicated to determining λ^* bounds and deriving ECMS-CESO algorithm for series HEVs. First, in section 5.3 the lower and upper bounds on λ^* are determined by an analytic procedure for series HEVs. In section 5.4, ECMS-CESO is developed for series HEVs, and the adaptive equation for estimating $\lambda(t)$ is derived. In Section 5.5, it is shown ECMS-CESO maintains the battery SOC between the desired limits. In section 5.6, the experimental setup used for validating the HEV model is explained. Finally, simulation results on several drivecycles are presented and discussed in section 5.7. Section 5.7 also presents a comparison between the performances of ECMS-CESO and two other types of EM strategies.

Chapter 2

Effects of Time Horizon on Model Predictive Control for Hybrid Electric Vehicles

2.1 Introduction

¹ The transportation sector is the main source of global greenhouse gas emissions and it is predicted that the demand for liquid fuel for transportation will grow even faster than any other segment of the economy, [27]. Many technologies have been

¹The material contained in this chapter is previously published: © 2015, IFAC. Published in IFAC PapersOnLine, vol. 48, no. 15, pp. 252–256

introduced to improve Fuel Economy (FE) and emissions of conventional vehicles. Electric vehicles are an alternative to improve FE and emission. However, because of current restrictions on battery technologies, the range of electric vehicles is short and also their charging time is long. As a result, Hybrid Electric Vehicles (HEVs) can be considered as a temporary solution to the problem. HEVs use both conventional fuel and electricity to yield good range and good FE. Therefore, the energy management or control strategy of HEVS plays an important role in improving the FE and exhaust emissions. Control strategies can be categorized in different ways, for example: rule-based controllers, Instantaneous Optimal Controllers (IOC), predictive controllers, and a globally optimized controller, which are shown in Fig. 2.1. The GOC requires the advance knowledge of DDP for the whole trip. In addition, GOC has a large computational burden. For these reasons, GOC is practically impossible to implement. But since GOC yields the maximum achievable FE, it is used for evaluating the other methods.

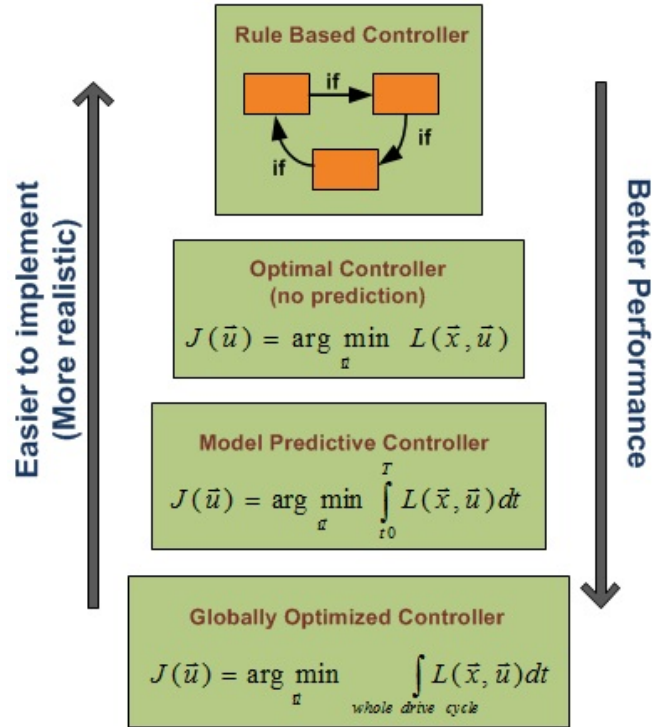


Figure 2.1: A representation of different control strategies

2.2 A review on control strategies

2.2.1 Rule-based control

Rule-Based controllers are the most common controllers for HEVs produced by different companies. These controllers are reliable, fast and easy to implement. However, developing control rules takes time and needs extensive experimental data for a specific HEV. The rules may be defined explicitly, or in the Fuzzy domain [28] [29] [30],

[31] [32]). The main disadvantage of rule-based controllers is that they are not optimal and there is considerable room for improving performance using other control strategies. To resolve this problem, some suggested extracting optimal rules from GOC actions, [18, 29]. However, this method is drive-cycle dependent and extracting optimal rules from the distribution of GOC control actions is challenging. In [18], stochastic dynamic programming is used to make extracted rules independent of drive cycle and in [33], an artificial neural network is trained and replaced with rules in order to avoid the process of extracting explicit optimal rules.

2.2.2 Instantaneous optimal control (IOC)

IOC tries to find the best control actions at each moment by minimizing a cost function as shown in Fig. 2.1. For example, [9] introduced the Equivalent Consumption Minimization Strategy (ECMS) with the cost function:

$$J(\vec{u}) = \underset{\vec{u}}{\operatorname{argmin}} \{ \dot{m}_{fuel}(\vec{x}, \vec{u}) + \lambda(t)P_{bat,C}(\vec{x}, \vec{u}) \} \quad (2.1)$$

where \dot{m}_{fuel} is the rate of fuel consumption (g/s), $P_{bat,C}$ is the battery chemical power (W), and λ is the penalty factor for using the battery power. ECMS states that using battery power $P_{bat,C}$ at any moment must be compensated by fuel in the future to

charge the battery, so a punishment term for using battery power should be included in the cost function, [9]. The cost function in Eq.2.1 is shown to optimize the energy management in HEVs, [8].

2.2.3 Model Predictive Control (MPC)

MPC is a branch of predictive control techniques that tries to find the best control actions by simulating (modeling) the plant on a predictive time horizon. As shown in Fig. 2.1, at the present moment t_0 , MPC predicts the future reference inputs of the system for T seconds. MPC then determines the best control actions $\vec{u}(t_0)$ by optimizing the cost function $L(\vec{x}, \vec{u})$ over the time horizon $[t_0 \ t_0 + T]$ (Fig. 2.2).

Knowing the reference input of the system $v(t)$ (the driver's demanded velocity) and the environmental variables $\vec{d}(t)$ at each moment, the DDP or $P_D(t)$ can be determined. The controller then tries to optimally divide $P_D(t)$ among the powertrain energy sources. So, MPC needs to predict $v(t)$ and $\vec{d}(t)$ in order to have an estimation of the future DDP. Fortunately, prediction of some of environmental variables, like speed limits, traffic conditions, road curves and road grades, is possible by using GPS devices and a geographic information system. Still, the main problem is predicting the drivers's demanded velocity $v(t)$.

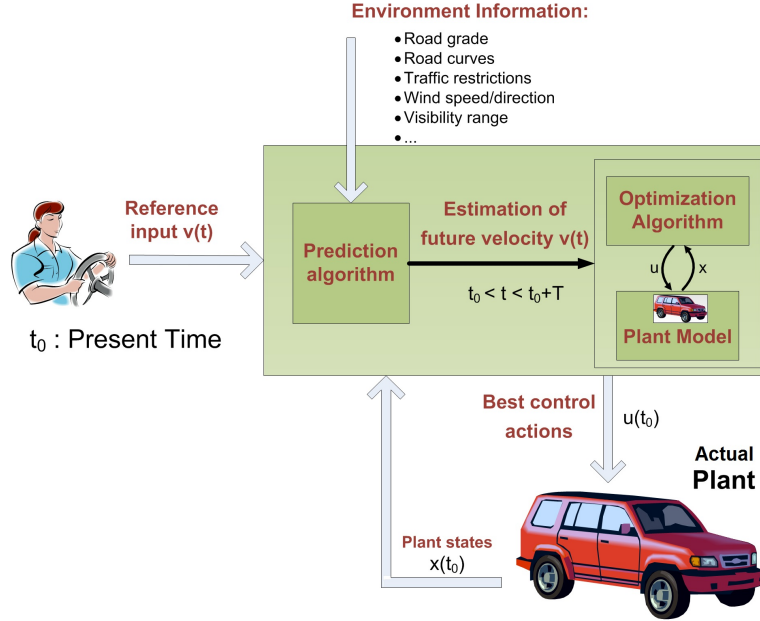


Figure 2.2: Units of a model predictive controller

2.3 Applied approach for analyzing MPC

2.3.1 Simulation approaches

Since the goal of this work is to evaluate the performance of MPC versus time horizon, a perfect predication has been assumed. In this way, the inevitable errors in predication that happen in practice, will not affect the results. So, by using a backward simulation on a flat road, the driver's demanded power $P_D(t)$ for both city (UDDS) and highway (HWFET) drive cycles were calculated. As a result in the simulation, the MPC will have access to exact values of $v(t)$ and $P_D(t)$ for any horizon length.

2.3.2 HEV configuration and equations

A hybrid vehicle with parallel configuration and controllable transmission was chosen for this study. This configuration yields the power split equations:

$$P_{eng}(t) = P_D(t)/\eta_t(g) - P_{em}(t) \quad , \quad P_D(t) \geq 0 \quad (2.2a)$$

$$F_{brk}(t) \cdot v(t) = P_D(t) - P_{em}(t)/\eta_t(g) \quad , \quad P_D(t) < 0 \quad (2.2b)$$

where t refers to time, P_D is driver's demanded power (DDP), P_{em} and P_{eng} are e-machine and engine power respectively, F_{brk} is friction brake force, v is vehicle velocity, g is the transmission gear number, and η_t is the combined efficiency of the transmission and the final drive.

The constraint Eqs. 2.2a and 2.2b limit the number of variables that are used as control inputs. P_{eng} is determined by P_D (given), P_{em} , and g as shown in Eq. 2.2a. Similarity, F_{brk} is determined by the demanded power, the velocity, P_{em} , and g as shown in Eq. 2.2b. Since P_D and v are specified by the driver (drive cycle), the set of control inputs can be reduced to:

$$\vec{u} = \begin{bmatrix} u_1 \\ u_2 \end{bmatrix} = \begin{bmatrix} P_{em} \\ g \end{bmatrix}$$

The battery power is:

$$P_{bat,E} = i(\vec{u})V_{bat,oc}(x) - i^2(\vec{u})R_{bat}(x) \quad (2.3)$$

where $P_{bat,E}$ is the electric power provided by the battery (W), i is the battery pack current (A), $V_{bat,oc}$ and R_{bat} are the open circuit voltage (V) and resistance of the battery pack respectively (Ω), \vec{u} is the vector of control variables, and x is the battery state of charge (SOC) defined by:

$$x(t) = SOC(t) = \frac{Q_{bat} - \int_0^t i dt}{Q_{bat}} \quad (2.4)$$

where Q_{bat} is the battery pack initial charge (A·s), and t is the time (s). From the above equation and Eq. 2.3, the system state equation is:

$$\dot{x} = -\frac{i}{Q_{bat}} = -\frac{V_{bat,oc}(x) - \sqrt{V_{bat,oc}^2(x) - 4R_{bat}(x)P_{bat,E}(\vec{u})}}{2Q_{bat}R(x)} \quad (2.5)$$

Dynamics with fast response times, compared to the overall system response time, can typically be ignored. So, the dynamics of the engine and the e-machine can be ignored when there is a slow changing state variable such as $x = SOC$ [16][22][23][34][35][36].

The vehicle longitudinal dynamics equation is:

$$P_D = (F_{gravity} + F_{rolling}(v) + F_{drag}(v)) v + m_e \dot{v}$$

where m_e is the effective vehicle mass (Kg), and v is the vehicle velocity (m/s). The above equation also represents one state variable: v . But, v is measured at each moment via a speed sensor or is predicted via MPC, and it is a known parameter to the controller. So, for the vehicle model at the heart of MPC, v can be seen as a known constant parameter at each moment.

Hence, the dynamics of a parallel HEV are given by equations (2.2) and (2.5). Of course, the x and \vec{u} variables are subjected to boundary constraints determined by physical limits of each components in the power-train.

2.3.3 Cost function and optimization method

At the present time t_0 , MPC predicts the reference signal $P_D(t)$ for the next T seconds and then uses the following cost function for the optimization algorithm:

$$J(\vec{u}) = \int_{t_0}^{t_0+T} \dot{m}_{fuel} dt$$

Since, the MPC is done via a computer program, a discrete version of the above cost function is used. Assuming the drive cycle duration is N seconds (vehicle stops after N seconds), the discrete version of the above cost function is:

$$J(\vec{u}(k)) = \sum_{n=k}^{n=k+T} \dot{m}_{fuel}(n)$$
$$0 \leq k \leq N - 1$$

where k is time, and T refers to the horizon length. In the model that is used for this work, no restriction was applied to the MPC regarding the vehicle driveability. So, the optimal controller that uses the above cost function will try to minimize $J(\vec{u}(k))$ regardless of what the driver might experience. For example, the controller might switch the gear every 1 s and also the gear shifting might happen from gear 1 to 5 directly if it helps to minimize $J(\vec{u}(k))$. So, the above cost function was modified by

adding a penalty factor for frequent gear shifting:

$$\begin{aligned}
 J(\vec{u}(k)) &= \sum_{n=k}^{n=k+T} (\dot{m}_{fuel}(n) + \delta |g(n+1) - g(n)|) \\
 &0 \leq k \leq N - 1 \\
 &\text{and for } n = k + T \rightarrow \delta = 0
 \end{aligned} \tag{2.6}$$

where g is the gear number, and δ is the punishment factor for frequent gear shifting.

Also, no penalty is included for the desired final state values $\phi(x(N-1))$. So, the net energy consumption of the battery is not zero at the end of each simulation which affects the final value of MPG for different simulations. Of course, it is more desirable to have $SOC(0) = SOC(N)$, but it is practically impossible to make that happen in an optimal way unless the predicted horizon is very long and accurate. So instead of MPG , the criteria MPG_{ge} is employed, [37]:

$$(MPG_{ge})_{UDDS} = 5\text{-cycle city FE} = \frac{1}{0.003259 + \frac{1.1805}{d/(G_g + G_{ge})}}$$

$$(MPG_{ge})_{HWFET} = 5\text{-cycle hwy FE} = \frac{1}{0.001376 + \frac{1.3466}{d/(G_g + G_{ge})}}$$

where d is the total miles derived for each drive cycle, G_g is consumed gasoline (Gal), and G_{ge} is the gasoline equivalent of the consumed electric energy. By using MPG_{ge} as the criteria for comparing results, $SOC(0) \neq SOC(N)$ can be compensated.

In addition, dynamic programming is the employed optimization algorithm. This method is computationally intensive and is not a good choice for real time applications, but, it guarantees a global optimal solution given the predicted horizon.

2.3.4 Vehicle model

A quasi-static model for the Honda Civic IMA was implemented in the Simulink environment (Appendix A). The model incorporates the equations in the previous section. However, for the engine and e-machine, look up tables from Honda Civic have been used to include their efficiencies at each moment. A rule-based controller was developed and tuned for this model in order to achieve a performance similar to that published by the manufacturer. Some of the parameters that were tuned are:

SOC range in the charge-sustaining mode, the minimum speed where regenerative braking is allowed, etc. The results are presented in Table 2.1.

Table 2.1
Validation of model performance with manufacturer data

	Manufacturer	Achieved
Top Speed (mph)	115	105
Accel. 0-40mph	5.9s	7s
Accel. 0-60mph	11.3s	14s
Accel. 0-80mph	21s	25s
mpg (City)	44	47.7
mpg (Highway)	44	40.4
mpg (Combined)	44	44.1

Unlike rule-based controllers, optimal controllers like the instantaneous optimal controller and MPC, need a model of the plant. These optimal controllers search for optimal actions on the model first and apply the optimal control actions to the plant. So, in order to replace the rule-based controller with optimal controllers, the plant Simulink model was duplicated in the MATLAB script language to be used as the vehicle model in the heart of the optimal controllers. In this way, any uncertainty between the plant model and the model inside the optimal controllers, is avoided (See Fig. 2.1).

2.4 Simulation results

2.4.1 MPC performance versus time horizon

Figure 2.3 presents the results for the UDDS and HWFET drive cycles. The most noticeable point in Fig. 2.3 is that for both city and highway drive cycles, FE is almost independent of horizons longer than 60 s. Note that a horizon of 10 s on the highway and 20 s in the city yields a performance very close to the GOC performance.

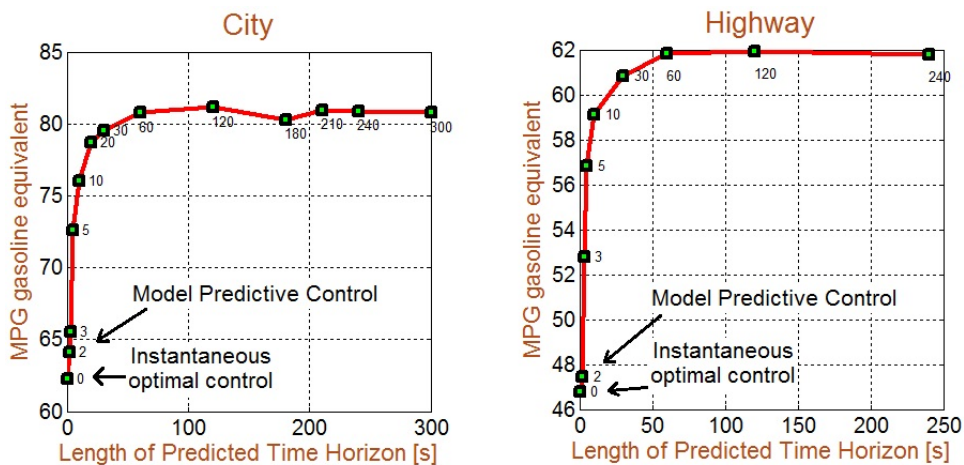


Figure 2.3: Effect of predicted horizon on fuel economy in the city (UDDS) and Highway (HWFET) driving (The high values for mpg comes from using the plant model as the actual plant in simulations)

In Fig. 2.3, a fluctuation can be seen in the city drivecycle for the MPC with 180 s horizon length. This fluctuation is mainly the result of not having a constraint on the final $SOC(N - 1)$. Thus, the MPC with 180 s horizon has different final SOC

than the other simulations. This different final SOC has created a fluctuation on the MPG samples. However, since no fluctuation exists before and after this particular sample, the main conclusion is still valid.

Figure 2.3 also shows that an IOC (equivalent to MPC with 0 prediction) performs poorly in comparison with MPC. But in comparison with the rule-based controller designed in section 2.3.4, instantaneous optimal controller achieves considerable improvement in fuel economy. Table 2.2 shows the amount of FE improvement for different control strategies.

Table 2.2
Improvement of fuel economy (MPG) by different control strategies.

	rule-based		IOC		GOC
City	48	→	62	→	81
Highway	40	→	47	→	62

2.5 Conclusion

While instantaneous optimal control can nearly achieve the GOC performance under certain conditions, in general, more information is needed in order to find the optimal trajectory of $\lambda(t)$ in (2.1). On the other hand, MPC suffers from prediction errors and long computational times. But the results show that under ideal conditions for the simulated HEV, short time prediction is enough for MPC to perform very close to the GOC in both city and highway driving.

In the city, MPC needs a longer horizon in comparison with highway driving which results from higher fluctuations in speed and environmental variables in the city. But on highways, where speed/disturbance fluctuations are not fast, prediction of a short horizon (10 s for the simulated HEV in this report) is particularly easy and fast, specially when the car is in Cruise mode. Since the horizon length is short, real-time implementation is also easier.

Chapter 3

Estimation of the ECMS

Equivalent Factor Bounds for

Hybrid Electric Vehicles

3.1 Introduction

¹ Hybrid electric vehicles (HEVs) have at least 2 energy sources. The efficient split of the driver's demanded power between the energy sources, is a control problem

¹The material contained in this chapter is submitted to the IEEE Transactions on Control Systems Technology: A. Rezaei, Jeffrey B. Burl, and Bin Zhou. Estimation of the ECMS Penalty Factor Bounds for Hybrid Electric Vehicles. IEEE Transactions on Control Systems Technology, Under Review, 2017.

that has been studied by many research groups. There are different energy management (EM) strategies and the most common strategies are rule-based control (RBC), instantaneous optimal control (IOC), model predictive control (MPC), and globally optimized control (GOC).

Rule-based control strategies are more common for commercial vehicles than the other EM strategies [19] [21]. RBCs are easy to implement, fast for real-time applications, and reliable for safety concerns. However, finding efficient rules requires extensive simulations and tests on the vehicle, which generally takes more development time than optimal controllers [19] [22]. In addition, theoretically optimal controllers can achieve better fuel economy in comparison with RBCs [2] [7][12] [23].

Globally optimized control yields the maximum achievable fuel economy, or mile per gallon (MPGmax). The GOC can be obtained using dynamic programming. The main challenge for implementing GOC, is acquiring the advanced knowledge of the whole drive-cycle or Driver's Demanded Power P_D [24]. In addition, given the full P_D , finding the optimal solution requires intensive calculation, which is time-consuming. However, assuming the problem of computational time can be resolved by a powerful on-board computational processor, the uncertainty on the predicted P_D can still affect the expected optimal fuel economy [24].

Model predictive control (MPC) can yield a suboptimal solution close to MPGmax [7]. In addition, unlike GOC, model predictive control is based on short term P_D

prediction. Therefore, the effect of prediction uncertainty on MPC is less severe in comparison with GOC [24]. However, like GOC, MPC suffers from model uncertainty.

Instantaneous optimal control is based on the calculus of variations or Pontryagin's Minimum Principle (PMP). A well-known IOC strategy is the Equivalent Consumption Minimization Strategy (ECMS) [9]. The main challenge for employing IOC or ECMS is estimating the optimal trajectory of the co-states used in IOC, or the battery equivalent factor in ECMS [10][12][23][25]. In fact, since PMP generally yields a two point boundary value problem, the numerical solution requires an iterative approach with full knowledge of P_D over the whole trip. For real-time applications, such advance knowledge of P_D either is not available, or is subjected to uncertainty [24] [26]. Therefore, many approaches have been proposed to estimate the optimal trajectory of the ECMS equivalent factor for causal systems [10][11][12][13][23] .

This work does not seek to estimate the optimal equivalent factor λ^* directly. Instead, the upper and lower bounds of λ^* are estimated, which can be employed to estimate λ^* in other applications such as adaptive ECMS (A-ECMS) [10][25]. Whereas, λ^* depends to the drive-cycle, the proposed bounds for λ^* are independent of the drive-cycle, which is useful in estimating λ^* . For instance, a sample application of λ^* bounds is presented by designing a new adaptive ECMS based on the proposed range for λ^* . The simulation results comparing the proposed A-ECMS with another type of A-ECMS from [12] , show the introduced A-ECMS has comparable performance

thanks to employing the bounds of λ^* . Furthermore, unlike the A-ECMS in [12], no speed prediction is required for the proposed A-ECMS, which makes it easier for implementation and faster for real-time applications. The main reason for the good performance of the introduced A-ECMS is applying the proposed λ^* bounds that offer a small range that contains λ^* , regardless of the drive-cycle. Thus, the proposed formula for calculating λ^* bounds for the parallel HEVs is considered as the main contribution of this work.

This work reviews the PMP solution for a parallel HEV to derive the ECMS cost function in section 3.2. Then in section 3.3, by assuming the vehicle is in charge-sustaining mode, a formula is derived to calculate the bounds of the ECMS optimal equivalent factor for using battery power. To demonstrate a sample application of λ^* bounds, section 3.4 introduces a new real-time adaptive ECMS developed based on λ^* bounds for parallel HEVs. In section 3.5, simulation results for a mild and a full parallel HEV for several drive cycles are presented. For all of simulations, λ^* falls within the proposed range. Section 3.5 also presents the simulation results comparing the fuel economy of the introduced adaptive ECMS with another type of A-ECMS and GOC. The results show whereas the introduced A-ECMS has no information about the future, it has comparable performance with the other tested A-ECMS which has access to the future driving conditions.

3.2 Pontryagin's Minimum Principle (PMP) AND ECMS

3.2.1 Vehicle Model

The driver uses brake or acceleration pedals to adjust P_D in order to achieve the desired speed. Therefore, a hard constraint of an EM strategy is providing $P_D(t)$ at time t :

$$P_D(t) = P_{ptr}(t) + P_{brk}(t) \quad (3.1)$$

where P_{ptr} is the power provided by the power-train at the wheels in watts (W), and P_{brk} is the dissipated power by the conventional friction brake system (W).

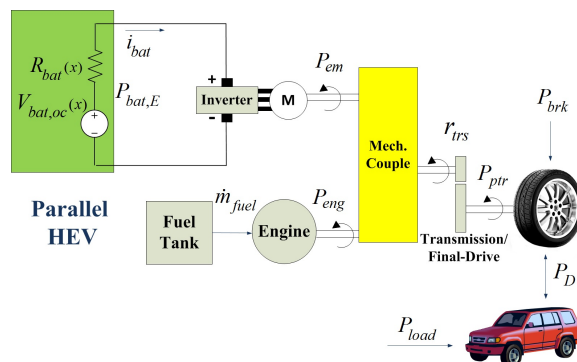


Figure 3.1: Typical configuration of a parallel HEV.

For the parallel HEV shown in Fig. 3.1, (3.1) becomes:

$$\left\{ \begin{array}{l} \text{Brake, Coast } P_D \leq 0 : \quad P_{brk}(t) = P_D(t) - \frac{P_{em}(t)}{\eta_{trs}(r_{trs}(t))} \\ \text{Acceleration } P_D > 0 : \quad P_{eng}(t) = \frac{P_D(t)}{\eta_{trs}(r_{trs}(t))} - P_{em}(t) \end{array} \right. \quad (3.2)$$

where P_{em} and P_{eng} are the mechanical powers (W) provided by the electric machine and engine, respectively, and $\eta_{trs}(r_{trs})$ is the total efficiency of the transmission and final drive when the total gear ratio is r_{trs} . In (3.2), P_D is known. Hence, the plant control inputs for energy management are:

$$\mathbf{u}(t) = [r_{trs}(t) \quad P_{em}(t)]^T \quad (3.3)$$

The chemical power out of the battery pack $P_{bat,C}$ is:

$$P_{bat,C}(x(t), \mathbf{u}(t)) = V_{bat,oc}(x(t)) i_{bat}(\mathbf{u}(t)) \quad (3.4)$$

where x is the battery state of charge (SOC), $V_{bat,oc}$ is the battery open circuit voltage in volts (V), and i_{bat} is the current of the battery pack in amperes (A). $P_{bat,C} < 0$ means the battery is being charged, and $P_{bat,C} > 0$ represents battery discharging.

Using (3.4) and the definition of SOC, the battery state equation is:

$$x(t) = 1 - \frac{\int_0^t i_{bat}(\mathbf{u}(\tau))d\tau}{Q_{bat}} \Rightarrow \dot{x}(t) = -\frac{P_{bat,C}(x(t), \mathbf{u}(t))}{Q_{bat} V_{bat,oc}(x(t))} \quad (3.5)$$

where Q_{bat} is the total battery capacity in (A·s).

The longitudinal dynamics of the vehicle is:

$$P_D(t) = P_{load}(v(t)) + m_e v(t) \dot{v}(t)$$

where v is the vehicle velocity in meter/s, m_e is the vehicle effective mass in Kg, and P_{load} is the road load power (W) which includes gravity, rolling, and drag load forces. The above equation, represents the vehicle speed $v(t)$ as another state variable. However, as long as the EM strategy maintains the hard constraint (3.1), P_D is provided and the driver's desired speed is tracked accordingly. Hence, the EM strategy can consider $v(t)$ as a known quantity at each moment instead of a state variable.

To consider the transient behaviors of the other power-train components, more state variables should be defined. However, transient behaviors can typically be ignored if their response times are much faster than the overall system response time. Therefore, in comparison with SOC and vehicle speed, the transient dynamics of the engine, e-machine, etc. are ignored. These simplifications for developing the vehicle model are

reasonable and sufficient [22][23][34][35][36].

3.2.2 Control Problem

Maximizing fuel economy or miles per gallon (MPG) is desirable because it lowers trip cost, as well as some pollutant emissions. The control problem is summarized by the equations:

$$\mathbf{u}^* = \arg \min_{\mathbf{u}} \left\{ \int_0^{t_f} \dot{m}_{fuel}(x, \mathbf{u}) dt \right\} \quad (3.6)$$

$$\dot{x}(t) = - \frac{P_{bat,C}(x(t), \mathbf{u}(t))}{Q_{bat} V_{bat,oc}(x(t))} \quad (3.7)$$

$$P_D(t) = P_{ptr}(t) + P_{brk}(t) \quad (3.8)$$

$$x(0) = c_0 \quad , \quad x(t_f) = c_1 \quad (3.9)$$

$$\text{Charge-Sustaining Mode: } SOC_L \leq x(t) \leq SOC_H \quad , \quad t \in [0 \quad t_f] \quad (3.10)$$

$$\mathbf{u} \in U \quad (3.11)$$

where \dot{m}_{fuel} is the fuel mass flow rate (g/s) , t_f is the final time at the end of the drive-cycle, c_0 and c_1 are the boundary values, and U is the space of the admissible control actions which do not violate any power/speed limit on any of the components in the power-train.

For parallel HEVs, the hard constraint (3.8) can be represented by (3.2). \dot{m}_{fuel} can be expressed as a function of control actions and the reference signal P_D by using (3.2):

$$\dot{m}_{fuel}(t) = \frac{P_{eng}(\mathbf{u}(t), P_D(t))}{Q_{lhv}\eta_{eng}(\mathbf{u}(t))} = \dot{m}_{fuel}(\mathbf{u}(t), P_D(t)) \quad (3.12)$$

where Q_{lhv} is the fuel lower heating value in J/g, and η_{eng} is the engine efficacy.

Therefore, the equations for the Hamiltonian and the optimal co-state are:

$$H = \dot{m}_{fuel}(\mathbf{u}(t), P_D(t)) + p(t)\dot{x}(x(t), \mathbf{u}(t)) \quad (3.13)$$

$$\dot{p}^*(t) = -\frac{\partial H}{\partial x} = -p^*(t)\frac{\partial \dot{x}}{\partial x} \quad (3.14)$$

In charge-sustaining mode, when (3.10) is maintained, $V_{cell,oc}$ and $P_{bat,C}$ in (3.7) are almost independent of x :

$$p^*(t) = -p^*(t)\frac{\partial \dot{x}}{\partial x} \approx 0 \quad \Rightarrow \quad p^* = \text{constant} . \quad (3.15)$$

Hence, a constant value for the co-state p yields the global optimal solution, as long as the boundary condition (3.9) and the constraint (3.10) are met, and the following condition is maintained [17]:

$$H(x^*, \mathbf{u}^*, p^*, P_D(t)) \leq H(x^*, \mathbf{u}, p^*, P_D(t)) \quad , \quad \forall \mathbf{u} \in U$$

Defining $\lambda = -p(t)/(Q_{bat}V_{bat,oc}(x))$, the Hamiltonian (3.13) can be converted into the ECMS cost function by using (3.5):

$$H = \dot{m}_{fuel}(\mathbf{u}(t), P_D(t)) + \lambda(t, x) P_{bat,C}(x(t), \mathbf{u}(t)) \quad . \quad (3.16)$$

$V_{bat,oc}$ is almost constant in charge-sustaining mode, therefore from (3.15), the optimal value of λ would also be a constant:

$$\lambda^* = \text{constant} \quad . \quad (3.17)$$

3.3 Bounds of the Optimal ECMS Equivalent Factor

The control problem posed in the previous section is a two-point boundary value problem that has to be solved for a nonlinear system. Numerical solution to such problems, requires an iterative procedure to find the optimal constant value for λ^* that doesn't violate any of the constraints [17]. Much research has focused on finding λ^* [10][12] [23]. Instead of direct estimation of λ^* , this work proposes formulas for calculating lower and upper bounds of λ^* in (3.16). The proposed bounds are independent of the drive-cycle or trip duration. The λ^* bounds can be employed for designing new types of adaptive ECMS [25]. A sample application of λ^* bounds is presented in designing a new adaptive ECMS in section 3.4.

3.3.1 Lower Bound for Optimal ECMS Equivalent Factor

The optimal control (3.6) with the boundary condition (3.9) is equivalent to minimizing the total consumed fuel energy or total dissipated energy E_{loss} during the trip.

Therefore, (3.6) with the boundary condition (3.9) can also be represented by:

$$\mathbf{u}^* = \arg \min_{\mathbf{u}} \{E_{loss}(x, \mathbf{u})\} \quad (3.18)$$

The energy conservation principle requires that:

$$E_{fuel} + E_{bat,C} = E_D + E_{loss}$$

where E_{fuel} and $E_{bat,C}$ are the total consumed chemical energies from the fuel and battery, respectively, and E_D is the total required energy for finishing the trip. In charge-sustaining mode:

$$\begin{aligned} \mathbf{u}^* &= \arg \min_{\mathbf{u}} \{E_{loss}\} = \arg \min_{\mathbf{u}} \{E_{fuel} + E_{bat,C} - E_D\} \\ &= \arg \min_{\mathbf{u}} \left\{ \int_0^{t_f} (P_{fuel} + P_{bat,C} - P_D) dt \right\} \end{aligned} \quad (3.19)$$

P_D is known since it is provided by the driver at each moment. Therefore:

$$\begin{aligned}
\mathbf{u}^* &= \arg \min_{\mathbf{u}} \left\{ \int_0^{t_f} (P_{fuel} + P_{bat,C}) dt \right\} \\
&= \arg \min_{\mathbf{u}} \left\{ \int_0^{t_f} (\dot{m}_{fuel} Q_{lhv} + P_{bat,C}) dt \right\} \\
&= \arg \min_{\mathbf{u}} \left\{ \int_0^{t_f} \left(\dot{m}_{fuel} + \frac{1}{Q_{lhv}} P_{bat,C} \right) dt \right\}
\end{aligned} \tag{3.20}$$

Hence, in order to minimize the *instantaneous* consumed power, the ECMS cost function should be:

$$J_{ECMS}(\cdot) = \dot{m}_{fuel} + \frac{1}{Q_{lhv}} P_{bat,C} . \tag{3.21}$$

Comparison of (3.21) with (3.16) suggests:

$$\lambda^* = \frac{1}{Q_{lhv}} . \tag{3.22}$$

The above derivation proves $1/Q_{lhv}$ is the optimal value for the ECMS equivalent factor λ in (3.16), if SOC never reaches its bounds in (3.10). But in general, the calculated value for λ in (3.22) is not necessarily optimal because the state constraint

(3.10) has been ignored in deriving (3.22). Thus, if for $\lambda = 1/Q_{thv}$, SOC reaches its limits, then $1/Q_{thv}$ is no longer optimal for λ . Simulations show by setting $\lambda = 1/Q_{thv}$, the battery SOC quickly reaches the lower bound SOC_L . A λ value lower than $1/Q_{thv}$ makes the battery energy even less valuable and thus, increases the battery discharge rate in comparison with $\lambda = 1/Q_{thv}$. Therefore, if a drive-cycle exists such that $\lambda^* < 1/Q_{thv}$, then for $\lambda = 1/Q_{thv}$ SOC will not reach SOC_L and thus: $\lambda^* = 1/Q_{thv}$ would also be optimal for that drive-cycle based on (3.22). As a result, in general the optimal ECMS equivalent factor for using the battery chemical power in (3.16) is equal or higher than $1/Q_{thv}$, depending on the drive-cycle:

$$\lambda_{\min}^* = \frac{1}{Q_{thv}} \leq \lambda^* . \quad (3.23)$$

Please note that the applied procedure for deriving (3.23), is independent of the power-train configuration, drive-cycle, or trip duration.

3.3.2 Upper Bound for Optimal ECMS Equivalent Factor

When the ECMS equivalent factor is too large, ECMS tends to charge the battery up to $SOC = SOC_H$ and then be in fuel only mode for most of the trip. Under these circumstances, the driver's demanded power is provided by the engine because using

the engine is considered more efficient. In other words, the EM strategy would force the use of engine only mode since any positive $P_{bat,C}$ (battery discharge) increases the cost function (3.16) significantly.

In the admissible control space U in (3.11), any admissible control \mathbf{u} can be categorized as belonging to one of the following subsets:

$$U = \{\mathbf{u}_{eom}\} \cup \{\mathbf{u}_{cm}\} \cup \{\mathbf{u}_{hm}\} \cup \{\mathbf{u}_{bom}\} \cup \{\mathbf{u}_{bcm}\} \cup \{\mathbf{u}_{stop}\}$$

where \mathbf{u}_{eom} , \mathbf{u}_{cm} , \mathbf{u}_{hm} , \mathbf{u}_{bom} , \mathbf{u}_{bcm} , and \mathbf{u}_{stop} are the actions that will bring the HEV into one of the modes: engine only mode (*eom*), charging mode (*cm*), hybrid mode (*hm*), battery only mode (*bom*), brake/coasting mode (*bcm*), and stop mode (*stop*), respectively. According to (3.8), no matter what subset \mathbf{u} belongs to, since it is assumed to be admissible, it provides P_D at the wheels. Therefore, depending on $P_D(t)$, some of the above subsets might be empty at time t . Battery charging can happen only if the \mathbf{u}^* belongs to the subsets *cm* (charge by engine) or *bcm* (charge by regenerative braking). On the other hand, battery discharging can happen only if \mathbf{u}^* belongs to the subsets *hm* (discharge in hybrid mode) or *bom* (discharge in battery only mode). As a reminder, in *cm*: $P_{(bat,C)} < 0$, and in *hm* or *bom*: $P_{(bat,C)} > 0$.

For the brake/coasting mode where $P_D \leq 0$, the clear optimal action is to recover

energy as much as possible via regenerative braking. Thus, the effect of λ in (3.16) matters when $P_D > 0$. Let's assume at a specific time, $\text{SOC}=\text{SOC}_H$ and the driver demands a positive power P_D via the acceleration pedal. Since $P_D > 0$, the subsets *bcm* and *stop* will be empty. Also, since $\text{SOC}=\text{SOC}_H$, the subset *cm* will be empty. Now, at that moment, the ECMS has to find the optimal control \mathbf{u}^* that minimizes the cost function (3.16). Therefore, it is expected that:

$$\left. \begin{array}{l} x = \text{SOC}_H \\ P_D > 0 \end{array} \right\} \Rightarrow \mathbf{u}^* \in \{\mathbf{u}_{eom}\} \cup \{\mathbf{u}_{bom}\} \cup \{\mathbf{u}_{hm}\}$$

Now, if $\mathbf{u}^* \in \{\mathbf{u}_{eom}\}$, the optimal Hamiltonian in (3.16) at that moment can be represented by (for simplicity, the time symbol t is dropped):

$$H(\mathbf{u}_{eom}^*) = \dot{m}_{fuel}(\mathbf{u}_{eom}^*, P_D)$$

where \mathbf{u}_{eom}^* represents that among all admissible controls $\mathbf{u} \in U$, the optimal \mathbf{u}^* belongs to the subset $\{\mathbf{u}_{eom}\}$ which brings the HEV into *eom*. Similarly, if $\mathbf{u}^* \in \{\mathbf{u}_{bom}\}$:

$$H(\mathbf{u}_{bom}^*) = \lambda P_{bat,C}(x, \mathbf{u}_{bom}^*)$$

and if $\mathbf{u}^* \in \{\mathbf{u}_{hm}\}$:

$$H(\mathbf{u}_{hm}^*) = \dot{m}_{fuel}(\mathbf{u}_{hm}^*, P_D) + \lambda P_{bat,C}(x, \mathbf{u}_{hm}^*)$$

If λ is too big, then the possibility of \mathbf{u}^* being a member of $\{\mathbf{u}_{eom}\}$ increases. For example if λ becomes infinite, then based on (3.16) the ECMS never discharges the battery. Thus when λ is too big, SOC will go up to SOC_H and after that the HEV will be in *eom* for any $P_D > 0$ over the whole trip. The discussed statement in mathematical term is presented by:

$$\left. \begin{array}{l} x = SOC_H \\ \lambda \gg \frac{1}{Q_{thv}} \end{array} \right\} \stackrel{\forall \mathbf{u} \in U}{\Rightarrow} \left\{ \begin{array}{l} \forall P_D > 0 : H(\mathbf{u}_{eom}) < H(\mathbf{u}_{bom}^*) \\ \text{and} \\ \forall P_D > 0 : H(\mathbf{u}_{eom}) < H(\mathbf{u}_{hm}^*) \end{array} \right.$$

Clearly, such a high value for λ cannot be optimal for any drive-cycle. For instance, $\lambda \rightarrow \infty$ keeps the HEV in *eom* for the whole trip and thus, cannot be optimal. Therefore, there should be an upper bound for λ^* such that when $SOC = SOC_H$, other modes, like *bom* or *hm*, will also have a chance to be optimal. In other words, the upper bound of λ^* should be such that there exists at least a $P_D > 0$ with $\mathbf{u}^* \in \{\mathbf{u}_{bom}\} \cup \{\mathbf{u}_{hm}\}$:

$$\left. \begin{array}{l} x = SOC_H \\ \lambda = \lambda_{max}^* \end{array} \right\} \stackrel{\forall \mathbf{u} \in U}{\Rightarrow} \left\{ \begin{array}{l} \exists P_D > 0 : H(\mathbf{u}_{com}) > H(\mathbf{u}_{bom}^*) \\ \text{or} \\ \exists P_D > 0 : H(\mathbf{u}_{com}) > H(\mathbf{u}_{hm}^*) \end{array} \right. \quad (3.24)$$

The inequalities in (3.24), simply state the upper bound of λ^* should allow battery discharging (*bom* or *hm*) to be optimal. Another interpretation for (3.24) is that there exists at least one drive-cycle where $\lambda^* = \lambda_{max}$, and beyond λ_{max} there is no drive-cycle with $\lambda^* > \lambda_{max}$. To calculate λ_{max} , each of the inequalities in (3.24) yields an upper bound for λ^* : λ_{max1}^* and λ_{max2}^* . If one chooses $\lambda_{max}^* = \min\{\lambda_{max1}^*, \lambda_{max2}^*\}$, then both *bom* and *hm* will have a chance to be optimal when $SOC = SOC_H$. However, even if only one of *bom* or *hm* are optimal, then the goal for allowing battery discharging when $SOC = SOC_H$, is met. Therefore, λ_{max}^* should be the maximum of λ_{max1}^* and λ_{max2}^* .

The derivation of the upper bound (3.24) is performed using the control inputs given in (3.3). But the derivation is the same for HEVs with more control actions. Therefore, the procedure for deriving (3.24) is independent of the HEV configuration, provided the HEV can be modeled with SOC as the only state variable. In addition, since no limiting assumption was made on the vehicle speed in derivation of (3.24), the determined upper bound is independent of the drive-cycle.

For a parallel HEV with the configuration in Fig. 3.1, the first inequality in (3.24)

and the constraint (3.8) yields:

$$\lambda^* \leq \frac{\dot{m}_{fuel}(\mathbf{u}_{eom}^*, P_D)}{P_{bat,C}(x, \mathbf{u}_{bom}^*)} = \frac{\frac{P_{eng}(\mathbf{u}_{eom}^*)}{Q_{lhw}\eta_{eng}(\mathbf{u}_{eom}^*)}}{\frac{P_{em}(\mathbf{u}_{bom}^*)}{\eta_{em}(\mathbf{u}_{bom}^*)\eta_{inv}(\mathbf{u}_{bom}^*)\eta_{bat}(\mathbf{u}_{bom}^*)}}$$

$$\Rightarrow \lambda_{\max 1}^* = \frac{\frac{P_D/\eta_{trs}(\mathbf{u}_{eom}^*)}{Q_{lhw}\eta_{eng}(\mathbf{u}_{eom}^*)}}{\frac{P_D/\eta_{trs}(\mathbf{u}_{bom}^*)}{\eta_{em}(\mathbf{u}_{bom}^*)\eta_{inv}(\mathbf{u}_{bom}^*)\eta_{bat}(\mathbf{u}_{bom}^*)}}$$

$$\lambda_{\max 1}^* = \frac{\eta_{trs}(\mathbf{u}_{bom}^*) \eta_{em}(\mathbf{u}_{bom}^*) \eta_{inv}(\mathbf{u}_{bom}^*) \eta_{bat}(\mathbf{u}_{bom}^*)}{\eta_{trs}(\mathbf{u}_{eom}^*) Q_{lhw} \eta_{eng}(\mathbf{u}_{eom}^*)}$$

where η_{trs} , η_{eng} , η_{em} , η_{inv} and η_{bat} are the efficiencies of the transmission, engine, e-machine, inverter, and battery, respectively. The above inequality shows the upper λ^* bound is a function of control actions at each moment. Define L and M as the least and the most efficient operating points of a component in the HEV power-train, respectively. Also, assume ϵ is a very small positive number. In the above inequality, the worst case is when η_{eng} is minimum and $\eta_{em}\eta_{inv}\eta_{bat}$ is maximum. If $\lambda_{\max 1}^*$ is chosen based on the worst case, then there will be only a particular value for $P_D(t) = C_0$ that *bom* becomes optimal. In other words, the only chance for $\mathbf{u}^* \in \{\mathbf{u}_{bom}\}$ is only

when the EM strategy has to choose either *ecom* with the engine working at L, or *bom* with e-machine, inverter, and battery, all working at M. Therefore, if a moment later P_D changes from C_0 to $C_0 + \epsilon$ then *ecom* will be able to operate engine in a more efficient point than L, which leads to $\mathbf{u}^* \in \{\mathbf{u}_{ecom}\}$. During the trip, the possibility of $P_D(t) = C_0$ is very low. For simulations or on the dynamometer, it is possible to test the HEV on a drive-cycle with $P_D(t) = C_0$ for $0 \leq t \leq t_f$. However, in reality the possibility of a constant long-term $P_D(t) = C_0$ is very rare due to numerous statistical factors like the road grade, wind speed or direction, traffic, etc. Therefore, $\lambda_{\max 1}$ is highly overestimated if it is chosen based on minimum η_{eng} . Instead, it is more reasonable to use the average efficiency of the engine in the above inequality: $\bar{\eta}_{eng}$. With the same argument, in the numerator, it is more reasonable to use the average efficiencies $\bar{\eta}_{trs}$, $\bar{\eta}_{em}$, $\bar{\eta}_{inv}$ and $\bar{\eta}_{bat}$, instead. Hence:

$$\lambda_{\max 1}^* = \frac{\bar{\eta}_{em}\bar{\eta}_{inv}\bar{\eta}_{bat}}{Q_{lhw}\bar{\eta}_{eng}} . \quad (3.25)$$

From the second inequality in (3.24) and constraint (3.8):

$$\begin{aligned}
\lambda^* &\leq \frac{\dot{m}_{fuel}(\mathbf{u}_{eom}^*, P_D) - \dot{m}_{fuel}(\mathbf{u}_{hm}^*, P_D)}{P_{bat,C}(x, \mathbf{u}_{hm}^*)} \\
\Rightarrow \lambda_{\max 2}^* &= \frac{\frac{P_D/\bar{\eta}_{trs}}{Q_{lhv} \bar{\eta}_{eng}} - \frac{P_D/\bar{\eta}_{trs} - P_{em}(\mathbf{u}_{hm}^*)}{Q_{lhv} \bar{\eta}_{eng}}}{\frac{P_{em}(\mathbf{u}_{hm}^*)}{\bar{\eta}_{em} \bar{\eta}_{inv} \bar{\eta}_{bat}}} \\
\Rightarrow \lambda_{\max 2}^* &= \frac{\bar{\eta}_{em} \bar{\eta}_{inv} \bar{\eta}_{bat}}{Q_{lhv} \bar{\eta}_{eng}} \tag{3.26}
\end{aligned}$$

Therefore, the upper bound of λ^* for the parallel HEV in Fig. 3.1 is:

$$\lambda^* \leq \lambda_{\max}^* = \max \{ \lambda_{\max 1}^*, \lambda_{\max 2}^* \} = \frac{\bar{\eta}_{em} \bar{\eta}_{inv} \bar{\eta}_{bat}}{Q_{lhv} \bar{\eta}_{eng}} . \tag{3.27}$$

3.3.3 summary

The bounds on the optimal equivalent factor λ^* are:

$$\frac{1}{Q_{lhv}} \leq \lambda^* \leq \max \{ \lambda_{\max 1}^*, \lambda_{\max 2}^* \}$$

where $\lambda_{\max 1}$ and $\lambda_{\max 2}$ can be obtained from the first and the second following inequalities, respectively:

$$\left. \begin{array}{l} x = SOC_H \\ \\ \lambda = \lambda_{max}^* \end{array} \right\} \stackrel{\forall \mathbf{u} \in U}{\Rightarrow} \left\{ \begin{array}{l} \exists P_D > 0 : H(\mathbf{u}_{eom}) > H(\mathbf{u}_{bom}^*) \\ \\ \text{or} \\ \\ \exists P_D > 0 : H(\mathbf{u}_{eom}) > H(\mathbf{u}_{hm}^*) \end{array} \right.$$

using the average efficiencies of the components in the HEV power-train. The above equations for calculating λ^* bounds, were derived regardless of the HEV configuration, drive-cycle, or trip duration.

For a parallel HEV with the configuration in Fig. 3.1, the optimal equivalent factor λ^* lies within the range:

$$\frac{1}{Q_{thv}} \leq \lambda^* \leq \frac{1}{Q_{thv}} \frac{\bar{\eta}_{em} \bar{\eta}_{inv} \bar{\eta}_{bat}}{\bar{\eta}_{eng}} . \quad (3.28)$$

The equivalent factor bounds for a series HEV are presented in the Appendix.

3.4 A Real-Time Adaptive ECMS

This section introduces a new adaptive ECMS to demonstrate a sample application of λ^* bounds calculated in previous section. Although, the introduced adaptive ECMS is new, but the main contribution of this work is the calculation of λ^* bounds that can be employed to design different new ECMS strategies.

As was mentioned previously, adaptive ECMS (A-ECMS) is a causal EM strategy that tries to estimate the optimal equivalent factor λ^* in (3.16) at each moment during the trip. Many different A-ECMS have been suggested by different works. A-ECMS types can be divided into two main groups: predictive A-ECMS which tries to estimate λ^* using a predicted drive-cycle horizon [10][11][12][13] and instantaneous A-ECMS which estimates λ^* based on the current driving condition with no information about the future [14][15][25]. Considering different A-ECMSs, the suggested formula to calculate $\lambda(t)$ can be represented by [10][11][12][13][14][15]:

$$\lambda(t) = \lambda^0 + \zeta (SOC_{ref}(t) - x(t)) \quad (3.29)$$

where λ^0 is a constant. In predictive A-ECMS, ζ is a function (usually a PID controller) defined to track a desired SOC trajectory $SOC_{ref}(t)$. $SOC_{ref}(t)$ is calculated

from applying an optimization algorithm to the predicted driving horizon. In instantaneous A-ECMS, ζ is a linear function with a constant gain and offset.

For instance, reference [12] suggests:

$$\left\{ \begin{array}{l} \lambda(t) = \lambda(t-1) + k_P \Delta x(t-1) - k_I \int_{t_0}^t \Delta x(\tau) d\tau \\ \text{Set } \lambda(t_0) = \frac{\bar{\eta}_{em}}{\bar{\eta}_{eng}} \end{array} \right. \quad (3.30)$$

where k_P and k_I are the tuning parameters of the PI controller, and $\Delta x(t) = SOC_{ref}(t) - x(t)$. The above adaptive ECMS is referred by ECMS₂ in the next section.

The suggested A-ECMS in this work is a type of instantaneous A-ECMS with $\lambda(t)$ calculated from (3.32). Equation (3.28) presents λ^* bounds for the parallel HEV shown in Fig. 3.1. In addition, from (3.17), λ^* is a constant and therefore, each drive-cycle is associated with a specific constant λ^* that might be any value from $1/Q_{lhv}$ to $\bar{\eta}_{em} \bar{\eta}_{inv} \bar{\eta}_{bat} / (Q_{lhv} \bar{\eta}_{eng})$, depending on the drive-cycle. Thus, another interpretation for (3.28) is that there is no drive-cycle associated with a λ^* outside of the range (3.28). Hence, a new ECMS is designed with an adaptive equivalent factor $\lambda(t)$, where $\lambda(t)$ always remains inside the range in (3.28):

$$\frac{1}{Q_{lhv}} \leq \lambda(t) \leq \frac{1}{Q_{lhv}} \frac{\bar{\eta}_{em} \bar{\eta}_{inv} \bar{\eta}_{bat}}{\bar{\eta}_{eng}} . \quad (3.31)$$

to make sure for any drive-cycle, $\lambda(t)$ is not far away from the actual λ^* . In addition, to have $\lambda(t)$ tracking λ^* during the trip, one can define a linear relationship between the $\lambda(t)$ and battery SOC by matching the SOC bounds with λ^* bounds, as shown in Fig. 3.2:

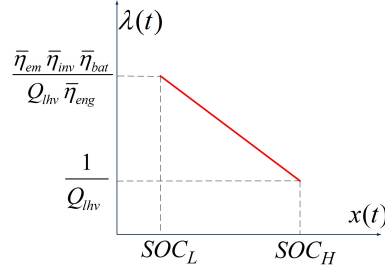


Figure 3.2: A new ECMS with an adaptive equivalent factor $\lambda(t)$ as a linear function of SOC bounds and calculated λ^* bounds.

$$\lambda(t) = \frac{1}{Q_{lhv}} + \left(\frac{\bar{\eta}_{em} \bar{\eta}_{inv} \bar{\eta}_{bat}}{Q_{lhv} \bar{\eta}_{eng}} - \frac{1}{Q_{lhv}} \right) \frac{SOC_H - x(t)}{SOC_H - SOC_L} \quad (3.32)$$

An intuitive explanation for how $\lambda(t)$ in (3.32) tracks λ^* is as following: during the trip, the possibility of $\lambda(t) \approx \lambda^*$ is for short moments, since λ^* is constant whereas $x(t)$ and $\lambda(t)$ change at each moment. Thus, depending on $x(t)$, at any moment $\lambda(t)$ is either overestimating λ^* or underestimating λ^* . If $\lambda(t)$ is overestimating λ^* , then according to (3.16), the battery energy becomes more valuable and hence, *cm* or *com*

are more likely to be optimal than *hm* or *bom*. Therefore, the battery is more likely to be charged which increases SOC. Please note that, even with an overestimated $\lambda(t)$, *hm* or *bom* might still be optimal occasionally, depending on the driver's demanded power P_D . However, for a range of P_D that might be requested by the driver in the future, *hm* or *bom* have less chance to be optimal since $\lambda(t)$ is big and battery energy is valuable. As SOC increases, from (3.32) or Fig. 3.2, $\lambda(t)$ decreases. Therefore, the overestimated $\lambda(t)$ is more likely to be driven toward λ^* in the future. Alternatively, if $\lambda(t)$ in (3.32) is an underestimation of λ^* , then the battery energy becomes less valuable and *hm* or *bom* are more likely to be optimal than *cm* or *eom*. Therefore, in the future driving conditions, the battery is more likely to be discharged (SOC decreases) than charged which increases $\lambda(t)$. Therefore, the underestimated $\lambda(t)$ is more likely to be driven toward λ^* as time passes. The main advantage of the introduced A-ECMS is employing (3.28) which ensures $\lambda(t)$ is always within a reasonable distance from λ^* .

3.5 Simulation Results

Two Parallel HEVs with different degrees of hybridization were chosen for simulation: a Honda Civic IMA (mild parallel HEV) and a plug-in hybrid electric Truck being developed in the HEV Enterprise at Michigan Tech. University (full parallel plug-in HEV). Both vehicles have the same configuration as shown in Fig. 3.1. The

main specifications of the simulated vehicles are presented in Table 3.1. The vehicles were simulated in the AMESim environment and the EM strategy was developed in Simulink. Also, a simpler vehicle model was created in Simulink using SOC as the only state variable to be implemented inside the EM strategy for the optimization algorithm.

To validate (3.28), λ^* values for both HEVs on different drive-cycles was calculated. For these simulations, λ^* is defined as λ that satisfies the boundary condition: $x(0) = x(t_f)$. Thus, for each drive-cycle, numerous simulations were run by testing different λ values. The results are presented in Table 3.2. As can be seen in Table 3.2, for all drive-cycles and for both HEVs, λ^* lies within the proposed range in (3.28). Although, the proposed bounds are derived analytically in section 3.3, the simulations results also show the proposed range in (3.28) contains λ^* , regardless of the drive-cycle.

Table 3.1

Vehicle parameters used in the simulations. The initial SOC is 68.5% and the allowed SOC range is 50% to 70%.

Main Specifications	Honda Civic IMA	Michigan Tech. HEV Truck
Configuration	Mild Parallel	Plugin Full Parallel
Vehicle mass	1279 Kg	1588 Kg
Engine max torque	120 N.m@3500rpm	454 N.m@4000rpm
E-machine max torque	62 N.m@1500rpm	315 N.m@2200rpm
Battery energy	0.93 KW.hr	12.2 KW.hr
Battery max discharge power	continues: 14KW	continues: 40KW
Battery max charge power	continues: 7KW	continues: 13KW
range of $Q_{thv}\lambda^*$	1 to 3.38	1 to 3.74

The simulation results are presented in Table 3.3. For each vehicle, 4 different EM

strategies are tested on several drive-cycles: RBC, the introduced adaptive ECMS in this section (A-ECMS), the ECMS based on PMP (ECMS-PMP), and GOC based on dynamic programming (DP). The RBC has been carefully tuned to maximize the MPG. The ECMS-PMP has access to the full drive-cycle trajectory in advance. For each drive-cycle, ECMS-PMP was run by sweeping different constant values of λ , in order to find the λ^* that yields the same final SOC as the introduced A-ECMS. Finally, DP was run with similar final SOC.

Table 3.2

λ^* values for 2 different HEVs on different drive-cycles with the boundary condition: $x(0) = x(t_f)$. The results are provided to validate (3.28), which gives $1 \leq Q_{thv}\lambda^* \leq 3.38$ for the mild HEV, and $1 \leq Q_{thv}\lambda^* \leq 3.74$ for the full HEV.

Drive-Cycle	$Q_{thv}\lambda^*$ (Mild parallel HEV)	$Q_{thv}\lambda^*$ (Full parallel HEV)
UDDS (D)	3.30	3.39
HWFET (H)	3.38	3.40
US06 (U)	2.73	3.16
SC03 (S)	3.38	3.30
NEDC	3.33	3.22
ECE-15	3.42	3.44
Japan-1015	3.33	3.30
H+H	3.38	3.40
D+H+D	3.30	3.39
D+H+U	2.95	3.28
U+S+H	3.38	3.40
45mph for 600s	3.38	3.73
60mph for 600s	2.39	3.25

To evaluate the performance of the introduced A-ECMS, different control strategies were simulated for both HEVs on the standard drive-cycles. The results are presented in Table 3.3, where ECMS₁ represents the introduced A-ECMS in this work, ECMS₂

is the A-ECMS introduced in [12] , and GOC represents the global optimal control obtained from dynamic programming.

The MPG of the simulated control strategies can be *fairly* compared if all of controllers start from the same initial SOC and finish at the same final SOC. Thus, the following procedure is followed for the simulations: 1) The introduced A-ECMS (ECMS₁) is run for each drive-cycle to find $x(t_f)$ or the final SOC, 2) Dynamic programming is run starting from the obtained $x(t_f)$ in order to find the optimal trajectory of SOC 3) The optimal SOC trajectory is used as the reference SOC signal for the ECMS₂ which is the A-ECMS in [12]. Since, ECMS₂ tracks the optimal SOC trajectory via the PI controller (3.30), it may yield a final SOC slightly different than the target value. Therefore the PI controller (3.30) was tuned to have the maximum difference of 0.1% between the obtained final SOC from ECMS₂ and the target $x(t_f)$ obtained from ECMS₁. Figure 3.3 represents the SOC trajectories of the 3 controllers in Table 3.3 for the UDDS drive-cycle.

For the full parallel HEV in Table 3.3, the infinite MPG values indicate the HEV has been in electric only mode for the whole trip because the battery energy and power had been enough for finishing the drive-cycle. Also, the ECMS₂ performs poorly for the routes than can be fully traveled in electric only mode. This behavior is caused by the PI controller that tries to track the optimal SOC. When $x(t)$ becomes less than $SOC_{ref}(t)$, the PI controller increases $\lambda(t)$. As $\lambda(t)$ increases, the cost of using

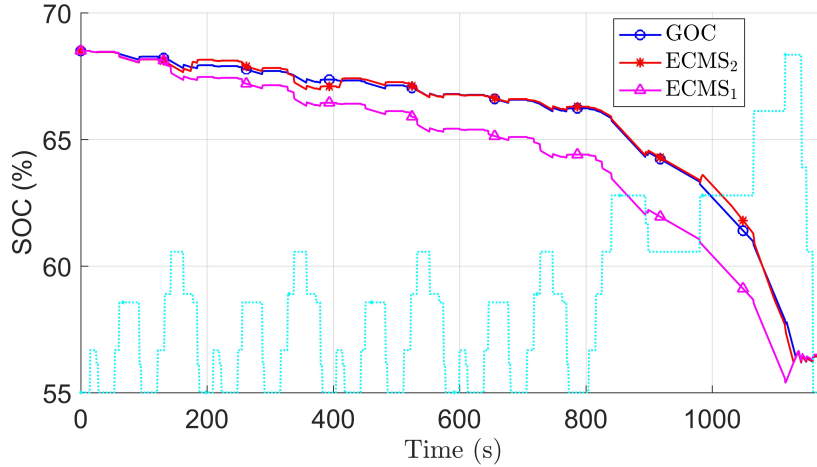


Figure 3.3: The SOC trajectory of the Full HEV for 3 different controllers on the NEDC drive-cycle (The speed profile is plotted with free offset/scale).

the electric energy in (3.16) increases. Therefore, the possibility of turning the engine on becomes higher.

From Table 3.3, $ECMS_1$ achieves a reasonably good performance in comparison with the $ECMS_2$ which knows the optimal SOC trajectory in advance. Please note that the good performance of the the introduced A-ECMS has been achieved without any horizon prediction thanks to employing the optimal λ^* bounds in (3.28). Furthermore, $ECMS_2$ requires predicting the future driving conditions and also an optimization algorithm to find SOC_{ref} from the predicted horizon. Therefore, in comparison with $ECMS_2$, the introduced A-ECMS is easier for implementation and also is computationally faster.

Table 3.3

Simulation results for a mild and a full parallel HEV for several drive-cycles, comparing the achieved MPG by 3 different EM strategies.

Drive-Cycle	MPG (Mild parallel HEV)			MPG (Full parallel HEV)		
	ECMS ₁	ECMS ₂	GOC	ECMS ₁	ECMS ₂	GOC
UDDS	86	73	94	∞	857	∞
HWFET	63	61	64	72	72	85
US06	42	42	43	49	48	55
SC03	91	78	93	∞	688	∞
NEDC	57	57	63	113	107	135
ECE-15	170	134	312	∞	512	∞
Japan-1015	78	75	87	253	243	259

3.6 Conclusion

ECMS is a fast and easy to implement EM strategy that has the ability to perform close to the GOC. The challenge for employing ECMS is estimation of the optimal equivalent factor for using the battery power. A formula for calculating the lower and upper bounds of the optimal equivalent factor for a parallel HEV is derived. The procedure for deriving the formula is independent of the drive-cycle. The simulation results show the optimal equivalent factor is always inside or close to the edge of the proposed range. To demonstrate an application of the derived formula, a new type of adaptive ECMS is introduced, employing the optimal equivalent factor bounds. Simulation results for 2 parallel HEVs are used to evaluate the performance of the introduced A-ECMS. Comparing the MPG of the introduced A-ECMS with the MPG of another A-ECMS and GOC, demonstrates promising performance for the introduced

A-ECMS. The equivalent factor bounds, would be useful for designing new types of A-ECMS or any approach that tries to estimate the ECMS optimal equivalent factor.

Chapter 4

A Real-Time Optimal Energy Management Strategy for Parallel Hybrid Electric Vehicles

4.1 Introduction

¹ Unlike conventional vehicles, hybrid electric vehicles (HEVs) have more than one energy source. Therefore, the strategy for splitting the energy request from the driver

¹The material contained in this chapter is submitted to the IEEE Transactions on Control Systems Technology: Amir Rezaei, Jeffrey Burl, and Bin Zhou. A new real-time optimal energy management strategy for hybrid electric vehicles. IEEE Transactions on Control Systems Technology, Under Review, 2016.

among the available energy sources impacts the fuel economy of the HEV, significantly [1][2]. Model predictive control (MPC)[2][3][4][5] [6][7], equivalent consumption minimization strategy (ECMS) [8][9][10][11][12][13][14][15][16], dynamic programming (DP) [2][16][17], and rule-based control (RBC)[18][19][20], are some of the well-studied energy management (EM) strategies for HEVs.

Given P_D (demanded power by the driver) for the entire drivecycle, DP yields the maximum fuel economy (FE). ECMS, which is based on Pontryagin's Minimum Principle (PMP) [8][17], performs similar to DP if 1) the entire drive-cycle is known in advance, 2) the battery state of charge (SOC) never exceeds its limits, as shown later. In practice, full prior knowledge of P_D is not available. Thus, DP and ECMS are not feasible as practical EM strategies. Instead, casual EM strategies like MPC, RBC, adaptive ECMS (A-ECMS), etc. are employed in practical applications.

ECMS, which was first introduced in [9] and [38], suggests in addition to minimizing the fuel consumption, consuming the battery energy must also be penalized. Later, in different works including [8], mathematical explanations for ECMS were provided showing that ECMS is based on PMP. Unfortunately, the ECMS *optimal* equivalent factor λ^* can be determined only if P_D is fully known, *a priori* (The symbol * denotes optimal value) [10][11]. To overcome the challenge of estimating λ^* for causal systems, adaptive ECMS (A-ECMS) was introduced [8][9][10][11][12][13][14][15][16][39].

A-EMCS either estimates λ^* using a predicted drive-cycle [10][11][12][13] or tries to

estimate λ^* with no information about the future [14][15]. The proposed EM strategy in this chapter falls into the latter group.

For instance, reference [25] defines S_{dis} and S_{chg} as empirical bounds of λ^* . Then the adaptive $\lambda(t)$ is calculated at the present time t by: $\lambda(t) = z(t)S_{dis} + (1 - z(t))S_{chg}$, where $z(t)$ is a probability function that depends to the drivecycle energy. According to [25] and [16], calculation of S_{dis} , S_{chg} , and $z(t)$ requires prior knowledge of the drivecycle. Although, [25] argues the performance of A-ECMS is not very sensitive to the choice of drivecycle energy, and thus, full prior knowledge of the drivecycle is not required.

Reference [10] adopts S_{dis} and S_{chg} from [25], as bounds of λ^* . The bounds are estimated by predicting the future P_D . Then the adaptive $\lambda(t)$ is calculated at the present time t using the determined bounds and $x_1(t)$, where $x_1(t)$ is the current feedback of SOC. Similarly, reference [40] calculates $\lambda(t)$ based on S_{dis} , S_{chg} , $x_1(t)$. However, [40] determines S_{dis} , S_{chg} from the average efficiencies of the powertrain components.

Reference [11] investigates A-ECMS with three different levels of information about the future P_D . For each information level, a method is proposed for calculating $\lambda(t)$. For calculating $\lambda(t)$ with no preview of P_D , the suggested approach in [40] is applied.

Reference [12] proposed an artificial neural network for predicting P_D in the future.

Then, an optimization algorithm is applied on the predicted horizon of P_D to find the optimal SOC trajectory. Given the optimal SOC trajectory over the future horizon x_1^* , a PI controller is employed to track $x_1^*(t)$ by setting $\lambda(t)$ based on the error signal $x_1^*(t) - x_1(t)$.

Other forms of A-ECMS are also introduced that try to estimate λ^* with no prior knowledge of P_D . These types of A-ECMS suggest calculating $\lambda(t)$ by the linear function $\lambda(t) = \lambda^0 + K_p(x_1(t) - SOC_{sp})$, where SOC_{sp} is a constant set point, and λ^0 and K_p are two constants to be estimated or tuned [14] [15]. No real-time formula for calculating the constants λ^0 and K_p is suggested by [14] or [15]. Instead, they rely on off-line simulations to estimate the constants for each drive-cycle.

The proposed EM strategy in this work is an instantaneous A-ECMS and is named ECMS-CESO. CESO is short for catch energy saving opportunity. Similar to the introduced A-ECMSs in [10][25][40], ECMS-CESO also uses λ^* bounds and the current SOC feedback to calculate $\lambda(t)$ at each moment. However, unlike [10], no P_D prediction is required for determining λ^* bounds. In addition, a theoretical background is provided for ECMS-CESO by introducing soft bounds or constraints on SOC. SOC is allowed to exceed the soft bounds if an energy saving opportunity is available. In order to limit excursions past the soft bounds, the ECMS-CESO penalty factor modified when the soft bound is exceeded. Since predicting P_D is eliminated, the required hardware and sensors for predicting P_D are no longer needed, which

makes implementation of ECMS-CESO cheaper than prediction-based EM strategies. In addition, implementation of ECMS-CESO in a real-time system is easier and more tractable than prediction-based EM strategies due to eliminating the intensive calculations for prediction and optimization on the predicted horizon of P_D .

The chapter is organized as follows: Section 4.2 presents the optimal control problem for parallel HEVs. Section 4.3, introduces ECMS-CESO and the equations for applying ECMS-CESO to a parallel HEV are derived. In this section, it is also proved that ECMS-CESO maintains the SOC limits in charge-sustaining mode. In addition, the robustness of ECMS-CESO in terms of providing P_D is discussed. Finally, in Section 4.4, the simulation results are presented, comparing ECMS-CESO with RBC and PMP, and an instantaneous A-ECMS.

4.2 Problem Statement

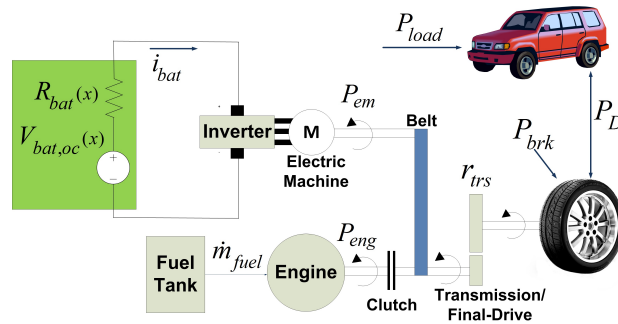


Figure 4.1: The configuration of the power-train in a parallel HEV.

The EM strategy has to find the optimal control actions in order to minimize the

total consumed fuel:

$$\mathbf{u}^* = \arg \min_{\mathbf{u}} \left\{ \int_0^{t_f} \dot{m}_{fuel}(\mathbf{x}, \mathbf{u}) dt \right\} \quad (4.1)$$

where \dot{m}_{fuel} is the fuel mass flow rate (g/s), t_f is the final time at the end of the drive-cycle, and \mathbf{u} and \mathbf{x} are the vectors of control actions and state variables, respectively.

The above optimization problem is subject to constraints on the control inputs:

$$\mathbf{u} \in U \quad (4.2)$$

where U is the set of all admissible control actions that do not violate any of the constraints in the system (For instance the constraints on the engine speed or torque).

The EM strategy must also provide the driver demanded power on the wheels $P_D(t)$ at each moment (See Fig. 4.1):

$$\left\{ \begin{array}{l} \text{Brake,Coast } P_D(t) \leq 0 : P_{brk}(t) = P_D(t) - \frac{P_{em}(t)}{\eta_{trs}(r_{trs}(t))} \\ \text{Acceleration } P_D(t) > 0 : P_{eng}(t) = \frac{P_D(t)}{\eta_{trs}(r_{trs}(t))} - P_{em}(t) \end{array} \right. \quad (4.3)$$

where P_{em} and P_{eng} are the useful mechanical powers (W) provided by the electric

machine and engine, respectively, P_{brk} is the dissipated power at the wheels by the friction brake system (W), and $\eta_{trs}(r_{trs})$ is the total efficiency of the transmission and final drive when the total gear ratio is r_{trs} . The efficiency of the clutch and the belt in Fig. 4.1 are assumed to be 1. Also, in (4.3) it is assumed that the EM strategy opens the clutch when the engine is off or when $P_D(t) < 0$.

The battery state of charge (SOC), denoted x_1 , is a state variable of the system with the state equation [16][41]:

$$\dot{x}_1(t) = -\frac{P_{bat,C}(x_1, \mathbf{u})}{Q_{bat}V_{bat,oc}(x_1)} \quad (4.4)$$

where $P_{bat,C}$ is the battery chemical power (W), $V_{bat,oc}$ is the battery open circuit (V), and Q_{bat} is the battery capacity (A·s).

Deep charge-discharge cycles can shorten the battery life. Thus, in charge-sustaining mode, SOC is limited to a certain range to avoid deep charge-discharge cycles:

$$\text{Charge-Sustaining Mode: } SOC_L \leq x_1(t) \leq SOC_H \quad , \quad t \in [0 \quad t_f] \quad (4.5)$$

The above range is usually defined to be the most efficient SOC range of the battery cells. Constraints on the initial and final values of the SOC make comparison of

different control strategies possible:

$$x_1(0) = c_0 \quad , \quad x_1(t_f) = c_1 \quad (4.6)$$

where c_0 and c_1 are two arbitrary known constants. The above constraint forces the strategies to consume the same amount of battery energy during the same drivecycle. Hence, it is possible to fairly compare the FEs of multiple EM strategies.

The equation for the longitudinal dynamics of the HEV is:

$$P_D(t) = P_{load}(v(t)) + m_e v(t) \dot{v}(t) \quad (4.7)$$

where v is the vehicle velocity in m/s, m_e is the vehicle effective mass in Kg, and P_{load} is the road load power (W) which includes gravity, rolling, and drag load forces. In the above equation $v(t)$ is determined by P_D . Thus, if (4.3) is maintained, P_D will be provided, which consequently satisfies (4.7). Hence, (4.7) can be ignored from the control problem.

The battery SOC and the vehicle velocity have slower dynamics in comparison with the fast transient behaviors of components like the engine, e-machine, transmission, etc. Hence, the fast transient dynamics are ignored due to slow overall system response [4][22][23][34][35][36].

P_D is a known parameter in (4.3). Hence, the independent variables in (4.3) are then considered as the plant control inputs:

$$\mathbf{u}(t) = [r_{trs}(t) \quad P_{em}(t)]^T \quad , \text{ where: } \quad \mathbf{u} \in U \quad (4.8)$$

From (4.3) the engine useful power P_{eng} is independent of the system state vector \mathbf{x} . Thus, for a parallel HEV:

$$\dot{m}_{fuel} = \dot{m}_{fuel}(\mathbf{u}(t), P_D(t)) \quad (4.9)$$

To account for the state inequality constraint in (4.5), the common approach is defining a new state variable x_2 [17]:

$$\begin{aligned} \dot{x}_2 = & (x_1 - SOC_L)^2 S(x_1 - SOC_L) + \\ & (SOC_H - x_1)^2 S(SOC_H - x_1) \end{aligned} \quad (4.10)$$

with the boundary condition:

$$x_2(t_f) = x_2(0) = 0 \quad (4.11)$$

where $S = 1$ if its argument is negative; Otherwise $S = 0$.

PMP solves the control problem (4.1) to (4.6) by augmenting the cost function (4.1) with the state constraints using co-state variables. Using PMP, the Hamiltonian is:

$$H = \dot{m}_{fuel}(\mathbf{u}(t), P_D(t)) + p_1(t)\dot{x}_1(t) + p_2(t)\dot{x}_2(t) \quad (4.12)$$

where p_1 and p_2 are the co-states. Finally, a PMP solution must consider the constraint (4.2), by satisfying the following condition for $0 \leq t \leq t_f$:

$$H(\mathbf{x}^*, \mathbf{u}^*, \mathbf{p}^*, P_D) \leq H(\mathbf{x}^*, \mathbf{u}, \mathbf{p}^*, P_D) \quad , \forall \mathbf{u} \in U \quad (4.13)$$

By defining λ as:

$$\lambda = \frac{-p_1(t)}{Q_{bat}V_{bat,oc}(x_1)} \quad (4.14)$$

the Hamiltonian in (4.12) becomes:

$$H = \dot{m}_{fuel}(\mathbf{u}(t), P_D(t)) + \lambda P_{bat,C}(x_1(t), \mathbf{u}(t)) + p_2 \dot{x}_2(t) \quad (4.15)$$

which is the ECMS cost function with λ as the penalty or equivalent factor for using

the battery power. Note that by using PMP, equations (4.4), (4.6), (4.10), (4.11), (4.12), and (4.13) represent the same control problem as (4.1) to (4.6).

4.3 Catch Energy Saving Opportunities (CESO),

The Proposed Optimal EM Strategy

Consider the situation $x_1(t) = SOC_L$ at the moment t . A moment later, assuming $P_D(t + dt) > 0$, there is a possibility that the hybrid or battery only modes are optimal. However, hybrid or battery only modes require battery discharging. Hence, the optimal EM strategy has to reject those desired modes, leading to sub-optimal FE. On the other hand, if $x_1(t) = SOC_H$ and $P_D(t + dt) \leq 0$, the opportunity for regenerative braking will be missed. Missing such opportunities might happen frequently during a trip as $P_D(t + dt)$ or in general, the future trajectory of P_D is unknown, *a priori*. Predicting P_D in MPC or some types of A-ECMS is one solution to avoid missing energy saving opportunities. However, the predicted P_D is subject to uncertainties [24][26] which may lead to sub-optimal FE. To the authors best knowledge, no *practical* real-time causal solution has been suggested to achieve optimal FE, regardless of the drive-cycle or trip duration. Similarly, the proposed approach in this work does not guarantee achieving optimal FE, in general. However, ECMS-CESO is designed to catch energy saving opportunities (CESO) without the

need for predicting P_D .

In order to avoid missing such opportunities, the authors propose replacing (4.5) with:

$$SOC_L^{soft} \leq x_1(t) \leq SOC_H^{soft} \quad (4.16)$$

where SOC_L^{soft} and SOC_H^{soft} are new bounds of SOC. Unlike the hard bounds in (4.5), x_1 is allowed to exceed either of SOC_L^{soft} or SOC_H^{soft} by at most θ_{max} (See Fig. 4.2a). Exceeding these bounds will be *penalized* by increasing or decreasing $\lambda(t)$, as shown in Fig. 4.2b. Thus, (4.16) shall be named a soft constraint. If the EM strategy guarantees that the soft constraints will be exceeded by at most θ_{max} , then the original constraint (4.5) is still satisfied, as shown in Fig. 4.2a.

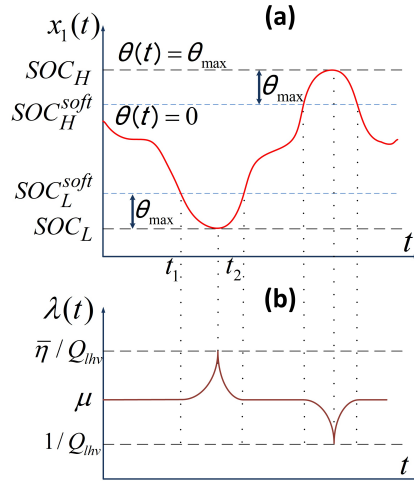


Figure 4.2: (a) Replacing the SOC hard bounds in (4.5) with soft constraints SOC_L^{soft} and SOC_H^{soft} . x_1 is allowed to exceed the soft bounds by at most θ_{max} . (b) ECMS-CESO maintains $\lambda(t)$ inside the range (4.30).

The main advantage of this technique is that the EM strategy will be able to catch energy saving opportunities, even without knowing the future P_D . Consider the previously discussed scenario again where $x_1(t) = SOC_L^{soft}$. A moment later, if $P_D(t + dt) > 0$, then the hybrid or battery only modes will not be rejected since the battery can be further discharged by exceeding SOC_L^{soft} .

4.3.1 Deriving the ECMS-CESO Equations

Replacing (4.5) with (4.16), requires modifying (4.10):

$$\begin{aligned} \dot{x}_2 = & \left(x_1 - SOC_L^{soft}\right)^2 S\left(x_1 - SOC_L^{soft}\right) + \\ & \left(SOC_H^{soft} - x_1\right)^2 S\left(SOC_H^{soft} - x_1\right) \end{aligned} \quad (4.17)$$

Since ECMS-CESO is allowed to exceed the soft constraint (4.16), the boundary condition (4.11) can be eliminated. Again, it should be emphasized that the above modifications to the original control problem makes ECMS-CESO a sub-optimal control strategy. In other words, the optimal control problem (4.4), (4.6), (4.10), (4.11), (4.12), and (4.13) is now reduced to the sub-optimal control problem (4.4), (4.6), (4.12), (4.13), and (4.17). However, the original optimal control problem is not solvable for practical applications. Thus, employing sub-optimal EM strategies is a reasonable alternative.

The co-state equations in (4.12) are:

$$\dot{p}_1^* = -\frac{\partial H}{\partial x_1} = -p_1^* \frac{\partial \dot{x}_1}{\partial x_1} - p_2^* \frac{\partial \dot{x}_2}{\partial x_1} \approx -p_2^* \frac{\partial \dot{x}_2}{\partial x_1} \quad (4.18)$$

$$\dot{p}_2^* = -\frac{\partial H}{\partial x_2} = 0 \quad \Rightarrow \quad p_2^* = \text{constant} \quad (4.19)$$

ECMS-CESO is designed to maintain SOC in the range (4.5). In this range, the profiles of $V_{bat,oc}$ and R_{bat} are almost flat with respect to SOC variations. In other words, for the range in (4.5), $V_{bat,oc}$, R_{bat} P_{bat} are almost independent of x_1 [16][19][42].

Thus in (4.18): $\partial \dot{x}_1 / \partial x_1 \approx 0$. Using (4.14), (4.18) becomes:

$$\dot{\lambda}^* \approx \frac{p_2^*}{Q_{bat} V_{bat,oc}} \frac{\partial \dot{x}_2}{\partial x_1} \quad (4.20)$$

From (4.17):

$$\begin{aligned}
\frac{\partial \dot{x}_2}{\partial x_1} = & 2 \left(x_1 - SOC_L^{soft} \right) S \left(x_1 - SOC_L^{soft} \right) \\
& + 2 \left(SOC_H^{soft} - x_1 \right) S \left(SOC_H^{soft} - x_1 \right) \\
& + \left(x_1 - SOC_L^{soft} \right)^2 \delta \left(x_1 - SOC_L^{soft} \right) \\
& + \left(x_1 - SOC_H^{soft} \right)^2 \delta \left(SOC_H^{soft} - x_1 \right)
\end{aligned} \tag{4.21}$$

where δ is the impulse function. The impulse functions are multiplied by 0^2 and can be omitted from (4.21). Substituting this result into (4.20) gives:

$$\dot{\lambda}^* = \begin{cases} 0 & , SOC_L^{soft} \leq x_1 \leq SOC_H^{soft} \\ \frac{2p_2^*}{Q_{bat} V_{bat,oc}} \left(x_1 - SOC_L^{soft} \right) & , x_1 < SOC_L^{soft} \\ \frac{2p_2^*}{Q_{bat} V_{bat,oc}} \left(SOC_H^{soft} - x_1 \right) & , x_1 > SOC_H^{soft} \end{cases} \tag{4.22}$$

Defining the variable θ as (shown in Fig. 4.2a):

$$\theta(t) = \begin{cases} 0 & , SOC_L^{soft} \leq x_1(t) \leq SOC_H^{soft} \\ SOC_L^{soft} - x_1 & , x_1(t) < SOC_L^{soft} \\ x_1 - SOC_H^{soft} & , x_1(t) > SOC_H^{soft} \end{cases} \tag{4.23}$$

equation (4.22) simplifies to:

$$\dot{\lambda}^*(t) = \frac{-2p_2^* \theta(t)}{Q_{bat} V_{bat,oc}} \quad (4.24)$$

$\theta(t)$ is the amount by which the lower or upper soft bounds are exceeded and always non-negative: $\theta(t) \geq 0$. To solve (4.24), different cases of θ must be considered: when SOC is inside the soft bounds, $\theta(t) = 0$, and hence, the constant μ is defined as:

$$\theta(t) = 0 \Rightarrow \dot{\lambda}^*(t) = 0 \Rightarrow \lambda^*(t) = \text{constant} = \mu^* \quad (4.25)$$

Assuming during the arbitrary times t_1 to t_2 , SOC goes below SOC_L^{soft} (See Fig. 4.2a), then from (4.23) and (4.24)

$$\begin{aligned} \int_{\lambda^*(t_1)}^{\lambda^*(t)} d\lambda &= \frac{-2p_2^*}{Q_{bat} V_{bat,oc}} \int_{t_1}^t \theta(\tau) d\tau \\ \Rightarrow \lambda^*(t) &= \lambda^*(t_1) + \frac{-2p_2^*}{Q_{bat} V_{bat,oc}} \Psi(\theta(t), t) \end{aligned} \quad (4.26)$$

where $\Psi(\theta(t), t)$ is a time-varying drivecycle dependent function defined as:

$$\Psi(\theta(t), t) = \int_{t_1}^t \theta(\tau) d\tau.$$

When $t = t_1$: $\lambda^*(t_1) = \mu^*$. Therefore, (4.26) becomes:

$$x_1 < SOC_L^{soft} \Rightarrow \lambda^*(t) = \mu^* - \frac{2p_2^* \Psi(\theta(t), t)}{Q_{bat} V_{bat,oc}} \quad (4.27)$$

Similarly:

$$x_1 > SOC_H^{soft} \Rightarrow \lambda^*(t) = \mu^* - \frac{2p_2^* \Psi(\theta(t), t)}{Q_{bat} V_{bat,oc}} \quad (4.28)$$

In the next section, it is shown:

$$\left\{ \begin{array}{l} \text{if } x_1 = SOC_L \Rightarrow \lambda = \bar{\eta}/Q_{lhv} \text{ prevents discharging} \\ \text{if } x_1 = SOC_H \Rightarrow \lambda = 1/Q_{lhv} \text{ prevents charging} \end{array} \right. \quad (4.29)$$

where $\bar{\eta} = \bar{\eta}_{em}\bar{\eta}_{inv}\bar{\eta}_{bat}/\bar{\eta}_{eng}$, and Q_{lhv} is the fuel lower heating value. $\bar{\eta}_{eng}$, $\bar{\eta}_{em}$, $\bar{\eta}_{inv}$ and $\bar{\eta}_{bat}$ are the average efficiencies of the engine, e-machine, inverter, and battery, respectively.

Thus, $\lambda(t)$ must be limited to the following range:

$$\frac{1}{Q_{lhv}} \leq \lambda(t) \leq \frac{\bar{\eta}_{bat} \bar{\eta}_{inv} \bar{\eta}_{em}}{Q_{lhv} \bar{\eta}_{eng}} = \frac{\bar{\eta}}{Q_{lhv}} \quad (4.30)$$

or the battery will be constantly charged or discharged, resulting in rapidly exceeding the state of charge bounds.

As was discussed previously, the optimal values of μ^* and p_2^* in (4.25), (4.27), and (4.28) cannot be found without full prior knowledge of P_D . Instead, to maintain (4.5), μ^* and p_2^* shall be chosen such that $\lambda^*(t)$ always remains within the range (4.30) during the trip. In the following, since the chosen values for μ^* and p_2^* might not be optimal, the optimal symbols of μ^* and p_2^* and $\lambda^*(t)$ are dropped.

The first case in (4.27) leads to (4.25).

For the case $x_1(t) \leq SOC_L^{soft}$ in (4.27), as shown in Fig. 4.3, it is desired to have:

$$\mu < \lambda(t) \leq \frac{\bar{\eta}}{Q_{lhv}} \Rightarrow 0 > p_2 \Psi(\theta(t), t) \geq \frac{\mu - \bar{\eta}/Q_{lhv}}{2/(Q_{bat} V_{bat,oc})} \quad (4.31)$$

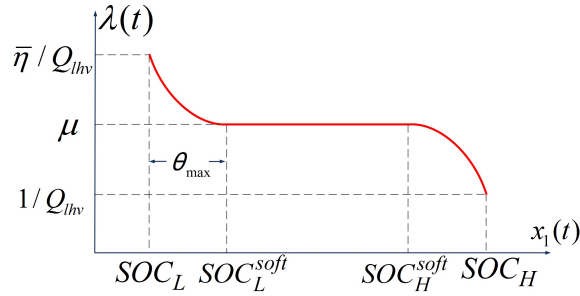


Figure 4.3: ECMS-CESO sets $\lambda(t)$ based on the current value of SOC.

From the inequality (4.31) the desired features of the function $p_2 \Psi(\theta(t), t)$ should be:

$$\left\{ \begin{array}{l} \lim_{\theta(t) \rightarrow 0} p_2 \Psi(\theta(t), t) = 0 \\ p_2 \Psi(\theta(t), t)|_{\theta(t)=\theta_{max}} = \frac{\mu - \bar{\eta}/Q_{lhv}}{2/(Q_{bat} V_{bat,oc})} \\ p_2 \Psi(\theta(t), t) \text{ should be a monotonic function of } \theta(t) \end{array} \right. \quad (4.32)$$

where the last feature is desired because as $\theta(t)$ increases from the lower soft constraint, we want the penalty or equivalent factor $\lambda(t)$ be increased accordingly.

To satisfy the features in (4.32) for the case $x_1(t) < SOC_L^{soft}$, the following expression is proposed for p_2 . This expression also cancels the effect of $\Psi(\theta(t), t)$:

$$p_2 = \frac{\mu - \bar{\eta}/Q_{lhv}}{2/(Q_{bat} V_{bat,oc})} \frac{(\theta(t)/\theta_{max})^2}{\Psi(\theta(t), t)} \quad (4.33)$$

Selection of a quadratic function for $\theta(t)$ in (4.33) is intuitively justified as follows: from Fig. 4.2, the quadratic function $(\theta(t)/\theta_{max})^2$ is small when the SOC is close to the soft bound SOC_L^{soft} . Thus, when SOC exceeds SOC_L^{soft} to catch an energy saving opportunity, the penalty or equivalence factor $\lambda(t)$ will be small. This behavior will keep the interference of the penalizing procedure small. However, as the SOC gets far from the soft bound, the quadratic function $(\theta(t)/\theta_{max})^2$ quickly grows and eventually stops ECMS-CESO from a violation of more than θ_{max} .

Similarly, for the case in (4.28), it is desired to (See Fig. 4.3):

$$\frac{1}{Q_{lhv}} \leq \lambda(t) < \mu \Rightarrow \frac{\mu - 1/Q_{lhv}}{2/(Q_{bat} V_{bat,oc})} \geq p_2 \Psi(\theta(t), t) > 0 \quad (4.34)$$

Reasoning similar to that used for the lower soft constraint, the case $x_1(t) > SOC_H^{soft}$ leads to:

$$p_2 = \frac{\mu - 1/Q_{lhv}}{2/(Q_{bat} V_{bat,oc})} \frac{(\theta(t)/\theta_{max})^2}{\Psi(\theta(t), t)} \quad (4.35)$$

Substituting (4.33) into (4.27), and (4.35) into (4.28), yields the final adaptive law of ECMS-CESO:

$$\lambda(t) = \begin{cases} \mu & , SOC_L^{soft} \leq x_1 \leq SOC_H^{soft} \\ \mu + \left(\frac{\bar{\eta}}{Q_{lhv}} - \mu \right) \left(\frac{\theta(t)}{\theta_{max}} \right)^2 & , x_1 < SOC_L^{soft} \\ \mu - \left(\mu - \frac{1}{Q_{lhv}} \right) \left(\frac{\theta(t)}{\theta_{max}} \right)^2 & , SOC_H^{soft} < x_1 \end{cases} \quad (4.36)$$

where $\theta(t)$ is defined in (4.23). Since, it is desired to maintain $\lambda(t)$ within the range (4.30), a reasonable estimate for μ is the mid-point of this range (See Fig. 4.3): $SOC_L^{soft} \leq x_1(t) \leq SOC_H^{soft}$: $\lambda(t) = \mu = (\bar{\eta} + 1)/(2Q_{lhv})$. For θ_{max} value in

(4.36), the authors propose a quarter of the range in (4.5). However, depending on the HEV configuration, this value can be tuned for better FE based on experiments or simulations. Regarding $\bar{\eta}$, the initial value must be: $\bar{\eta} = \bar{\eta}_{em}\bar{\eta}_{inv}\bar{\eta}_{bat}/\bar{\eta}_{eng}$. To calculate $\bar{\eta}_{eng}$ for the engine, a uniform distribution of *admissible* operating points is assumed on the efficiency map. Similarly, $\bar{\eta}_{em}$, $\bar{\eta}_{inv}$, and $\bar{\eta}_{bat}$ can be found. After finding $\bar{\eta}$, the authors recommend running a simulation on an aggressive drivecycle like US06 or two successive HWFETs. If at any time SOC goes below SOC_L , then $\bar{\eta}$ must slightly be increased.

4.3.2 Achieving Hard SOC Constraints With ECMS-CESO

This section investigates the previous claim about (4.29). When the driver is pressing the brake pedal (braking), or no pedal (coasting), the clear optimal control is to recover energy as much as possible via regenerative braking. Thus, the effect of EM strategy on FE mostly matters when the driver is pressing the accelerator pedal: $P_D > 0$. In that case, it is expected:

$$P_D > 0 \quad \Rightarrow \quad \mathbf{u}^* \in \{\mathbf{u}_{em}\} \cup \{\mathbf{u}_{cm}\} \cup \{\mathbf{u}_{hm}\} \cup \{\mathbf{u}_{bom}\}$$

where \mathbf{u}_{em} , \mathbf{u}_{cm} , \mathbf{u}_{hm} , and \mathbf{u}_{bom} are the control actions that will bring the HEV into

one of the modes: engine only mode (*ecom*), charging mode (*cm*), hybrid mode (*hm*), and battery only mode (*bom*), respectively.

To prove the first case in (4.29), it is enough to show that setting $\lambda = \bar{\eta}/Q_{lhv}$ makes the cost of *ecom* less than *hm* or *bom* (battery will be discharged only in *hm* or *bom*):

$$\begin{aligned} \lambda = \bar{\eta}/Q_{lhv} &\Rightarrow \forall \mathbf{u} \in \{\mathbf{u}_{ecom}\} \cup \{\mathbf{u}_{hm}\} \cup \{\mathbf{u}_{bom}\} : \\ &\exists \mathbf{u}_{ecom}^0 \in \{\mathbf{u}_{ecom}\} \quad \text{such that:} \quad H(\mathbf{u}_{ecom}^0) < H(\mathbf{u}) \end{aligned} \quad (4.37)$$

There is no need to consider *cm* in (4.37), as *cm* charges the battery. In (4.37), u_{ecom}^0 is not required to be optimal. Only the existence of u_{ecom}^0 is enough to guarantee the battery will not be further discharged. In (4.37), $H(\mathbf{u}_{ecom}^0) < H(\mathbf{u})$ requires:

$$\begin{cases} H(\mathbf{u}_{ecom}^0) < H(\mathbf{u}_{bom}) & , \quad \forall \mathbf{u}_{bom} \in \{\mathbf{u}_{bom}\} \\ H(\mathbf{u}_{ecom}^0) < H(\mathbf{u}_{hm}) & , \quad \forall \mathbf{u}_{hm} \in \{\mathbf{u}_{hm}\} \end{cases} \quad (4.38)$$

Using (4.15), the above inequalities become:

$$\begin{cases} \dot{m}_{fuel}(\mathbf{u}_{ecom}^0) < \lambda P_{bat,C}(x_1, \mathbf{u}_{bom}) \\ \dot{m}_{fuel}(\mathbf{u}_{ecom}^0) < \dot{m}_{fuel}(\mathbf{u}_{hm}) + \lambda P_{bat,C}(x_1, \mathbf{u}_{hm}) \end{cases} \quad (4.39)$$

From the constraint (4.3) for the parallel HEV in Fig. 4.1, (4.46) becomes:

$$\left\{ \begin{array}{l} \frac{P_D/\bar{\eta}_{trs}}{Q_{lhv} \bar{\eta}_{eng}} < \lambda \frac{P_D/\bar{\eta}_{trs}}{\bar{\eta}_{em} \bar{\eta}_{inv} \bar{\eta}_{bat}} \\ \frac{P_D/\bar{\eta}_{trs}}{Q_{lhv} \bar{\eta}_{eng}} < \frac{P_D/\bar{\eta}_{trs} - (P_{em})_{hm}}{Q_{lhv} \bar{\eta}_{eng}} + \lambda \frac{(P_{em})_{hm}}{\bar{\eta}_{em} \bar{\eta}_{inv} \bar{\eta}_{bat}} \end{array} \right. \quad (4.40)$$

where $\bar{\eta}_{trs}$ is the average efficiency of the transmission. Both inequalities in (4.40) give:

$$\frac{\bar{\eta}_{em} \bar{\eta}_{inv} \bar{\eta}_{bat}}{Q_{lhv} \bar{\eta}_{eng}} = \frac{\bar{\eta}}{Q_{lhv}} < \lambda \quad (4.41)$$

which shows if λ becomes slightly higher than $\bar{\eta}/Q_{lhv}$ then it prevents battery discharge.

To prove the second case in (4.29), it is enough to show that setting $\lambda = 1/Q_{lhv}$ makes the cost of *bom* less than *cm*:

$$\begin{aligned} P_D > 0 \quad \text{and} \quad \lambda = 1/Q_{lhv} &\Rightarrow \forall \mathbf{u} \in \{\mathbf{u}_{cm}\} \cup \{\mathbf{u}_{bom}\} : \\ \exists \mathbf{u}^0 \in \{\mathbf{u}_{bom}\} \quad \text{such that:} \quad &H(\mathbf{u}^0) < H(\mathbf{u}) \end{aligned} \quad (4.42)$$

There is no need to consider *com* or *hm* here, because these modes do not charge the battery. In (4.42), Let us assume the cost of *cm* is less than the cost of *bom*:

$$H(\mathbf{u}_{bom}) > H(\mathbf{u}_{cm}) \quad (4.43)$$

Using (4.15) and substituting λ with $1/Q_{lhw}$, (4.43) becomes:

$$\frac{P_{bat,C}(x_1, \mathbf{u}_{bom})}{Q_{lhw}} > \dot{m}_{fuel}(\mathbf{u}_{cm}) + \frac{P_{bat,C}(x_1, \mathbf{u}_{cm})}{Q_{lhw}} \quad (4.44)$$

Using the constraint (4.3), the above inequality becomes:

$$\begin{aligned} \frac{P_D/\bar{\eta}_{trs}}{Q_{lhw} \bar{\eta}_{em} \bar{\eta}_{inv} \bar{\eta}_{bat}} &> \frac{P_D/\bar{\eta}_{trs} - (P_{em})_{cm}}{Q_{lhw} \bar{\eta}_{eng}} \\ &\quad + \frac{\bar{\eta}_{em} \bar{\eta}_{inv} \bar{\eta}_{bat}}{Q_{lhw}} (P_{em})_{cm} \\ \frac{P_D(\bar{\eta}_{eng} - \bar{\eta}_{em} \bar{\eta}_{inv} \bar{\eta}_{bat})}{\bar{\eta}_{trs} \bar{\eta}_{em} \bar{\eta}_{inv} \bar{\eta}_{bat} \bar{\eta}_{eng}} &> \frac{\bar{\eta}_{em} \bar{\eta}_{inv} \bar{\eta}_{bat} \bar{\eta}_{eng} - 1}{\bar{\eta}_{eng}} (P_{em})_{cm} \end{aligned}$$

Since the total efficiency of the electric components is expected to be higher than the engine efficiency, then the left side of the above inequality is negative. Also, since $(P_{em})_{cm} < 0$, the right side of the above inequality is positive, which is not possible.

Therefore, (4.43) is wrong and:

$$\lambda = \frac{1}{Q_{lhv}} \quad \Rightarrow \quad H(\mathbf{u}_{bom}) < H(\mathbf{u}_{cm}) \quad (4.45)$$

which proves the second part of (4.29).

4.3.3 Achieving Driver Requested Power With ECMS-CESO

ECMS-CESO might occasionally fail to provide the driver requested power $P_D(t)$: When $x_1(t) = SOC_L$, if the driver asks for a high power, the engine might not be powerful enough to deliver $P_D(t)$, without electrical assist. However, such situations can happen for any control strategy. One might argue that predictive controllers like MPC can avoid this situation, and thus, they are robust in terms of delivering $P_D(t)$. But, note that the uncertainty of the predicted horizon cannot be eliminated due to numerous statistical factors affecting $P_D(t)$ [24][26][43]. Therefore, predictive controllers could also occasionally fail in delivering high $P_D(t)$.

In addition, ECMS-CESO is designed to keep the SOC around SOC_L^{soft} . ECMS-CESO can exceed SOC_L^{soft} if there is an energy saving opportunity *or* if the engine only cannot provide $P_D(t)$. On the occasions that $x_1(t) = SOC_L$ and $P_D(t)$ is low, the equivalent factor $\lambda(t)$ is high enough that ECMS-CESO will tend to charge the battery via *cm*. In other words, the episodes of $x_1(t) = SOC_L$ are expected to be short, which

lowers the chance of having $x_1(t) = SOC_L$ and high $P_D(t)$, simultaneously.

4.4 Simulation Results

For simulations, a mild parallel HEV (Honda Civic IMA), and a full parallel HEV (plug-in parallel HEV Truck under construction at Michigan Technological University) with the same configuration as in Fig. 4.1, were modeled. The main specifications of both HEVs are presented in Table 4.1. A high fidelity model with 19 state variables was created in AMESim as the HEV plant. Each component of the AMESim model (engine, battery, e-machine, etc.) was initialized by the manufacturer published data (For the HEV truck the measured data were used for the body dynamics). Due to many state variables, the high fidelity model could not be used for the optimization algorithm. Therefore, a low fidelity quasi-static model with 4 state variables (SOC, engine on/off, gear number, velocity) was created in Simulink to be used as the optimization model. Both AMESim and quasi-static models have the same control inputs: engine on/off command, engine and e-machine requested torques, clutch and gear number commands, and friction brake command. The quasi-static model was validated by the high fidelity model in AMESim. The uncertainty between the optimization model and the plant model affects the results [44][45]. Therefore, to eliminate this effect on simulation results, the validated quasi-static model was used as the plant model as well.

Table 4.1
Vehicle Parameters Used in the Simulations.

Main Specifications	Honda Civic IMA	HEV Truck
Configuration	Mild Parallel	Plugin Full Parallel
Vehicle mass	1279 Kg	1588 Kg
Frontal Area	1.9 m ²	3.3 m ²
Engine max torque	120 N.m@3500rpm	454 N.m@4000rpm
E-machine max torque	62 N.m@1500rpm	315 N.m@2200rpm
Battery energy	0.93 KW.hr	12.2 KW.hr
Battery dis/chg power	14 KW / 7 KW	40 KW / 13 KW

For each vehicle in Table 4.1, four different EM strategies were tested: RBC, A-ECMS, ECMS-CESO, and ECMS-PMP:

1. PMP: Is the ECMS with the cost function (4.15) based on PMP. PMP has access to $P_D(t)$ for $0 \leq t \leq t_f$. PMP uses an iterative procedure to find λ^* that yields a final SOC as close as possible to CESO, which satisfies (4.6). The resulting SOC trajectory is optimal if (4.5) is not violated [8]. Otherwise, DP is used instead of PMP.
2. CESO: is the proposed EM strategy in this work which has no access to the future P_D .
3. A-ECMS: An instantaneous A-ECMS adopted from [40]. As was mentioned in section 4.1, a basic A-ECMS was introduced by [40]: $S_{dis} = 1/(\bar{\eta}_e^{(d)} \bar{\eta}_f)$ and $S_{chg} = \bar{\eta}_e^{(c)}/\bar{\eta}_f$, where $\bar{\eta}_e^{(c)}$ and $\bar{\eta}_e^{(d)}$ are the average efficiencies of the electric energy path for charge and discharge, respectively, and $\bar{\eta}_f$ is the average efficiency of the fuel energy path. Reference [40] suggested a bilinear relationship between

$\lambda(t)$ and SOC:

$$\left\{ \begin{array}{l} \lambda(t) = s_0 + \frac{s_0 - S_{chg}}{x_1^0 - SOC_H}(x_1(t) - x_1^0), x_1(t) \geq x_1^0 \\ \lambda(t) = s_0 + \frac{s_0 - S_{dis}}{x_1^0 - SOC_L}(x_1(t) - x_1^0), x_1(t) < x_1^0 \end{array} \right. \quad (4.46)$$

where $s_0 = \sqrt{S_{chg}S_{dis}}$ and $x_1^0 = (SOC_L + SOC_H)/2$.

4. RBC: a rule-based control strategy developed and tuned in Simulink to maximize the achieved FE for the tested drivecycles. The following are some of the rules: a) Stay in *bom* unless $x_1(t) < SOC_L + 0.1$ or e-machine only cannot deliver P_D . b) If $x_1(t) \leq SOC_L$, force *eom* or *cm* depending on lesser fuel consumption. c) If $x_1(t) \geq SOC_H$, avoid *cm* and regenerative braking. d) In *hm*, choose gear number based on the engine optimal operating line. e) If $x_1(t) < SOC_H - 0.05$ and driver requested torque is less than engine optimal torque, force *cm* and charge the battery.

The simulation results are presented in Tables 4.2 and 4.3. For all simulations: $SOC_L = 0.5$, $SOC_H = 0.7$, $\theta_{max} = 0.07$, initial SOC=0.65. Comparing CESO with PMP, shows that CESO performs close to PMP. Since the FE numbers are rounded, for some of the drivecycles, CECO and PMP have the same FE. Note that CESO performs close to PMP with no information about the future. The ∞ values in Table 4.3 indicate the HEV has been in *bom* for the entire drivecycle. Unfortunately,

since the final SOC for RBC, A-ECMS, and CESO are different a fair comparison is not possible.

Figure 4.4 presents the trajectories of SOC and fuel consumption on UDDS (mild HEV) and US06 (full HEV) drivecycles. A-ECMS tends to maintain SOC around the mid-point of SOC range, i.e. x_1^0 . From (4.46), if $x_1(t) < x_1^0$, A-ECMS increases $\lambda(t)$, which increases the chance of cm . Similarly, if $x_1(t) > x_1^0$, $\lambda(t)$ is decreased which favors hm or bom . For CESO, SOC is mostly around $SOC_L^{soft} = 57\%$. However, SOC exceeds this bound many times due to possible energy saving opportunities or to assist the engine in delivering P_D . For US06, the SOC trajectories of RBC and CESO are very close. However, CESO yields better FE (Table 4.3).

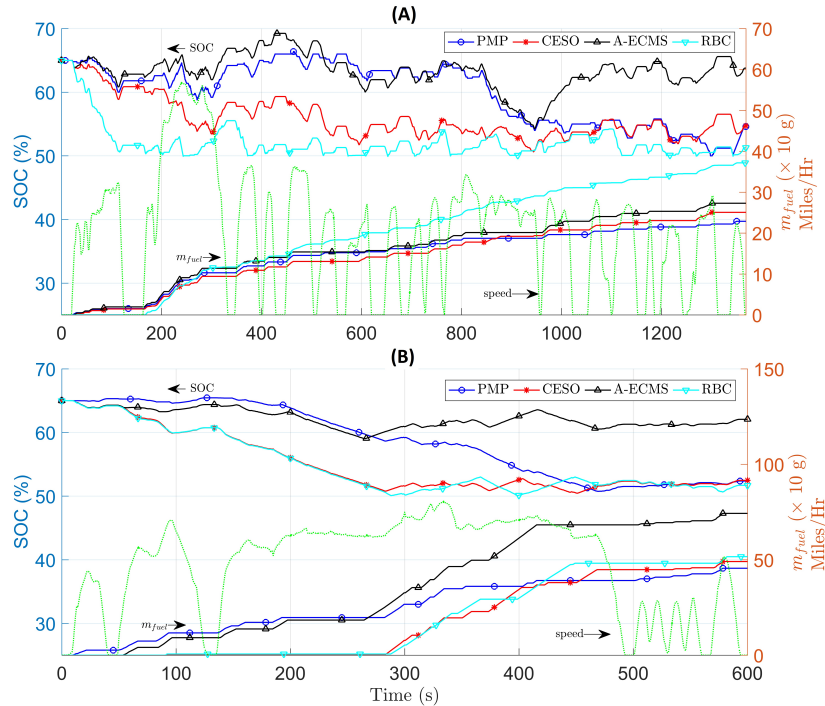


Figure 4.4: The SOC and fuel consumption trajectories for 4 different EM strategies: (a) mild parallel HEV on UDDS (b) full parallel HEV on US06.

With the same final SOC, the comparison between CESO and PMP is fair. Therefore, separate PMP simulations were done based on the final SOCs of RBC and A-ECMS on each drivecycle. Given the optimal FE value for each EM strategy, it is possible to normalize the FEs and compare the normalized values, fairly. Figure 4.5 presents the normalized FE values for both vehicles. The FE values in Tables 4.2 and 4.3 are achieved with $x_1(0) = 0.65$. To investigate the effect of $x_1(0)$ on results, a new set of simulation were done with $x_1(0) = 0.55$, as shown in Fig. 4.5.

Table 4.2
Results for a mild parallel HEV.

Drivecycle	Miles per gallon (Final SOC %)			
	RBC	A-ECMS	CESO	PMP
UDDS	57 (51.3)	75 (63.8)	84 (54.7)	91 (54.7)
HWFET	53 (55.4)	60 (69.6)	62 (58.8)	63 (58.8)
US06	38 (54.3)	40 (70.0)	42 (68.3)	42 (68.3)
SC03	62 (50.9)	76 (59.8)	86 (54.4)	87 (54.4)
NEDC	46 (52.9)	49 (68.2)	55 (55.9)	57 (55.9)

Table 4.3
Results for a full parallel HEV.

Drivecycle	Miles per gallon (Final SOC %)			
	RBC	A-ECMS	CESO	PMP
UDDS	160 (50.9)	84 (58.0)	615 (51.2)	924 (51.2)
HWFET	54 (53.5)	48 (56.6)	64 (52.0)	65 (52.0)
US06	44 (51.7)	30 (62.1)	46 (52.5)	50 (52.5)
SC03	∞ (57.6)	301 (58.8)	∞ (57.6)	∞ (57.6)
NEDC	65 (53.8)	35 (66.1)	124 (52.6)	137 (52.6)

As can be seen in Fig. 4.5, the performance of CESO is better than both RBC and A-ECMS on all of the drivecycles. The performance of A-ECMS is also good and close to CESO. However, on a low power drivecycle like SC03, A-ECMS performs poorly in comparison with CESO. For the full HEV with $x_1(0) = 0.65$, RBC has a

very good performance which is because the RBC was able to operate in *bom* for the entire trip. Based on the results in Fig. 4.5, in average, CESO improves FE by about 7% and 20% in compression with A-ECMS and RBC, respectively.

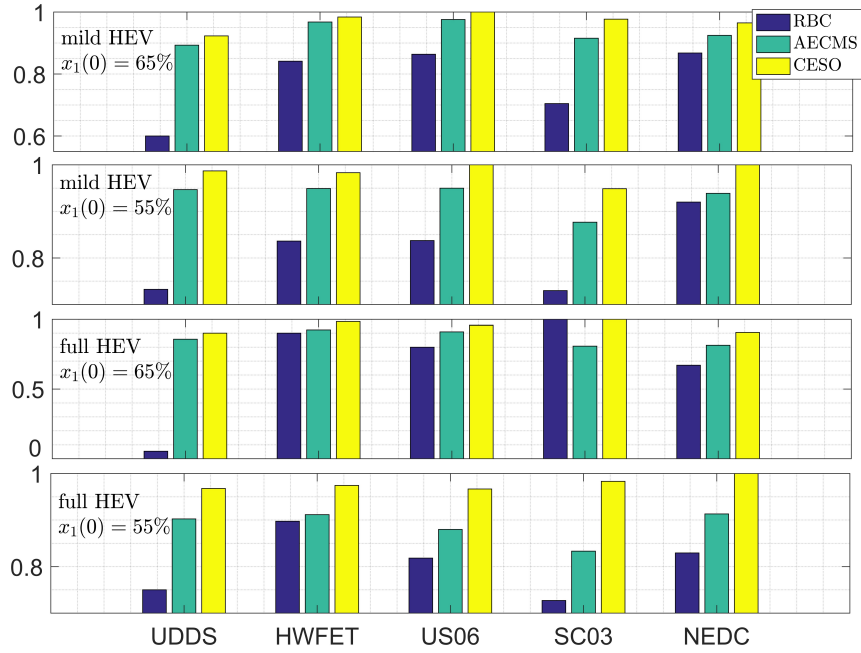


Figure 4.5: Normalized FEs for two HEVs with different initial SOC.

4.5 Conclusion

A new energy management strategy was introduced for HEVs that is suitable for practical real-time applications. The introduced EM strategy is a form of adaptive ECMS and is named ECMS-CESO. The required equations for implementing ECMS-CESO for a parallel HEV were derived. Based on the simulation results for a mild and a full parallel HEV, ECMS-CESO can yield FE reasonably close to the maximum FE.

Compared to an instantaneous A-ECMS, in average, ECMS-CESO improved the fuel economy by 7%. Unlike other causal optimal EM strategies like MPC or prediction-based A-ECMS, ECMS-CESO does not require predicting driver demanded power. Considering the cost of additional hardware/sensors for predicting the future power demand, ECMS-CESO is a cheap EM strategy. Also, in comparison with MPC or prediction based A-ECMS, the extensive calculations for prediction and optimization over the predicted horizon are no longer needed. As a result, ECMS-CESO would be easier to implement and faster for real-time applications.

Chapter 5

A Real-Time Optimal Energy Management Strategy for Series Hybrid Electric Vehicles

5.1 Introduction

The λ^* bounds in chapter 3 and the ECMS-CESO algorithm in chapter 4 are for parallel HEVs. Therefore, this chapter is dedicated to determining λ^* bounds and deriving ECMS-CESO algorithm for series HEVs. First, in section 5.3 the lower and upper bounds on λ^* are determined by an analytic procedure for series HEVs. In

section 5.4, ECMS-CESO is developed for series HEVs, and the adaptive equation for estimating $\lambda(t)$ is derived. In Section 5.5, it is shown ECMS-CESO maintains the battery SOC between the desired limits. In section 5.6, the experimental setup used for validating the HEV model is explained. Finally, simulation results on several drivecycles are presented and discussed in section 5.7. Section 5.7 also presents a comparison between the performances of ECMS-CESO and two other types of EM strategies.

5.2 Problem Statement

The control problem for series HEVs is similar to the control problem discussed in chapter 4.2 for parallel HEVs. The only difference is that (4.3) which was for parallel HEVs, must be modified for series HEVs. The following presents the control problem for series HEVs:

$$\mathbf{u}^* = \arg \min_{\mathbf{u}} \left\{ \int_0^{t_f} \dot{m}_{fuel}(\mathbf{x}, \mathbf{u}) dt \right\} \quad (5.1)$$

$$\mathbf{u} \in U \quad (5.2)$$

$$P_D(t) = P_{ptr}(\mathbf{x}, \mathbf{u}, t) + P_{brk}(\mathbf{x}, \mathbf{u}, t) \quad (5.3)$$

$$\dot{x}_1(t) = \frac{-P_{bat,C}(x_1, \mathbf{u})}{Q_{bat}V_{bat,oc}(x_1)} \quad (5.4)$$

$$\text{Charge-Sustaining Mode: } SOC_L \leq x_1(t) \leq SOC_H \quad , \quad t \in [0 \quad t_f] \quad (5.5)$$

$$x_1(0) = c_0 \quad , \quad x_1(t_f) = c_1 \quad (5.6)$$

where P_{ptr} is the power provided by the powertrain at the wheels in watts (W). Equation (5.3) is the equivalent of (4.3) for series HEVs. New state variable x_2 is defined in order to augment the cost function (5.1) with the inequality constraint (5.5) [17]:

$$\dot{x}_2 = (x_1 - SOC_L)^2 S(x_1 - SOC_L) + (SOC_H - x_1)^2 S(SOC_H - x_1) \quad (5.7)$$

where $S(a) = 1$ if $a < 0$; Otherwise $S(a) = 0$. The boundary conditions:

$$x_2(t_f) = x_2(0) = 0 \quad (5.8)$$

result in the inequality constraints (5.5) being enforced.

Augmenting (5.1) with the state equations (5.4) and (5.7), the Hamiltonian is:

$$H = \dot{m}_{fuel}(\mathbf{u}(t)) + \lambda P_{bat,C}(x_1(t), \mathbf{u}(t)) + p_2(t)\dot{x}_2(t) \quad (5.9)$$

where p_2 is the Lagrange multiplier, λ is the ECMS equivalent factor, and $\lambda^* \approx$ constant [16][19][41][42]. In (5.9), any bounded nonzero constant for p_2 is optimal since the optimal solution will keep $\dot{x}_2(t) = 0$ for the whole drivecycle to satisfy the constraint (5.5).

In (5.3), the power provided by the powertrain P_{ptr} depends on the HEV configuration. For the series HEV shown in Fig. 5.1: $P_{ptr} = P_D - P_{brk}$. Therefore, the mechanical power of the tractive electric machine, P_{em} , is:

$$P_{em}(t) = \frac{P_{ptr}(t)}{\eta_{trs}^n(r_{trs}(t))} = \frac{P_D(t) - P_{brk}(t)}{\eta_{trs}^n(r_{trs}(t))} \quad (5.10)$$

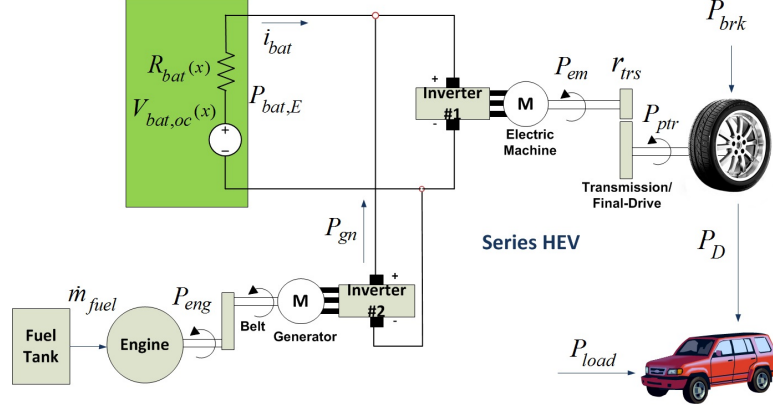


Figure 5.1: The configuration of the powertrain in a series HEV in this study.

where η_{trs} is the total efficiency of the transmission (including the final drive) at the gear ratio r_{trs} , and n is defined as:

$$n = \begin{cases} -1 & , \text{when braking/coasting: } P_D(t) \leq 0 \\ 1 & , \text{when accelerating: } P_D(t) > 0 \end{cases}$$

From Fig. 5.1, the electric power of the battery, $P_{bat,E}$, is (t is dropped for easier readability):

$$P_{bat,E} = \frac{P_{em}}{\eta_{em}^n \eta_{inv1}^n} + P_{gn} = \frac{P_D - P_{brk}}{\eta_{trs}^n (r_{trs}) \eta_{em}^n \eta_{inv1}^n} + P_{gn} \quad (5.11)$$

where η_{em} and η_{inv1} are the efficiency of the tractive electric machine and its inverter,

respectively, and P_{gn} is the electric power of the generator which is always non-positive: $P_{gn} \leq 0$. Thus, (5.11) is equivalent to (5.3) for the series HEV shown in Fig. 5.1. In (5.11), $P_{bat,E} < 0$ and $P_{bat,E} > 0$ represent battery charging and discharging, respectively.

During braking/coasting, the obvious optimal action is to keep mechanical P_{brk} as close as possible to 0 and use regenerative braking instead. Therefore, the optimal choice for P_{brk} is known for the EM strategy. As a result, the vector of control actions in (5.11) is:

$$\mathbf{u} = [r_{trs} \quad P_{gn}]^T \quad (5.12)$$

The combination of the generator-engine can be optimized offline based on P_{gn} . Therefore, for a known control P_{gn} , the optimal values of the engine torque and speed that give the minimum \dot{m}_{fuel} can be determined, as stated in (5.9).

5.3 Optimal Equivalent Factor Bounds For Series

HEVs

The value of λ^* in (5.9) depends to the drivecycle and thus, is an unknown constant for causal controllers. However, lower and upper bounds of λ^* can be found that are independent of the drivecycle [41]. Reference [41] shows that regardless of the vehicle configuration or drivecycle, the lower bound of λ^* in (5.9) is:

$$\lambda^* \geq \frac{1}{Q_{lhv}} \quad (5.13)$$

where Q_{lhv} is the fuel lower heating value. In addition, regarding the upper bound of λ^* , reference [41] argues: an infinite λ in (5.9) forces the ECMS to work in engine only mode (*ecom*) for the whole trip. Thus, λ^* must have an upper bound λ_{max} , such that no drivecycle exists with $\lambda^* > \lambda_{max}$. To find λ_{max} , let us assume a drivecycle with $\lambda^* = \lambda_{max}$ is known, where different values of $P_D(t)$ might be requested by the driver for $0 \leq t \leq t_f$. During that drivecycle, when $x_1(t) = SOC_H$, the hybrid mode (*hm*) or battery only mode (*bom*) must be optimal for at least one value of $P_D(t)$, otherwise the HEV remains in *ecom* for the rest of the drivecycle. When $x_1(t) = SOC_H$, if HEV remains in *ecom*, then the brake energy at the end of the drivecycle will be missed

which is not optimal. Therefore, in mathematical terms:

$$\left. \begin{array}{l} x_1 = SOC_H \\ \lambda^* = \lambda_{max} \end{array} \right\} \begin{array}{l} \forall \mathbf{u} \in U \\ \Rightarrow \end{array} \left\{ \begin{array}{l} \exists P_D > 0 : H(\mathbf{u}_{eom}) > H(\mathbf{u}_{bom}^*) \\ \text{or} \\ \exists P_D > 0 : H(\mathbf{u}_{eom}) > H(\mathbf{u}_{hm}^*) \end{array} \right. \quad (5.14)$$

where \mathbf{u}_{eom} , \mathbf{u}_{bom} , and \mathbf{u}_{hm} are the control actions that bring the HEV into one of the modes *eom*, *bom*, and *hm*, respectively. Reference [41] uses (5.14) to find λ_{max} for parallel HEVs. As follows, λ_{max} is calculated for series HEVs.

Substituting (5.9) in the first inequality of (5.14) gives:

$$\lambda^* \leq \frac{\dot{m}_{fuel}(\mathbf{u}_{eom}^*, P_D)}{P_{bat,C}(x, \mathbf{u}_{bom}^*)} \quad (5.15)$$

From Fig. 5.1, substituting (5.11) in (5.15) gives:

$$\lambda^* \leq \frac{\frac{P_{gn}(\mathbf{u}_{eom}^*)}{Q_{lhv} \bar{\eta}_{eng} \bar{\eta}_{btl} \bar{\eta}_{gn} \bar{\eta}_{inv2}}}{\frac{P_{bat,E}(\mathbf{u}_{bom}^*)}{\bar{\eta}_{bat}}} = \frac{\frac{P_{em} / (\eta_{em}^n \eta_{inv1}^n)}{Q_{lhv} \bar{\eta}_{eng} \bar{\eta}_{btl} \bar{\eta}_{gn} \bar{\eta}_{inv2}}}{\frac{P_{em} / (\eta_{em}^n \eta_{inv1}^n)}{\bar{\eta}_{bat}}} \quad (5.16)$$

where $\bar{\eta}_{eng}$, $\bar{\eta}_{btl}$, $\bar{\eta}_{gn}$, $\bar{\eta}_{inv2}$, and $\bar{\eta}_{bat}$ are the average efficiencies of the engine, belt,

generator, inverter #2, and battery, respectively, and η_{em} and η_{inv1} are the efficiencies of the tractive e-motor and inverter #1, respectively. From (5.16) the upper bound of λ^* becomes:

$$\lambda_{\max} = \frac{\bar{\eta}_{bat}}{Q_{lhv} \bar{\eta}_{eng} \bar{\eta}_{btl} \bar{\eta}_{gn} \bar{\eta}_{inv2}} \quad (5.17)$$

Similarly, substituting (5.9) in the second inequality of (5.14) gives:

$$\lambda^* \leq \frac{\dot{m}_{fuel}(u_{eom}^*, P_D) - \dot{m}_{fuel}(u_{hm}^*, P_D)}{P_{bat,C}(x, u_{hm}^*)} \quad (5.18)$$

and substituting (5.11) in (5.18) gives the same λ_{max} as (5.17).

Therefore, for the series HEV shown in Fig. 5.1 and for any drivecycle, λ^* is bounded by:

$$\frac{1}{Q_{lhv}} \leq \lambda^* \leq \frac{\bar{\eta}_{bat}}{Q_{lhv} \bar{\eta}_{eng} \bar{\eta}_{btl} \bar{\eta}_{gn} \bar{\eta}_{inv2}} = \frac{\bar{\eta}}{Q_{lhv}} \quad (5.19)$$

where $\bar{\eta}$ is defined as: $\bar{\eta} = \bar{\eta}_{bat} / (\bar{\eta}_{eng} \bar{\eta}_{btl} \bar{\eta}_{gn} \bar{\eta}_{inv2})$.

5.4 The Proposed Energy Management Strategy, ECMS-CESO, For Series HEVs

The proposed EM strategy, ECMS-CESO, has been previously introduced in [39] for parallel HEVs. This work develops ECMS-CESO for series HEVs. The main idea of ECMS-CESO is to catch energy saving opportunities (CESO) when possible. The constraint (5.5) restricts causal controllers from energy saving when the SOC is at a limit. For example when $x_1(t) = SOC_H$, if the driver presses the brake pedal ($P_D(t + dt) \leq 0$), then the EM strategy is not allowed to catch this energy saving opportunity via regenerative braking. The same scenario happens when $x_1(t) = SOC_L$ and $P_D(t + dt) > 0$ is such that *hm* or *bom* are optimal but cannot be applied due to (5.5). Predictive controllers can avoid such situations. However, a prediction of the driver demanded power is uncertain [24][26][43][46].

In order to catch energy saving opportunities, the authors propose defining soft SOC bounds inside the range (5.5) where the EM strategy is allowed to exceed these soft bounds, as presented in Fig. 5.2. ECMS-CESO replaces the hard SOC limits in (5.5) with the newly defined soft constraints:

$$SOC_L^{soft} \leq x_1(t) \leq SOC_H^{soft} \quad , \quad t \in [0 \quad t_f] \quad (5.20)$$

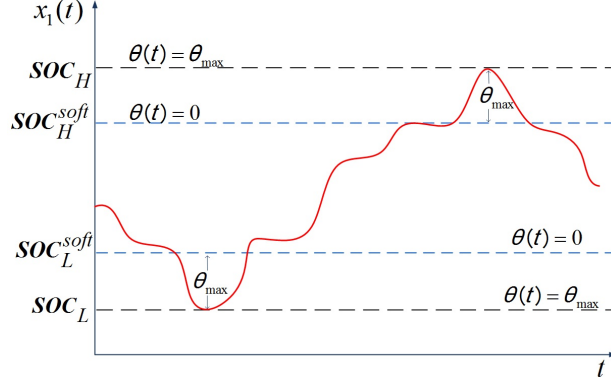


Figure 5.2: ECMS-CESO defines new soft bounds for the SOC inside the actual hard limits SOC_L and SOC_H . ECMS-CESO is allowed to exceed the soft bounds by $\theta(t)$ when there is an energy saving opportunity. When the soft bounds are exceeded, the equivalent factor is modified. If $\theta(t) = \theta_{max}$, the equivalent factor becomes modified enough that it prevents the ECMS-CESO from violating (5.5).

However, unlike (5.5), ECMS-CESO allows SOC to exceed (5.20) by $\theta(t)$ if an energy saving opportunity is available. To maintain (5.5), ECMS-CESO is punished for exceeding (5.20). As $\theta(t)$ becomes larger, the punishment becomes higher until the punishment becomes big enough that it prohibits $\theta(t) > \theta_{max}$. The main advantage of this strategy is that since (5.5) is replaced with (5.20), the EM strategy has a better chance in catching energy saving opportunities. Another advantage of ECMS-CESO is employing (5.19) for estimating λ^* which is explained as follows.

Using (5.20), (5.7) becomes:

$$\begin{aligned} \dot{x}_2 = & \left(x_1 - SOC_L^{soft}\right)^2 S\left(x_1 - SOC_L^{soft}\right) \\ & + \left(SOC_H^{soft} - x_1\right)^2 S\left(SOC_H^{soft} - x_1\right) \end{aligned} \quad (5.21)$$

where the boundary condition (5.8) can now be eliminated from the control problem because ECMS-CESO is allowed to exceed (5.20). Since (5.7) is changed, the derivation of (5.9), needs to be modified accordingly. From (5.1), (5.4), and (5.21), the Hamiltonian is [39]:

$$H = \dot{m}_{fuel}(\mathbf{u}(t)) + \lambda(t) P_{bat,C}(x_1(t), \mathbf{u}(t)) + p_2(t)\dot{x}_2(t) \quad (5.22)$$

which gives (to improve readability, the time variable t is dropped) [17]:

$$\dot{p}_2^* = -\frac{\partial H}{\partial x_2} = 0 \quad \Rightarrow \quad p_2^* = \text{constant} \quad (5.23)$$

$$\dot{\lambda}^* = \frac{1}{Q_{bat}V_{bat,oc}(x_1)} \frac{\partial H}{\partial x_1} = \frac{\lambda^* \frac{\partial P_{bat,C}}{\partial x_1} + p_2^* \frac{\partial \dot{x}_2}{\partial x_1}}{Q_{bat}V_{bat,oc}(x_1)} \quad (5.24)$$

The range (5.5) is chosen based on the SOC range where the battery is most efficient.

In this range, $V_{bat,oc}$ and $P_{bat,C}$ are almost independent of x_1 [1]. Thus:

$$\dot{\lambda}^* \approx \frac{p_2^*}{Q_{bat}V_{bat,oc}} \frac{\partial \dot{x}_2}{\partial x_1} \quad (5.25)$$

and from (5.21):

$$\dot{\lambda}^*(t) \approx \frac{-2p_2^* \theta(t)}{Q_{bat} V_{bat,oc}} \quad (5.26)$$

where the exceeding $\theta(t)$ is defined as:

$$\theta(t) = \begin{cases} 0 & , SOC_L^{soft} \leq x_1(t) \leq SOC_H^{soft} \\ SOC_L^{soft} - x_1(t) & , x_1(t) < SOC_L^{soft} \\ x_1(t) - SOC_H^{soft} & , x_1(t) > SOC_H^{soft} \end{cases} \quad (5.27)$$

For the first case in (5.27):

$$\dot{\lambda}^*(t) = 0 \Rightarrow \lambda^*(t) = \text{constant} = \mu \quad (5.28)$$

where μ is a constant to be chosen later. For the second case, assuming the exceeding $x_1(t) < SOC_L^{soft}$ starts at the time t_1 , then (5.26) gives:

$$\lambda^*(t) = \lambda^*(t_1) - \frac{2p_2^*}{Q_{bat} V_{bat,oc}} \Psi(\theta(t), t) \quad (5.29)$$

where $\Psi(\theta(t), t)$ is a drivecycle dependent function:

$$\Psi(\theta(t), t) = \int_{t_1}^t \theta(\tau) d\tau \quad (5.30)$$

According to (5.28), a moment before exceeding starts: $\lambda^*(t_1 - dt) = \mu$. Therefore, (5.29) becomes:

$$x_1(t) < SOC_L^{soft} \Rightarrow \lambda^*(t) = \mu - \frac{2p_2^* \Psi(\theta(t), t)}{Q_{bat} V_{bat,oc}} \quad (5.31)$$

Similarly, when $x_1(t) > SOC_H^{soft}$:

$$x_1(t) > SOC_H^{soft} \Rightarrow \lambda^*(t) = \mu - \frac{2p_2^* \Psi(\theta(t), t)}{Q_{bat} V_{bat,oc}} \quad (5.32)$$

To find a formula for calculating $\lambda^*(t)$ from (5.28), (5.31), and (5.32), values of μ and p_2^* must be found. Fortunately, the range of λ^* is known from (5.19). Thus, μ and p_2^* will be chosen such that $\lambda(t)$ always remains inside the range in (5.19). For μ the

author proposes the middle point of the range in (5.19):

$$\mu = \frac{\bar{\eta} + 1}{2Q_{lhv}} \quad (5.33)$$

Also, p_2^* is chosen to ensure $\lambda^*(t)$ always falls within (5.19). In other words, p_2^* will be chosen such that:

$$\begin{aligned} \theta(t) = \theta_{max} : \quad x_1(t) = SOC_L &\Rightarrow \lambda(t) = \bar{\eta}/Q_{lhv} \\ \theta(t) = \theta_{max} : \quad x_1(t) = SOC_H &\Rightarrow \lambda(t) = 1/Q_{lhv} \end{aligned} \quad (5.34)$$

where θ_{max} is the desired maximum distance that SOC is allowed to exceed from the soft constraints (See Fig. 5.2). Since, such selection for p_2^* is not necessarily optimal, ECMS-CESO becomes a sub-optimal controller and thus, the optimal symbol for p_2 is dropped. Therefore, to enforce (5.34) for $\lambda(t)$ in (5.31) and (5.32):

$$x_1(t) < SOC_L^{soft} \Rightarrow p_2 = \frac{\mu - \bar{\eta}/Q_{lhv}}{2/(Q_{bat} V_{bat,oc})} \left(\frac{\theta(t)}{\theta_{max}} \right)^2 \quad (5.35)$$

$$x_1(t) > SOC_H^{soft} \Rightarrow p_2 = \frac{\mu - 1/Q_{lhv}}{2/(Q_{bat} V_{bat,oc})} \left(\frac{\theta(t)}{\theta_{max}} \right)^2 \quad (5.36)$$

Finally, substituting (5.35) and (5.36) into (5.31) and (5.32), respectively, yields a formula for calculating the adaptive $\lambda(t)$ in ECMS-CESO:

$$\lambda(t) = \left\{ \begin{array}{l} \frac{\bar{\eta} + 1}{2 Q_{lhv}} \quad , SOC_L^{soft} \leq x_1 \leq SOC_H^{soft} \\ \frac{\bar{\eta} + 1}{2 Q_{lhv}} + \frac{\bar{\eta} - 1}{2 Q_{lhv}} \left(\frac{\theta(t)}{\theta_{max}} \right)^2 \quad , \theta(t) = SOC_L^{soft} - x_1 > 0 \\ \frac{\bar{\eta} + 1}{2 Q_{lhv}} - \frac{\bar{\eta} - 1}{2 Q_{lhv}} \left(\frac{\theta(t)}{\theta_{max}} \right)^2 \quad , \theta(t) = x_1 - SOC_H^{soft} > 0 \end{array} \right. \quad (5.37)$$

5.5 Achieving The Hard SOC Constraints

To ensure ECMS-CESO maintains (5.5), let us assume $x_1(t) = SOC_L$ and $P_D(t) > 0$.

It is enough to show under such situations battery discharging cannot be optimal.

Here, it is shown that if $x_1(t) = SOC_L$ and $P_D(t) > 0$, then the cost of *ecom* is less than the costs of *hm* or *bom*:

$$\begin{aligned}
 &P_D > 0 \quad \text{and} \quad x_1(t) = SOC_L \Rightarrow \\
 &\forall \mathbf{u} \in \{\mathbf{u}_{ecom}\} \cup \{\mathbf{u}_{hm}\} \cup \{\mathbf{u}_{bom}\} : \\
 &\exists \mathbf{u}_{ecom}^0 \in \{\mathbf{u}_{ecom}\} \quad \text{such that:} \quad H(\mathbf{u}_{ecom}^0) < H(\mathbf{u})
 \end{aligned} \tag{5.38}$$

In (5.38), $H(\mathbf{u}_{ecom}^0) < H(\mathbf{u})$ requires:

$$\left\{ \begin{array}{l} H(\mathbf{u}_{ecom}^0) < H(\mathbf{u}_{bom}) \quad , \quad \forall \mathbf{u}_{bom} \in \{\mathbf{u}_{bom}\} \\ H(\mathbf{u}_{ecom}^0) < H(\mathbf{u}_{hm}) \quad , \quad \forall \mathbf{u}_{hm} \in \{\mathbf{u}_{hm}\} \end{array} \right. \tag{5.39}$$

Using (5.22), the above inequalities become:

$$\left\{ \begin{array}{l} \dot{m}_{fuel}(\mathbf{u}_{ecom}^0) < \lambda P_{bat,C}(x_1, \mathbf{u}_{bom}) \\ \dot{m}_{fuel}(\mathbf{u}_{ecom}^0) < \dot{m}_{fuel}(\mathbf{u}_{hm}) + \lambda P_{bat,C}(x_1, \mathbf{u}_{hm}) \end{array} \right. \tag{5.40}$$

For series HEVs, substituting (5.11) into (5.40) gives:

$$\left\{ \begin{array}{l} \frac{P_{em}/(\bar{\eta}_{em} \bar{\eta}_{inv1})}{Q_{lhv} \bar{\eta}_{eng} \bar{\eta}_{blt} \bar{\eta}_{gn} \bar{\eta}_{inv2}} < \lambda \frac{P_{em}/(\bar{\eta}_{em} \bar{\eta}_{inv1})}{\bar{\eta}_{bat}} \\ \frac{P_{em}}{Q_{lhv} \bar{\eta}_{bat}/\bar{\eta}} < \frac{P_{em}}{Q_{lhv} \bar{\eta}_{bat}/\bar{\eta}} - \frac{P_{bat,E}}{Q_{lhv} \bar{\eta}_{bat}/\bar{\eta}} + \lambda \frac{P_{bat,E}}{\bar{\eta}_{bat}} \end{array} \right. \quad (5.41)$$

Both inequalities in (5.41) give:

$$\frac{\bar{\eta}}{Q_{lhv}} < \lambda \quad (5.42)$$

which indicates that when $x_1(t) = SOC_L$, if the A-ECMS sets $\lambda(t)$ *slightly* higher than the upper bound in (5.37), then the battery will not be further discharged.

In (5.41) the average efficiencies are used. However, the change in the efficiency of a component might be high from one operating point to another. Thus, one might argue (5.42) is not an accurate threshold for preventing $x_1(t) < SOC_L$. From (5.37), ECMS-CESO continues to increase $\lambda(t)$ if $x_1(t) < SOC_L$. Therefore, the violation from the lower bound, if it happens, will be limited. However, in order to enforce (5.5), the authors propose using (5.42) to tune $\bar{\eta}$ for ECMS-CESO. Based on the definition,

the initial $\bar{\eta}$ value can be acquired from: $\bar{\eta} = \bar{\eta}_{bat}/(\bar{\eta}_{eng} \bar{\eta}_{btt} \bar{\eta}_{gn} \bar{\eta}_{inv2})$. Then, ECMS-CESO should be tested on several different drivecycles. If $x_1(t) < SOC_L$ is observed, then $\bar{\eta}$ should be increased.

Regarding the SOC upper limit, when $x_1(t) = SOC_H$ and $P_D(t) > 0$, ECMS-CESO must avoid charging mode (cm). It is enough to show under such conditions, bom has less cost than cm :

$$\begin{aligned} P_D > 0 \text{ and } x_1(t) = SOC_H \text{ and } \lambda = 1/Q_{lhv} \\ \Rightarrow H(\mathbf{u}_{bom}) < H(\mathbf{u}_{cm}) \end{aligned} \quad (5.43)$$

Assuming the above statement is wrong and $H(\mathbf{u}_{bom}) > H(\mathbf{u}_{cm})$. Then, using (5.22):

$$\lambda P_{bat,C}(x_1, \mathbf{u}_{bom}) > \dot{m}_{fuel}(\mathbf{u}_{cm}) + \lambda P_{bat,C}(x_1, \mathbf{u}_{cm}) \quad (5.44)$$

For series HEVs, substituting (5.11) into (5.44) gives:

$$\lambda \frac{P_{em}}{\bar{\eta}_{em} \bar{\eta}_{inv1} \bar{\eta}_{bat}} > \frac{P_{em}}{\bar{\eta}_{em} \bar{\eta}_{inv1}} - \frac{P_{bat,E}}{Q_{lhv} \bar{\eta}_{bat} / \bar{\eta}} + \lambda P_{bat,E} \bar{\eta}_{bat} \quad (5.45)$$

Simplifying the above inequality by setting $\lambda = 1/Q_{lhv}$, gives:

$$(1 - \bar{\eta}) \frac{P_{em}}{\bar{\eta}_{em} \bar{\eta}_{inv1}} > (\bar{\eta}_{bat}^2 - \bar{\eta}) P_{bat,E} \quad (5.46)$$

In *cm*: $P_{bat,E} < 0$. Also, $P_D(t) > 0$ requires $P_{em} > 0$. In addition: $\bar{\eta} > 1$. Thus, the right side of the above inequality is positive and the left side is negative, which is not possible. Therefore, the statement (5.43) must be correct.

5.6 Experimental Setup

This section introduces the experimental setup that is designed and built at Michigan Technological University. More details on the experimental setup design can be found in [47]. The setup is comprised of a 2.0-liter spark ignition (SI) engine and a 100-kW electric powertrain, which are connected to a 465 hp double-ended AC dynamometer.

Figure 5.3 shows the developed experimental setup.



Figure 5.3: Developed hybrid electric powertrain experimental setup connected to a double-ended 465 hp AC dynamometer at Michigan Technological University.

The SI engine setup includes a GM 2.0-liter Ecotec Gasoline Direct Injection Turbocharged SI engine. Table 5.1 lists the engine specifications. Engine control units included dSPACE[®] MicroAutoBox (MABx) DS1511 and RapidPro units. Models for control of cam phasers, fuel pump, injectors, spark plugs, supercharger, throttle body, and EGR valve were developed in Simulink[®]. These models were compiled into a single engine control program, and related parameters were monitored and controlled in real-time using the dSPACE ControlDesk[®].

Table 5.1
Parameters of the SI engine in this study

Parameters	Value/Description
Engine Model	GM Ecotec LHU
Bore x Stroke	86 x 86 mm
Number of Cylinders	4
Displacement Volume	2.0 L
Compression Ratio	9.2:1
Connecting Rod Length	145.5 mm
Max Power	270 hp @6000 rpm
Fuel Injection System	Gasoline Direct Injection
Valve System	DOHC 4 Valves

Using the data acquired from dSPACE[®], LabVIEW[®] and ACAP[®], the combustion and performance parameters were calculated using an in-house Matlab[®] code. The brake specific fuel consumption (BSFC) maps were generated and the load limits for each of the combustion modes were determined. The test setup runs with a 100 kW synchronous induction Remy motor, which is controlled by RMS PM100DX inverter. Using the experimental data collected from the experimental setup, the e-motor efficiency map is calculated by measuring the e-motor input and output powers. Two LG Chem batteries are used to supply the electric energy for the electric motor

(see Table 5.2). The mechanical drivetrain, including the e-motor mount, coupling, and shafts, is designed and manufactured at Michigan Technological University. The high voltage battery during the operation is connected to the e-motor through a designed pre-charge circuit. The MABx is used as a supervisory controller to monitor sub-level controllers (i.e., battery, e-motor, etc.). The MABx communicates control commands on the CAN bus to the sub-level controllers. The LG Chem battery temperature is controlled through a fan and all the cooling systems are controlled by the supervisory controller. A fault-action module was developed in Matlab[®] to manage the setup during faults and extreme conditions.

Table 5.2
Battery specifications.

Parameters	Values
Energy Capacity (kWh)	5
Maximum Voltage (V)	410
Nominal Voltage (V)	360
Minimum Voltage (V)	260
SOC Operating Range (%)	30-70
Battery Pack Mass (kg)	90

5.7 Simulation Results

A quasi-static model for the series HEV shown in Fig. 5.1 was created in Simulink[®]. Each component of the model is individually validated by measured data from the experimental setup discussed in the previous section. The specifications of the simulated

vehicle is presented in Table 5.3

Table 5.3
Vehicle specifications.

Parameters	Values
Vehicle Curb Mass	1588 (Kg)
Frontal Area	3.3 (m^2)
Engine Motor Coupling Gear Ratio	1.5 (-)
Transmission Ratios	[1.34 0.63] (-)
Differential Ratio	3.73 (-)
Wheel Radius	0.36 (m)
Drag Coefficient	0.364 (-)
Rolling Resistance Coefficient	0.015 (-)

ECMS-CESO is a type of A-ECMS, and hence, its performance is compared with dynamic programming (DP) and a predictive A-ECMS based in [12]. In this predictive A-ECMS, first, a prediction of future driver's demanded power is made by an artificial neural network. Then, the optimal trajectory of the battery state of charge (SOC) on the predicted future horizon is calculated. Finally, a PI controller is implemented in predictive A-ECMS which calculates $\lambda(t)$ from the difference between the optimal SOC and the actual SOC, as follows:

$$\lambda(t) = \frac{\bar{\eta}_{em}}{\bar{\eta}_{eng}} + K_p(x_1^*(t) - x_1(t)) + K_i \int_0^t (x_1^*(t) - x_1(t)) dt \quad (5.47)$$

where x_1^* and x_1 are the optimal and actual SOC, respectively, K_p and K_i are the coefficients of the PI controller, and $\bar{\eta}_{em}$ and $\bar{\eta}_{eng}$ are the average efficiencies of the electric motor and the engine, respectively. DP yields the globally optimal performance. For

implementing the predictive A-ECMS, instead of using the specified prediction algorithm, the exact information about the future driving conditions are provided to the controller. Since the prediction uncertainty is eliminated, the performance of the simulated A-ECMS should be better than the proposed A-ECMS in [12]. For each drivecycle, the optimal SOC trajectory is obtained from DP and is used by the PI controller of A-ECMS as in (5.47).

Table 5.4 represents the simulation results for standard drivecycles. With respect to DP, the results show the performance of ECMS-CESO is better than A-ECMS. Also, for the UDDS drivecycle ECMS-CESO achieves better FE in comparison with the A-ECMS in [12]. For the HWFET and NEDC drivecycles, A-ECMS yields slightly higher FE than ECMS-CESO (MPG values are rounded). However, A-ECMS has also consumed more electric energy than ECMS-CESO on HWFET and NEDC (lower final SOC). Whereas, DP and A-ECMS have the benefit of knowing the entire drivecycle in advance, ECMS-CESO achieves a comparable performance with instantaneous optimization. As was mentioned, thanks to having perfect knowledge about the entire drivecycle, the performance of the simulated A-ECMS is equal or better than the proposed A-ECMS in [12]. Thus, with no prediction, ECMS-CESO has achieved comparable performance with respect to predictive A-ECMS.

Figure 5.4 shows the trajectories of SOC, fuel consumption rate, and λ on the UDDS drivecycle. As can be seen, the A-ECMS in [12] closely tracks the reference optimal

Table 5.4

Fuel economy (MPG) and final SOC $x_1(t_f)$ results for different control strategies. All simulations start at $x_1(0) = 60\%$. The SOC range in (5.5) is from 40% to 70%. For ECMS-CESO: $\theta_{max} = 6\%$, and $1 \leq Q_{lhw}\lambda^* \leq 4.78$. For all of simulations, the average and variance of speed tracking error are in orders of 0.005 (m/s) and 0.001, respectively

Drivecycle	MPG (Final SOC %)		
	ECMS-CESO	A-ECMS	DP
UDDS	72 (43.7)	69 (43.3)	75 (43.7)
HWFET	39 (45.2)	39 (44.4)	41 (45.2)
US06	26 (44.8)	25 (44.6)	27 (44.8)
NEDC	43 (42.9)	43 (40.8)	49 (42.9)

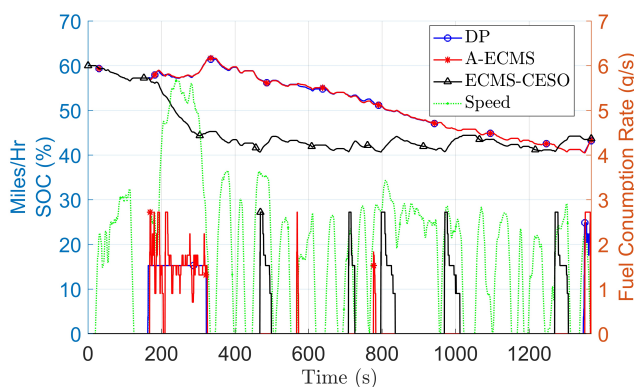


Figure 5.4: Trajectories of SOC and fuel consumption rate for the UDDS drivecycle

SOC trajectory obtained from DP. The PI controller in A-ECMS calculates $\lambda(t)$ from the difference between the optimal SOC and actual SOC. Thus, when the actual SOC becomes less than optimal SOC, A-ECMS increases $\lambda(t)$ to add more value to the battery power. According to (5.9), increasing $\lambda(t)$ raises the chance of consuming more fuel by the EM strategy. For instance, in Fig. 5.4, A-ECMS turns the engine on at times 570 and 780 s in response to the actual SOC being smaller than the optimal SOC. Thus, the achieved FE from A-ECMS becomes less than DP, and as can be seen in Table 5.4, becomes less than ECMS-CESO as well.

The effect of the soft constraints on the SOC trajectory of ECMS-CESO can be observed in Fig. 5.4. For this simulation: $SOC_L = 40\%$, $SOC_H = 70\%$, and $\theta_{max} = 6\%$. Therefore, ECMS-CESO tries to maintain the SOC in the range $46 \leq x_1(t) \leq 64$, unless an energy saving opportunity is available or the engine alone cannot provide the driver requested power $P_D(t)$. Under such conditions, ECMS-CESO exceeds either the soft constraint $SOC_L^{soft} = 46\%$, or $SOC_H^{soft} = 64\%$. The SOC of ECMS-CESO never reaches $SOC_L = 40\%$ which can be justified by the adaptive behavior of ECMS-CESO. According to (5.37), when $x_1(t) = SOC_L$, ECMS-CESO sets $\lambda(t) = \bar{\eta}/Q_{lhv}$ which is the upper bound of λ^* in (5.19). As a reminder, no driving condition exists with $\lambda^* > \bar{\eta}/Q_{lhv}$, which makes $\bar{\eta}/Q_{lhv}$ the highest optimal penalty value in (5.9). Thus, ECMS-CESO uses this high penalty at $x_1(t) = SOC_L$ only after a highly valuable energy saving opportunity has occurred. For the UDDS drivecycle in Fig. 5.4, such a valuable opportunity does not occur. Also, in Fig. 5.4 at the times 350, 500, 840, and 1050 s, ECMS-CESO exceeds $SOC_L^{soft} = 46\%$ to catch available energy saving opportunities. But, since the penalty factor $\lambda(t)$ rises for exceeding SOC_L^{soft} , ECMS-CESO turns the engine on and increases the SOC shortly after exceeding SOC_L^{soft} .

This desired behavior improves the robustness of ECMS-CESO in terms of providing the driver requested power. In addition, since the chance of $x_1(t) = SOC_L$ is low, ECMS-CESO is less likely to be limited by a depleted battery. This behavior is achieved by defining the soft constraints for ECMS-CESO and employing the bounds

on λ^* (5.19).

5.8 Conclusion

A new energy management strategy, previously introduced for parallel HEVs, was developed for a series HEV. Two characteristics distinguish ECMS-CESO from other types of A-ECMSs: 1) ECMS-CESO uses knowledge about the range of λ^* to set an adaptive $\lambda(t)$, 2) soft constraints on SOC are defined and exceeding these soft constraints is penalized. Here, the bounds on λ^* were determined for a series HEV. The λ^* bounds are drivecycle independent and thus, are used by ECMS-CESO to set an adaptive $\lambda(t)$. ECMS-CESO was designed to ensure the adaptive $\lambda(t)$ always remains inside the determined λ^* range. In addition, the SOC soft constraints allow ECMS-CESO to catch energy saving opportunities when available. In other words, ECMS-CESO was designed to maintain SOC between the soft bounds. However, when an energy saving opportunity is available, or when the engine only cannot deliver the demanded power, ECMS-CESO is allowed to exceed the SOC soft constraints. It was shown that even when exceeding the soft constraints, SOC still remains between the hard limits. Using experimental data, a model for a series HEV was developed to evaluate ECMS-CESO performance by comparing it with dynamic programming and a predictive-based A-ECMS. Results show that the performance of ECMS-CESO is equal or better than those obtained with the prediction-based A-ECMS. Note that

the performance of ECMS-CESO was achieved without any knowledge about future driving conditions. Therefore, the implementation of ECMS-CESO is cheap and easy, which makes it a tractable, real-time energy management strategy for HEVs.

References

- [1] A. Sciarretta and L. Guzzella, “Control of Hybrid Electric Vehicles,” *IEEE Control Systems Magazine*, vol. 27, no. 2, pp. 60–70, 2007.
- [2] A. Solouk, M. Shahbakhti, and M. Mahjoub, “Energy Management and Control of a Hybrid Electric Vehicle with an Integrated Low Temperature Combustion (LTC) Engine,” in *Proceedings of ASME 2014 Dynamic Systems and Control Conference*, San Antonio, TX, USA, 2014.
- [3] S. D. Cairano, D. Bernardini, A. Bemporad, and I. V. Kolmanovsky, “Stochastic MPC With Learning for Driver-Predictive Vehicle Control and its Application to HEV Energy Management,” *IEEE Transactions on Control Systems Technology*, vol. 22, no. 3, pp. 1018–1031, 2014.
- [4] H. Borhan, A. Vahidi, A. M. Phillips, M. L. Kuang, I. V. Kolmanovsky, and S. D. Cairano, “MPC-Based Energy Management of a Power-Split Hybrid Electric

- Vehicle,” *IEEE Transactions on Control Systems Technology*, vol. 20, no. 3, pp. 593–603, 2012.
- [5] Y. Huang, H. Wang, A. Khajepour, H. He, and J. Ji, “Model predictive control power management strategies for HEVs: A review,” *Journal of Power Sources*, vol. 341, pp. 91–106, 2017.
- [6] A. Solouk and M. Shahbakhti, “Energy Optimization and Fuel Economy Investigation of a Series Hybrid Electric Vehicle Integrated with Diesel/RCCI Engines,” *Energies*, vol. 9, no. 12, p. 1020, 2016.
- [7] A. Rezaei and J. B. Burl, “Effects of Time Horizon on Model Predictive Control for Hybrid Electric Vehicles,” *IFAC-PapersOnLine*, vol. 48, no. 15, pp. 252–256, 2015.
- [8] N. Kim, S. Cha, and H. Peng, “Optimal Control of Hybrid Electric Vehicles Based on Pontryagins Minimum Principle,” *IEEE Transactions on Control Systems Technology*, vol. 19, no. 5, pp. 1279 – 1287, 2011.
- [9] G. Paganelli, G. Ercole, A. Brahma, Y. Guezennec, and G. Rizzoni, “General supervisory control policy for the energy optimization of charge-sustaining hybrid electric vehicles,” *JSAE Review*, vol. 22, no. 4, pp. 511–518, 2001.
- [10] C. Musardo, G. Rizzoni, and B. Staccia, “A-ECMS: An Adaptive Algorithm for Hybrid Electric Vehicle Energy Management,” in *44th IEEE Conference on*

- Decision and Control and European Control Conference*, Seville, Spain, 2005, pp. 1816–1823.
- [11] C. Zhang and A. Vahidi, “Route Preview in Energy Management of Plug-in Hybrid Vehicles,” *IEEE Transactions on Control Systems Technology*, vol. 20, no. 2, pp. 546–553, 2012.
- [12] F. Tianheng, Y. Lin, G. Qing, H. Yanqing, Y. Ting, and Y. Bin, “A Supervisory Control Strategy for Plug-In Hybrid Electric Vehicles Based on Energy Demand Prediction and Route Preview,” *IEEE Transactions on Vehicular Technology*, vol. 64, no. 5, pp. 1691–1700, 2015.
- [13] M. Vajedi, A. Taghavipour, N. L. Azad, and J. McPhee, “A comparative analysis of route-based power management strategies for real-time application in plug-in hybrid electric vehicles,” in *American Control Conference (ACC)*, Portland, Oregon, USA, 2014, pp. 2612–2617.
- [14] A. Chasse, A. Sciarretta, and J. Chauvin, “Online optimal control of a parallel hybrid with costate adaptation rule,” *IFAC Proceedings Volumes*, vol. 43, no. 7, pp. 99–104, 2010.
- [15] A. Chasse, G. Hafidi, P. Pognant-Gros, and A. Sciarretta, “Supervisory Control of Hybrid Powertrains: an Experimental Benchmark of Offline Optimization and Online Energy Management,” *IFAC Proceedings Volumes*, vol. 42, no. 26, pp. 109–117, 2009.

- [16] S. Onori, L. Serrao, and G. Rizzoni, *Hybrid Electric Vehicles Energy Management Strategies*, ser. SpringerBriefs in Electrical and Computer Engineering Control, Automation and Robotics. Springer, 2016, chap. 4-7.
- [17] D. E. Kirk, *Optimal Control Theory: An Introduction*. Mineola, NY, USA: Dover Publications, 2004, chap. 5.
- [18] C.-C. Lin, H. Pengl, and J. Grizzle, “A Stochastic Control Strategy for Hybrid Electric Vehicles,” in *Proceedings of American Control Conference*, Boston, MA, USA, vol. 5, 2004, pp. 4710 – 4715.
- [19] N. Kim and A. P. Rousseau, “Comparison between Rule-Based and Instantaneous Optimization for a Single-Mode, Power-Split HEV,” *SAE Technical Paper No. 2011-01-0873*, 2011.
- [20] J. Peng, H. He, and R. Xiong, “Rule based energy management strategy for a seriesparallel plug-in hybrid electric bus optimized by dynamic programming,” *Applied Energy*, vol. 185, Part 2, pp. 1633–1643, 2017.
- [21] C. Vagg, S. Akehurst, C. J. Brace, and L. Ash, “Stochastic dynamic programming in the real-world control of hybrid electric vehicles,” *IEEE Transactions on Control Systems Technology*, vol. PP, no. 99, pp. 1–14, 2016.
- [22] C. Dextreit and I. V. Kolmanovsky, “Game Theory Controller for Hybrid Electric Vehicles,” *IEEE Transactions on Control Systems Technology*, vol. 22, no. 2, pp. 652–663, 2014.

- [23] Y. Hu, L. Yang, B. Yan, T. Yan, and P. Ma, “An Online Rolling Optimal Control Strategy for Commuter Hybrid Electric Vehicles Based on Driving Condition Learning and Prediction,” *IEEE Transactions on Vehicular Technology*, vol. 65, no. 6, pp. 4312–4327, 2016.
- [24] T. Cummings, T. H. Bradley, and Z. D. Asher, “The Effect of Trip Preview Prediction Signal Quality on Hybrid Vehicle Fuel Economy,” *IFAC-PapersOnLine*, vol. 48, no. 15, pp. 271–276, 2015.
- [25] A. Sciarretta, M. Back, and L. Guzzella, “Optimal Control of Parallel Hybrid Electric Vehicles,” *IEEE Transactions on Control Systems Technology*, vol. 12, no. 3, pp. 352–363, 2004.
- [26] A. Rezaei and J. B. Burl, “Prediction of Vehicle Velocity for Model Predictive Control,” *IFAC-PapersOnLine*, vol. 48, no. 15, pp. 257–262, 2015.
- [27] J. Conti and P. Holtberg, *International Energy Outlook 2011*. U.S. Energy Information Administration, 2011.
- [28] V. Freyermuth, E. Fallas, and A. Rousseau, “Comparison of Powertrain Configuration for Plug-in HEVs from a Fuel Economy Perspective,” *SAE Int. J. Engines*, vol. Vol. 1, no. Issue 1, pp. 392–398, 2008.
- [29] C.-C. Lin, H. Peng, and J. W. Grizzle, “Power Management Strategy for a Parallel Hybrid Electric Truck,” *IEEE Transactions on Control Systems Technology*, vol. VOL. 11, no. NO. 6, pp. 839 – 849, 2003.

- [30] M. Salman, N. J. Schouten, and N. A. Kheir, “Control strategies for parallel hybrid vehicles,” in *Proceedings of the American Control Conference, Chicago, Illinois*, 2000, pp. 524–528.
- [31] B. M. Baumann, G. Washington, B. C. Glenn, and G. Rizzoni, “Mechatronic design and control of hybrid electric vehicles,” *IEEE/ASME Transactions On Mechatronics*, vol. VOL. 5, no. NO. 1, p. 15, 2000.
- [32] N. J. Schouten, M. A. Salman, and N. A. Kheir, “Fuzzy Logic Control for Parallel Hybrid Vehicles,” *IEEE Transactions on Control Systems Technology*, vol. Vol. 10, p. 9, 2002.
- [33] J. Moreno, M. E. Ortuzar, and J. W. Dixon, “Energy-management system for a hybrid electric vehicle, using ultracapacitors and neural networks,” *Industrial Electronics, IEEE Transactions on*, vol. 53, no. 2, pp. 614–623, 2006.
- [34] S. Stockar, V. Marano, G. Rizzoni, and L. Guzzella, “Optimal Control for Plug-in Hybrid Electric Vehicle Applications,” in *American Control Conference (ACC)*, Baltimore, MD, USA, 2010, pp. 5024–5030.
- [35] A. Simon, P. Michel, D. Nelson-Gruel, Y. Chamaillard, and C. Nouillant, “Gasoline-HEV Equivalent Consumption and Pollutant Minimization Strategy,” in *Vehicle Power and Propulsion Conference (VPPC), 2015 IEEE*, Montreal, Canada, 2015, pp. 1–6.

- [36] G. Rousseau, D. Sinoquet, and P. Rouchon, “Constrained Optimization of Energy Management for a Mild-Hybrid Vehicle,” *Oil and Gas Science and Technology - Revue de l’IFP*, vol. 62, no. 4, pp. 623–634, 2007.
- [37] M. Maduro and G. Rohrauer, “Well-to-wheel energy use and greenhouse gas emissions analysis of hypothetical fleet of electrified vehicles in canada and the u.s.” SAE International, 2011, 2011-01-0910.
- [38] G. PAGANELLI, S. DELPRAT, T. GUERR, J. RIMAUX, and J. SANTIN, “Equivalent consumption minimization strategy for parallel hybrid powertrains,” in *Vehicular Technology Conference, 2002. VTC Spring 2002. IEEE 55th*, vol. 4, 2002, pp. 2076 – 2081.
- [39] A. Rezaei, J. Burl, B. Zhou, and M. Rezaei, “A New Real-Time Optimal Energy Management Strategy for Hybrid Electric Vehicles,” *IEEE Transactions on Control Systems Technology*, vol. Under Review, 2016.
- [40] C. Zhang, A. Vahidi, P. Pisu, X. Li, and K. Tennant, “Role of Terrain Preview in Energy Management of Hybrid Electric Vehicles,” *IEEE Transactions on Vehicular Technology*, vol. 59, no. 3, pp. 1139–1147, 2010.
- [41] A. Rezaei, J. B. Burl, and B. Zhou, “Estimation of the ECMS Penalty Factor Bounds for Hybrid Electric Vehicles,” *IEEE Transactions on Control Systems Technology*, vol. Under Review, 2017.

- [42] L. Guzzella and A. Sciarretta, *Vehicle Propulsion Systems, Introduction to Modeling and Optimization*, 3rd ed. Springer, 2013, chap. 7.
- [43] R. Langari and W. Jong-Seob, “Intelligent Energy Management Agent for a Parallel Hybrid Vehicle-Part I: System Architecture and Design of the Driving Situation Identification Process,” *IEEE Transactions on Vehicular Technology*, vol. 54, no. 3, pp. 925–934, 2005.
- [44] M. R. Amini, M. Shahbakhti, S. Pan, and J. K. Hedrick, “Bridging the gap between designed and implemented controllers via adaptive robust discrete sliding mode control,” *Control Engineering Practice*, vol. 59, pp. 1–15, 2017.
- [45] C. Manzie, O. Grondin, A. Sciarretta, and G. Zito, “Robustness of ECMS-based Optimal Control in Parallel Hybrid Vehicles,” *IFAC Proceedings Volumes*, vol. 46, no. 21, pp. 127–132, 2013.
- [46] Y. Yokoi, S. Ichikawa, S. Doki, S. Okuma, T. Naitou, T. Shiimado, and N. Miki, “Driving Pattern Prediction for an Energy Management system of Hybrid Electric Vehicles in a Specific Driving Course,” in *30th Annual Conference of IEEE, Industrial Electronics Society, 2004*, Busan, Korea, vol. 2, 2004, pp. 1727–1732
Vol. 2.
- [47] A. Solouk, M. Shakiba-herfeh, K. Kannan, H. Solmaz, P. Dice, M. Bidarvatan, N. N. T. Kondipati, and M. Shahbakhti, “Fuel Economy Benefits of Integrating a Multi-Mode Low Temperature Combustion (LTC) Engine in a Series Extended

- Range Electric Powertrain,” in *SAE 2016 Int. Powertrain, Fuels and Lubricants Conference*, Baltimore, MD, USA, 2016, SAE Technical Paper No. 2016-01-2361.
- [48] M. Amini, M. Shahbakhti, and J. K. Hedrick, “Discrete Sliding Controller Design with Robustness to Implementation Imprecisions via Online Uncertainty Prediction,” in *2016 American Control Conference (ACC)*, Boston, MA, USA, 2016, pp. 6537–6542.
- [49] S.-I. Ao, *Applied Time Series Analysis and Innovative Computing*, ser. Lecture Notes in Electrical Engineering. Springer, 2010, vol. 59.
- [50] A. E. Bryson and Y.-C. Ho, *Applied Optimal Control: Optimization, Estimation, And Control*. Washington, D.C.: Hemisphere Publishing Corporation, 1975.
- [51] K. Bo-Ah, L. Seung-Hi, L. Young Ok, and C. Chung Choo, “Comparative study of approximate, proximate, and fast model predictive control with applications to autonomous vehicles,” in *Control, Automation and Systems (ICCAS), 2012 12th International Conference on*, 2012, pp. 479–484.
- [52] G. E. P. Box, G. M. Jenkins, and G. C. Reinsel, *Time Series Analysis : Forecasting and Control*, 3rd ed. Prentice Hall Professional Technical Reference, 1995.
- [53] M. Debert, G. Colin, Y. Chamaillard, L. Guzzella, A. Ketfi-Cherif, and B. Bellicaud, “Predictive energy management for hybrid electric vehicles - Prediction

- horizon and battery capacity sensitivity,” in *6th IFAC Symposium Advances in Automotive Control*, 2010, pp. 270–275.
- [54] E. F. Camacho and C. Bordons, *Model Predictive control*, ser. Advanced Textbooks in Control and Signal Processing. Springer London, 2007.
- [55] Y. Fengjun, W. Junmin, and H. Kaisheng, “Hybrid Electric Vehicle Model Predictive Control Torque-Split Strategy Incorporating Engine Transient Characteristics,” *IEEE Transactions on Vehicular Technology*, vol. 61, no. 6, pp. 2458–2467, 2012.
- [56] Z. Fengqi, X. JunQiang, and R. Langari, “An adaptive Equivalent Consumption Minimization Strategy for Parallel Hybrid Electric Vehicle Based on Fuzzy PI,” in *2016 IEEE Intelligent Vehicles Symposium (IV)*, 2016, pp. 460–465.
- [57] A. Fotouhi, M. Montazeri-Gh, and M. Jannatipour, “Vehicle’s velocity time series prediction using neural network,” *International Journal of Automotive Engineering*, vol. 1, no. 1, p. 8, 2011.
- [58] T. D. Gillespie, *Fundamentals of Vehicle Dynamics*. Warrendale, PA : Society of Automotive Engineers, 1992.
- [59] J.v.Baalen, “Optimal Energy Management Strategy for the Honda Civic IMA,” Master’s Thesis, 2006.

- [60] L. Johannesson, M. Asbogard, and B. Egardt, "Assessing the potential of predictive control for hybrid vehicle powertrains using stochastic dynamic programming," in *8th International IEEE Conference on Intelligent Transportation Systems*, 2005.
- [61] H. Kazemi, B. Khaki, A. Nix, S. Wayne, and Y. P. Fallah, "Utilizing Situational Awareness for Efficient Control of Powertrain in Parallel Hybrid Electric Vehicles," in *2015 IEEE International Conference on Ubiquitous Wireless Broadband (ICUWB)*, Montreal, QC, Canada, 2015, pp. 1–5.
- [62] J. T. B. A. Kessels, M. W. T. Koot, P. P. J. v. d. Bosch, and D. B. Kok, "Online Energy Management for Hybrid Electric Vehicles," *IEEE Transactions on Vehicular Technology*, vol. 57, no. 6, pp. 3428–3440, 2008.
- [63] T. v. Keulen, G. Naus, B. d. Jager, R. v. d. Molengraft, M. Steinbuch, and E. Aneke, "Predictive cruise control in hybrid electric vehicles," *World Electric Vehicle Journal*, vol. 3, 2009.
- [64] M. Koot, J. T. B. A. Kessels, B. de Jager, W. P. M. H. Heemels, P. P. J. van den Bosch, and M. Steinbuch, "Energy Management Strategies for Vehicular Electric Power Systems," *IEEE Transactions on Vehicular Technology*, vol. 54, no. 3, pp. 771–782, 2005.
- [65] V. Marano, P. Tulpule, S. Stockar, S. Onori, and G. Rizzoni, "Comparative study of different control strategies for plug-in hybrid electric vehicles," 2009.

- [66] M. Miller, M. Reif, M. Pandit, W. Staiger, and B. Martin, "Vehicle speed prediction for driver assistance systems," in *SAE World Congress*. SAE International, 2004, 2004-01-0170.
- [67] A. Rezaei, J. B. Burl, A. Solouk, B. Zhou, M. Rezaei, and M. Shahbakhti, "Ecmsceso for series hybrid electric vehicles," *Applied Energy*, vol. Under Review, 2017.
- [68] G. Ripaccioli, D. Bernardini, S. Di Cairano, A. Bemporad, and I. V. Kolmanovsky, "A stochastic Model Predictive Control Approach for Series Hybrid Electric Vehicle Power Management," in *American Control Conference (ACC), Baltimore, MD., USA., 2010*, 2010, pp. 5844–5849.
- [69] L. Serrao, S. Onori, and G. Rizzoni, "ECMS as a realization of Pontryagin's minimum principle for HEV control," in *American Control Conference, 2009. ACC '09.*, 2009, pp. 3964–3969.
- [70] A. Solouk and M. Shahbakhti, "Modeling and Energy Management of an HCCI based Powertrain for Series Hybrid and Extended Range Electric Vehicles," 2016.
- [71] C. Sun, F. Sun, and H. He, "Investigating adaptive-ECMS with velocity forecast ability for hybrid electric vehicles," *Applied Energy*, vol. 185, Part 2, pp. 1644–1653, 2017.
- [72] P. Tulpule, V. Marano, and G. Rizzoni, "Effects of Different PHEV Control Strategies on Vehicle Performance," in *American Control Conference, 2009. ACC '09.*, 2009, pp. 3950–3955.

- [73] T. van Keulen, B. de Jager, J. Kessels, and M. Steinbuch, “Energy Management in Hybrid Electric Vehicles: Benefit of Prediction,” in *6th IFAC Symposium Advances in Automotive Control*, Schwabing, Germany, 2010, pp. 264–269.
- [74] W. Zhou, C. Zhang, J. Li, and H. Fathy, “A Pseudospectral Strategy for Optimal Power Management in Series Hybrid Electric Vehicles,” *IEEE Transactions on Vehicular Technology*, vol. PP, no. 99, pp. 1–1, 2015.

Appendix A

Vehicle Modeling And Simulation

A high fidelity model in AMESim with 19 state variables was developed (Fig. A.1 and A.2). The energy management (EM) strategies were created in Simulink (Fig. A.3). AMESim Co-simulation ability was used to run and control the AMESim model from Simulink.

In the AMESim model, there is a clutch located on the shaft of the e-motor. This clutch is just added in order to convert the parallel HEV model into a conventional vehicle model. For simulations, this clutch is always engaged.

As shown in Fig. A.4, an optimal EM strategy requires a model of the plant for the optimization algorithm. In addition, another model is required to simulate the actual HEV.

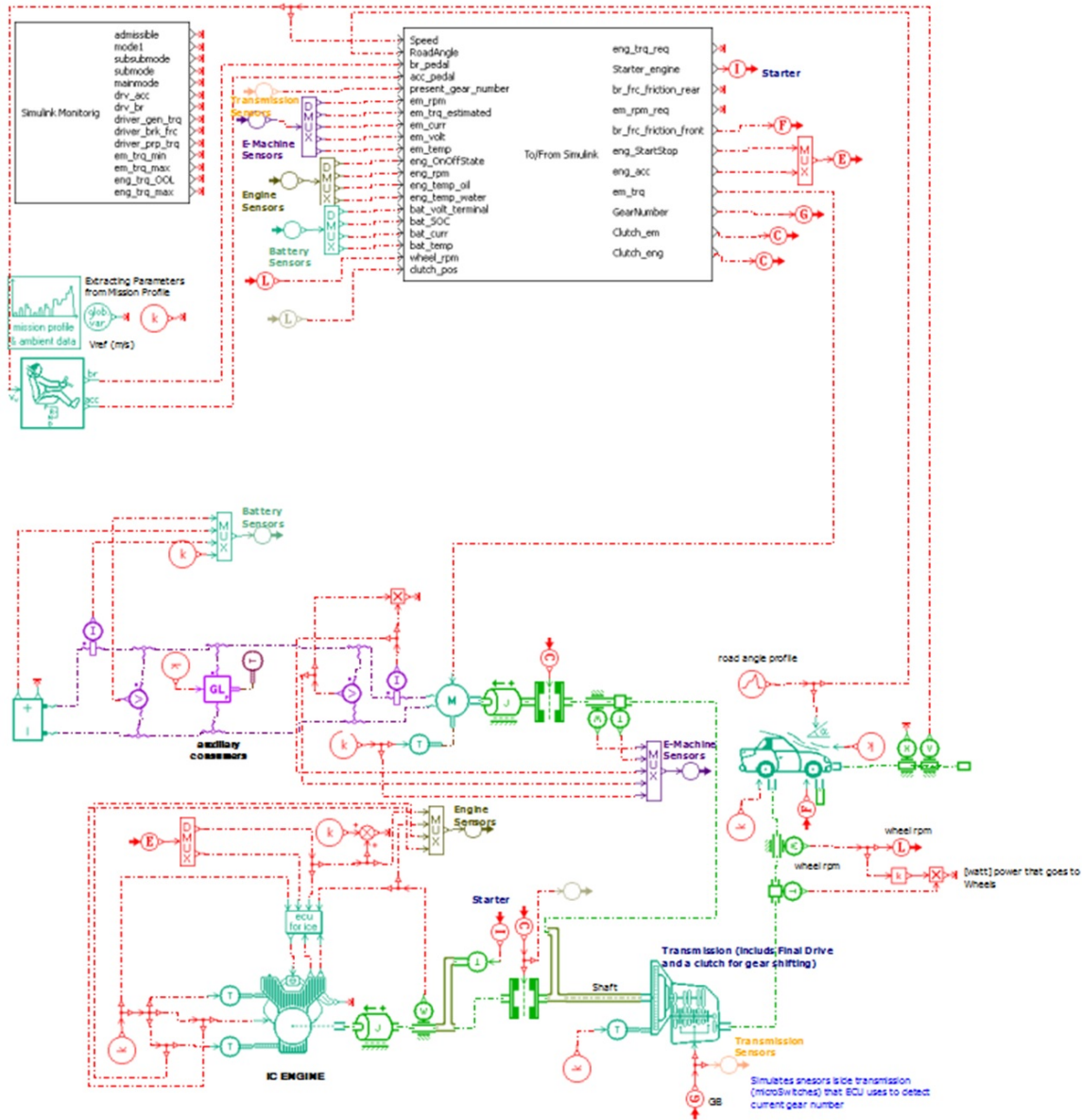


Figure A.1: High fidelity parallel HEV model in AMESim (19 state variables).

The AMESim model with 19 state variables is an acceptable model that considers many dynamics of the plant. However, because of too many state variables, this model cannot be directly used for the optimization algorithm inside the optimal EM strategy. Therefore, a quasi-static low fidelity model of the HEV was created in

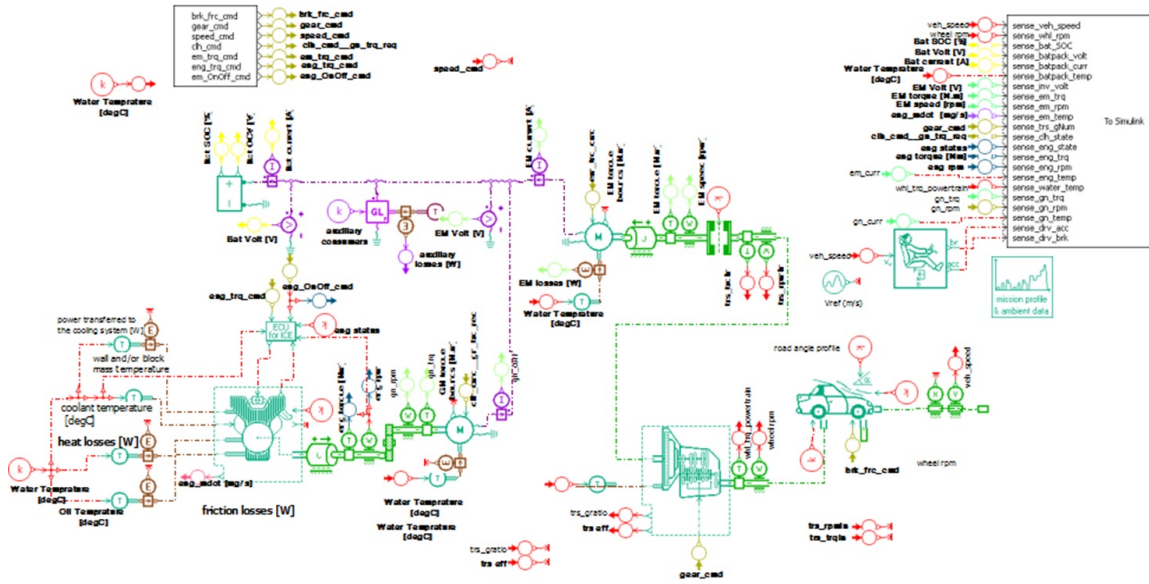


Figure A.2: High fidelity series HEV model in AMESim (22 state variables).

Simulink as shown in Fig. A.5:

Both AMESim and quasi-static models have similar control inputs: engine on/off command, engine and e-motor requested torques, clutch and gear number commands, and friction brake command. However, the quasi-static model has only 4 state variables: battery SOC, vehicle velocity, engine on/off, gear number.

To validate the quasi-static model, the following steps were performed:

- † All components (engine, battery, transmission, etc.) in both AMESim and quasi-static models were initialized by the manufacturer published data.
- † A rule-based controller (RBC) was designed and tuned in Simulink as shown in Fig. A.3 to run the AMESim model (Co-simulation).

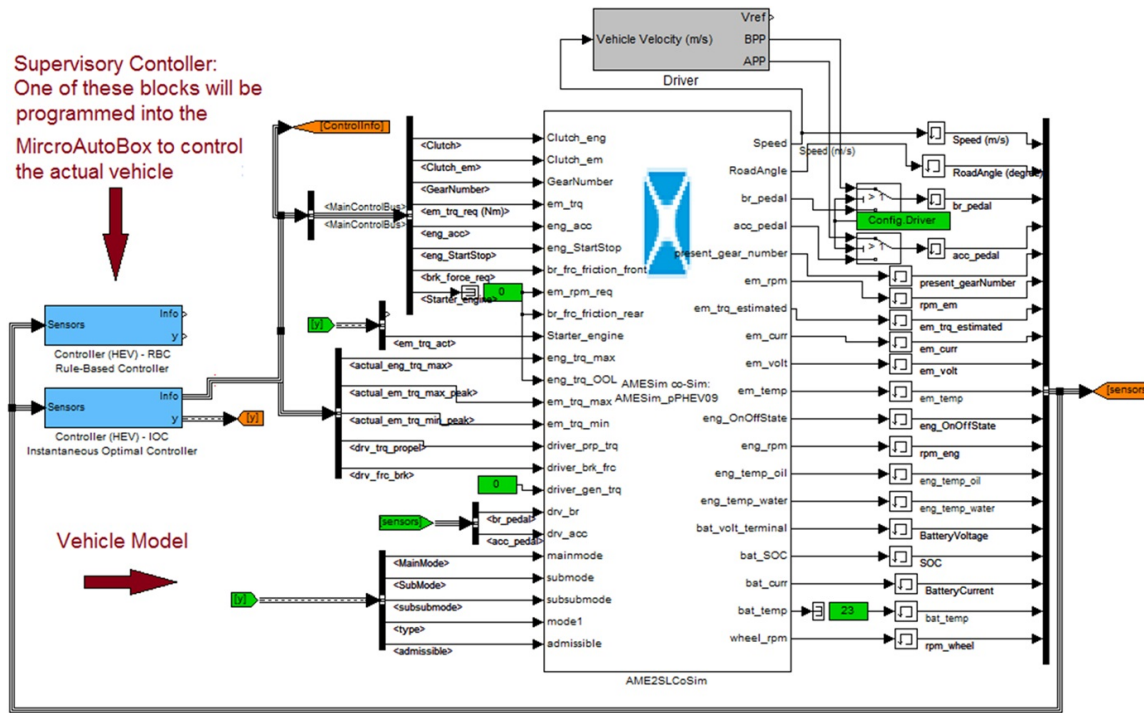


Figure A.3: Co-simulation between Simulink and AMESim: The energy management strategies are developed in Simulink.

- † The trajectory of control commands in the above simulation, were saved.
- † The saved trajectory of the control commands were applied to the quasi-static model (open loop control).

The following figure represents the results (note that both models are triggered with identical controls):

As can be seen in Fig. A.6, the quasi-static model (4 state variables) closely follows the behavior of the high fidelity model with 19 state variables. Although, the tracking is not perfect, but it is close enough to be used as a reliable model for simulations. As shown in Fig.3, the uncertainty between the model and the plant can affect the

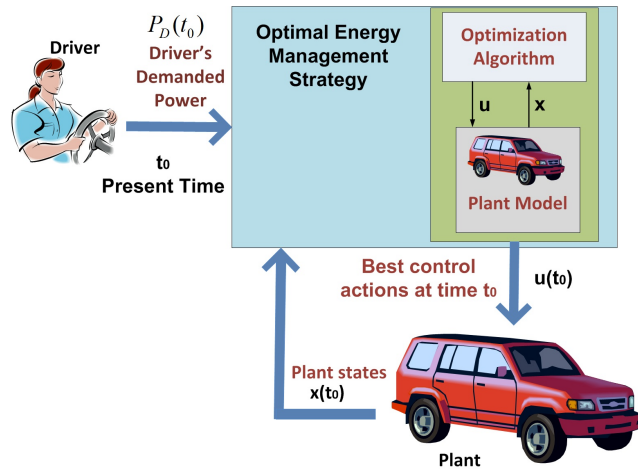


Figure A.4: Simulation requires two model of the HEV: the model inside the EM strategy for the optimization algorithm, and the actual HEV model which simulates the real plant.

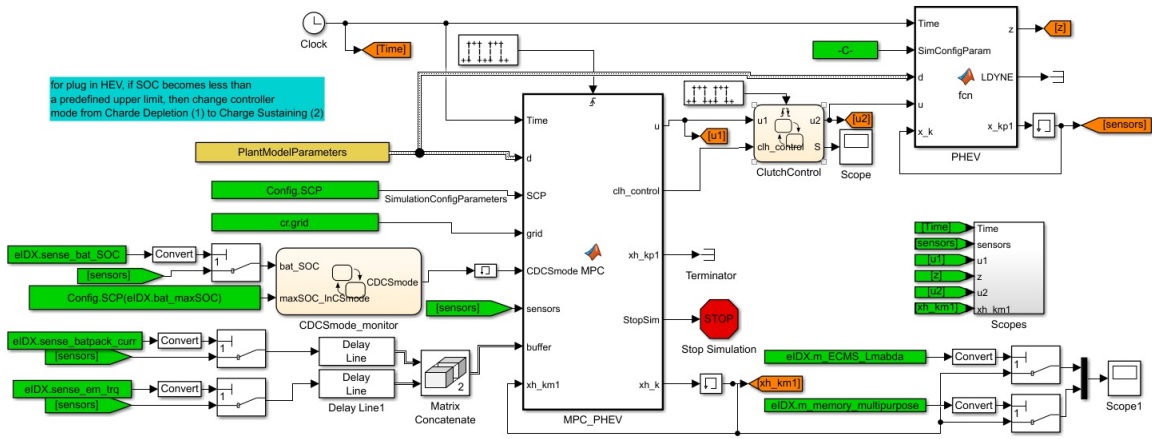


Figure A.5: The quasi static model (the right top block) created in Simulink and was validated with AMESim model.

simulation results. It was desired to only evaluate the performance of ECMS-CESO in comparison with other control strategies without any interference from uncertainty effects. Thus, the quasi-static model was used as the HEV plant as well.

Figure A.5 shows the main model that is used for the simulations in this work.

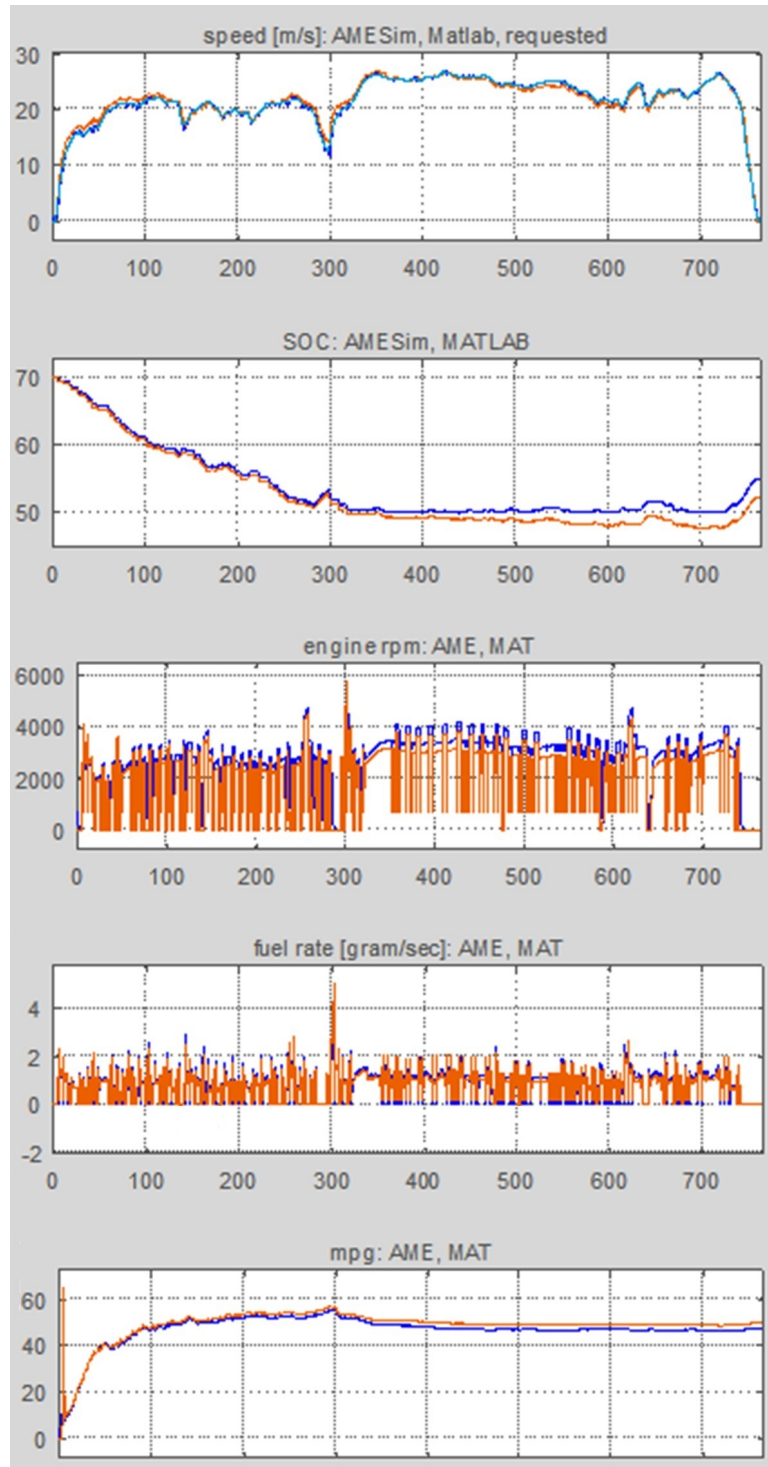


Figure A.6: AMESim model vs. quasi-static model on HWFET drivecycle for the parallel HEV. Both models are triggered with identical control actions. The dark blue lines are AMESim, and the red lines are created by the quasi-static model. The light blue line in the top window is the reference velocity.

Appendix B

Letters of Permission

Re: Enquiry: Request for using the contents of one of my published papers in my dissertation

1 message

Juan Antonio de la Puente <jpuente@dit.upm.es>
To: arezaei@mtu.edu
Cc: IFAC Secretariat <secretariat@ifac-control.org>

Sun, Feb 5, 2017 at 5:14 AM

Dear Amir Rezaei,

You can use the paper in your dissertation, provided you acknowledge copyright and publication by IFAC. The following text is suggested:

© 2015, IFAC. Published in IFAC-PapersOnLine, vol. 48, no. 15, pp. 252–256.

Best regards,
Juan de la Puente

Prof. Juan A. de la Puente
Universidad Politécnica de Madrid
EiC, IFAC-PapersOnLine

El 4 feb 2017, a las 7:25, arezaei@mtu.edu escribió:

The following enquiry was sent via the Elsevier Journal website:

-- Sender --
First Name: Amir
Last Name: Rezaei
Email: arezaei@mtu.edu

-- Message --
Dear Dr. Juan Antonio De La Puente,

I am a student at Michigan Tech. University and I am working on my PhD dissertation. I have a paper published in IFAC-PapersOnLine:

A. Rezaei and J. B. Burl, "Effects of Time Horizon on Model Predictive Control for Hybrid Electric Vehicles," IFAC-PapersOnLine, vol. 48, no. 15, pp. 252–256, Aug. 2015.

I would like to ask for your permission to use the contents of this paper in my dissertation. I look forward to hearing from you. Thanks in advance for your consideration.

Best Regards,
Amir Rezaei

--
This email was sent to you by Amir Rezaei (arezaei@mtu.edu) via the Elsevier Journal Editor contact form at <https://www.journals.elsevier.com:443/ifac-papersonline/editorial-board/juan-antonio-de-la-puente>
Elsevier B.V., Radarweg 29, 1043 NX Amsterdam, The Netherlands. Reg. No. 33156677.

Elsevier is not responsible for the content of this email, and anything written in this email does not necessarily reflect the views or opinions of Elsevier. Please note that neither the email address nor name of the sender have been verified.